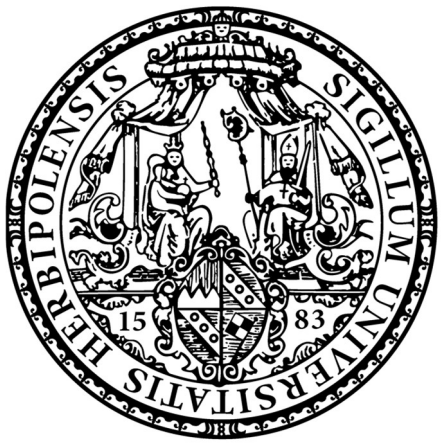

Dosimetry-based Assessment of Radiation-associated Cancer risk for ^{99m}Tc-MAG3 Scans in Infants and Optimization of Administered Activities for ^{68}Ga-labelled Peptides in Children and Adolescents

Dosimetrie-basierte Abschätzung des strahlungsassoziierten Krebsrisikos für ^{99m}Tc-MAG3-Scans bei Säuglingen und Optimierung der verabreichten Aktivitäten für ^{68}Ga-markierte Peptide bei Kindern und Jugendlichen

Doctoral thesis for a doctoral degree
at the Graduate School of Life Sciences,
Julius-Maximilians-Universität Würzburg,
Section Biomedicine.

submitted by

Jéssica Soares Machado

from

São Paulo, Brazil

Würzburg, 2019

Members of the Promotionskomitee

Chairperson: Prof. Dr. Michael Sendtner
Primary Supervisor: Prof. Dr. Michael Laßmann
Supervisor (Second): Prof. Dr. Gerhard Glatting
Supervisor (Third): Prof. Dr. med. Andreas K. Buck

Date of Public Defence: ……

Date of Receipt of Certificates: ……

Submitted on: ……
Office stamp

“Nothing in life is to be feared, it is only to be understood. Now is the time to understand more, so that we may fear less.”

Marie Curie

CONTENTS

I. SUMMARY

In 2006, 0.18 Mio pediatric nuclear medicine diagnostic exams were performed worldwide. However, for most of the radiopharmaceuticals used data on biokinetics and, as a consequence on dosimetry, are missing or have not been made publicly available. Therefore, most of the dosimetry assessments presented today for diagnostic agents in children and adolescents rely on the biokinetics data of adults. Even for one of the most common nuclear medicine exams for this patient group, renal scintigraphy with ^{99m}Tc-MAG3 for assessing renal function measured data on biokinetics is available only from a study performed on four children of different ages. In particular, renal scans are among the most frequent exams performed on infants and toddlers. Due to the young age, this patient group can be classified as a risk group with a higher probability of developing stochastic radiation effects compared to adults. As there are only limited data on biokinetics and dosimetry in this patient group, the aim of this study is to reassess the dosimetry and the associated radiation risk for a larger number of infants undergoing ^{99m}Tc-MAG3 renal scans based on a retrospective analysis of existing patient data.

Data were collected retrospectively from 34 patients younger than 20 months with normal (20 patients) and abnormal renal function (14 patients) undergoing ^{99m}Tc-MAG3 scans. The patient-specific organ activity was estimated based on a retrospective calibration which was performed based on a set of two 3D-printed infant kidneys (newborns: 8.6 ml; 1-year-old: 23.4 ml) filled with known activities. Both phantoms were scanned at different positions along the anteroposterior axis inside a water phantom, providing depth- and size-dependent attenuation correction factors for planar imaging. Time-activity curves were determined by drawing kidney, bladder, and whole body regions-of-interest for each patient, and subsequently applying the calibration factor for conversion of counts to activity. Patient-specific time-integrated activity coefficients were obtained by integrating the organ-specific time-activity curves. Absorbed and effective dose coefficients for each patient were assessed with OLINDA/EXM for the provided newborn and 1-year-old phantom. Based on absorbed dose values, the radiation risk estimation was performed individually for each of the 34 patients with the National Cancer Institute's Radiation Risk Assessment Tool.

The patients' organ-specific mean absorbed dose coefficients for the patients with normal renal function were 0.04±0.03 mGy/MBq for the kidneys and 0.27±0.24 mGy/MBq for the bladder. This resulted in a mean effective dose coefficient of 0.02±0.02 mSv/MBq. Based on the dosimetry results, the evaluation of the excess lifetime risk (ELR) for the development of radiation-induced cancer showed that the group of newborns has an ELR of 16.8 per 100,000 persons, which is higher in comparison with the 1-year-old group with an ELR of 14.7 per 100,000 persons. With regard to the 14 patients with abnormal renal function, the mean

values for the organ absorbed dose coefficients for the patients were: 0.40±0.34 mGy/MBq for the kidneys and 0.46±0.37 mGy/MBq for the bladder. The corresponding effective dose coefficients (mSv/MBq) was: 0.05±0.02 mSv/MBq. The mean ELR (per 100,000 persons) for developing cancer from radiation exposure for patients with abnormal renal function was 29.2±18.7 per 100,000 persons.

As a result, the radiation-associated stochastic risk increases with the organ doses, taking age- and gender-specific influences into account. Overall, the lifetime radiation risk associated with the ^{99m}Tc-MAG3 scans is very low in comparison to the general population risk for developing cancer.

Furthermore, due to the increasing demand for PET-scans in children and adolescents with ^{68}Ga-labelled peptides, in this work published data sets for those compounds were analyzed to derive recommendations for the administered activities in children and adolescents. The recommendation for the activities to be administered were based on the weight-independent effective dose model, proposed by the EANM Pediatric Dosage Card for application in pediatric nuclear medicine. The aim was to derive recommendations on administered activities for obtaining age-independent effective doses. Consequently, the corresponding weight-dependent effective dose coefficients were rescaled according to the formalism of the EANM dosage card, to determine the radiopharmaceutical class of ^{68}Ga-labeled peptides (“multiples”), and to calculate the baseline activities based on the biokinetics of these compounds and an upper limit of the administered activity of 185 MBq for an adult. Analogous to ^{18}F-fluoride, a minimum activity of 14 MBq is recommended. As a result, for those pediatric nuclear medicine applications involving ^{68}Ga-labeled peptides, new values for the EANM dosage card were proposed and implemented based on the results derived in this work.

Overall, despite the low additional radiation-related cancer risk, all efforts should be undertaken to optimize administered activities in children and adolescents for obtaining sufficient diagnostic information with minimal associated radiation risk.

II. ZUSAMMENFASSUNG

Im Jahr 2006 wurden weltweit 0,18 Mio. nuklearmedizinische Diagnostikuntersuchungen bei Kindern durchgeführt. Für die meisten Radiopharmazeutika fehlen jedoch Daten zur Biokinetik und damit zur Dosimetrie oder diese wurden nicht öffentlich zugänglich gemacht. Daher basieren die meisten der heute vorgestellten Dosimetriedaten für Diagnostika bei Kindern und Jugendlichen auf den biokinetischen Daten von Erwachsenen. Selbst für eine der häufigsten nuklearmedizinischen Untersuchungen für diese Patientengruppe, die Nierenszintigraphie mit ^{99m}Tc-MAG3 für Bestimmung der Nierenfunktion, wurden Daten zur Biokinetik bisher nur für vier Kinder unterschiedlichen Alters erhoben. Insbesondere Nierenuntersuchungen gehören zu den häufigsten Untersuchungen bei Säuglingen und Kleinkindern. Aufgrund des jungen Alters kann diese Patientengruppe als Hochrisikogruppe mit einer höheren Wahrscheinlichkeit für das Eintreten stochastischer Strahlenwirkungen im Vergleich zu Erwachsenen eingestuft werden. Da es in dieser Patientengruppe nur begrenzte Daten zur Biokinetik und Dosimetrie gibt, ist das Ziel dieser Arbeit, die Dosimetrie und das damit verbundene Strahlenrisiko für eine größere Anzahl von Kleinkindern, die sich ^{99m}Tc-MAG3-Nierenscans unterziehen, auf der Grundlage einer retrospektiven Analyse bestehender Patientendaten neu zu bewerten.

Die Daten wurden retrospektiv von 34 Patienten unter 20 Monaten mit normaler (20 Patienten) und eingeschränkter Nierenfunktion (14 Patienten) erhoben, bei denen ^{99m}Tc-MAG3-Scans durchgeführt wurden. Die patientenspezifische Organaktivität wurde basierend auf einer retrospektiven Kalibrierung abgeschätzt. Diese Kalibrierung basiert auf einem Satz von zwei 3D-gedruckten Säuglingsnieren, die mit bekannten Aktivitäten gefüllt wurden. Beide Phantome wurden an verschiedenen Positionen entlang der anteroposterioren Achse innerhalb eines Wasserphantoms gescannt und lieferten tiefen- und größenabhängige Schwächungskorrekturfaktoren für die planare Bildgebung. Die Zeit-Aktivitäts-Kurven wurden bestimmt, indem für jeden Patienten Nieren-, Blasen- und Ganzkörperregionen eingezeichnet und anschließend der entsprechende Kalibrierfaktor für die Umwandlung der Zählraten in Aktivität angewendet wurde. Patientenspezifische zeitintegrierte Aktivitätskoeffizienten wurden durch Integration der organspezifischen Zeit-Aktivitätskurven ermittelt. Die Energie- und effektiven Dosiskoeffizienten für jeden Patienten wurden mit OLINDA/EXM für das bereitgestellte Neugeborenen- und 1-Jahres-Phantom ermittelt. Basierend auf diesen Werten für die Energiedosen wurde eine individuelle Abschätzung des Strahlenrisikos für jeden der 34 Patienten mit dem Radiation Risk Assessment Tool des National Cancer Institute durchgeführt.

Die organspezifischen mittleren Energiedosiskoeffizienten der Patienten mit normaler Nierenfunktion lagen bei 0,04±0,03 mGy/MBq für die Nieren und 0,27±0,24 mGy/MBq für die

Blase, was in einem mittleren effektiven Dosiskoeffizienten von 0,02±0,02 mSv/MBq resultiert. Basierend auf den Ergebnissen der Dosimetrie, zeigte die Auswertung des zusätzlichen Lebenszeitrisikos ("excess lifetime risk", ELR) für die Entwicklung von strahleninduziertem Krebs, dass die Gruppe der Neugeborenen ein ELR von 16,8 pro 100.000 Personen aufweist, was höher ist als das der Gruppe der 1-jährigen mit 14,7 pro 100.000 Personen. Bei den 14 Patienten mit abnormaler Nierenfunktion waren die Mittelwerte für die Koeffizienten der organspezifischen Energiedosen für die Patienten: 0,40±0,34 mGy/MBq für die Nieren; 0,46±0,37 mGy/MBq für die Blase. Der effektivendosiskoeffizienten (mSv/MBq) waren: 0,05±0,02 mSv/MBq. Der mittlere ELR (pro 100.000 Personen) für die Entstehung von Krebs durch die Strahlenexposition von Patienten mit abnormaler Nierenfunktion betrug 29,2±18,7 pro 100.000 Personen.

Das mit der Strahlung verbundene stochastische Risiko steigt mit den Organdosen unter Berücksichtigung alters- und geschlechtsspezifischer Einflüsse. Im Allgemeinen ist das mit den ^{99m}Tc-MAG3-Scans verbundene lebenslange Strahlenrisiko im Vergleich zum allgemeinen Bevölkerungsrisiko für die Entstehung von Krebs sehr gering.

Aufgrund der steigenden Nachfrage nach PET-Scans bei Kindern und Jugendlichen mit ^{68}Ga-markierten Peptiden wurden zusätzlich publizierte Datensätze für diese Verbindungen analysiert, um Empfehlungen für zu verabreichende Aktivitäten bei Kindern und Jugendlichen abzuleiten.

Die Dosisberechnungen dazu basierten auf dem Modell einer gewichtsunabhängigen effektiven Dosis, das von der EANM Pediatric Dosage Card für den Einsatz in der pädiatrischen Nuklearmedizin vorgeschlagen wurde. Ziel war es, Empfehlungen zu verabreichenden Aktivitäten so aufzuteilen, dass sich altersunabhängige effektive Dosen ergeben. Dazu wurden die entsprechenden gewichtsabhängigen effektiven Dosiskoeffizienten gemäß dem Formalismus der EANM-Dosierungsempfehlung neu berechnet, um die radiopharmazeutische Klasse der ^{68}Ga-markierten Peptide ("Multiples") zu bestimmen und die Werte für Basisaktivität zu berechnen. Diese basierend auf den Biokinetiken dieser Verbindungen und einer Obergrenze der verabreichten Aktivität von 185 MBq für einen Erwachsenen. Analog zu ^{18}F-Fluorid, wird eine Mindestaktivität von 14 MBq empfohlen. Darauf basierend wurden für die pädiatrischen nuklearmedizinischen Anwendungen mit ^{68}Ga-markierten Peptiden neue Werte für die EANM-Dosierungsempfehlung vorgeschlagen.

Insgesamt sollten, trotz des geringen zusätzlichen strahlenbedingten Krebsrisikos, alle Anstrengungen unternommen werden, um die verabreichten Aktivitäten bei Kindern und Jugendlichen zu optimieren, um ausreichende diagnostische Informationen bei minimalem zusätzlichem Strahlenrisiko zu erhalten.

1. INTRODUCTION

Nuclear medicine plays a major role in clinical areas such as cancer therapy and diagnostic imaging consequently, contributing to healthcare and life quality of the worldwide population [1]. In particular, nuclear medicine diagnostics is an important tool in pediatric patients since it combines physiologic information with high sensitivity imaging [2]. Based on information of the National Council on Radiation Protection and Measurements [3] report 160 (RERF), the number of nuclear medicine exams increased from 6.3 million (1984) to 18 million (2006) out of which 1% of these procedures are for pediatric patients [4]. In general, the most common nuclear medicine exams in pediatrics are renal, bone, brain, gastric and gastroesophageal (reflux studies), gastrointestinal, thyroid, liver and cardiac imaging [4]. Renal scintigraphy allows the evaluation of renal morphology, structure, and function [2]. It is highly indicated for the detection of pyelonephritis or cortical scars (subsequent to an acute condition) [2]. Bone scintigraphy is the second most common examination in pediatric nuclear medicine [4]. It is a method that detects disorders of bone metabolism. Compared to 2D scintigraphy, hybrid 3D imaging with SPECT/CT or PET/CT improve the diagnostic accuracy as it is possible to detect, with sufficient spatial resolution, sources of pain, trauma in small bones and soft tissues, infection, and tumors in an early stage [4]. Brain imaging and neuroblastoma imaging performed with hybrid scans are one of the most frequent procedures in pediatric oncology because of their high specificity (>90%) [2]. Gastrointestinal imaging enables the detection of bleeding from organs' mucosa. Hepatobiliary scintigraphy is the most precise imaging test for cholecystitis, while it is also applied for biliary atresia in small children [2]. In comparison to CT pulmonary angiography, perfusion-ventilation lung scans with usually lower radiation exposure are a low-risk diagnostic procedure for children with a suspect of pulmonary embolism [2].

With respect to radiation safety, medical procedures should be in agreement with the International Commission on Radiological Protection (ICRP) fundamental principles for radiation protection [5]:

1st *Justification* - "any decision that alters the radiation exposure situation should do more good than harm" [5];

2nd *Optimization of Protection* – doses should all be kept "*as low as reasonably achievable"* (*ALARA*), taking into account economic and societal factors" [5];

3rd *Dose Limitation* - "the total dose to an individual should not exceed the appropriate limits" [5-7].

With regard to risk-benefit, nuclear medicine exams for pediatric patients have advantages that justify the risk of radiation exposure. The procedures are non-invasive, allow

detecting initial stages of pathologies, and can be applied as a guide for oncology therapies [2, 8]. In these applications, the amount of the administered activity such that the absorbed doses to both the imaged and the non-imaged tissues are very low and, thus, risks of cancer induction are substantially outweighed by the diagnostic benefit of the imaging procedure [2, 9].

The principle of optimization of protection is associated with the optimization of an adequate quantity of administered activity. Thus, a minimum quantity must be sufficient to acquire an image quality and, consequently, to obtain reliable diagnostic information [6]. Therefore, the majority of pediatric nuclear medicine exams for diagnostics are kept at low radiation exposure when performed according to the national and international guidelines and recommendations [9].

Considering the dose limitation, it is important to mention that there are in principle no dose limits determined for medical studies. However, due to an increasing number of medical exposures by medical imaging [2, 10], *Diagnostic Reference Levels (DRL)* have been determined for patients. According to an IAEA publication [6] for nuclear medicine, “DRLs are investigation levels based on an easily measured quantity (administered activity)” [5-7]. DRLs are usually defined by national regulatory bodies responsible for radiation protection and have the purpose of optimizing radiation safety while providing meaningful diagnostic information [5-7].

The optimizing of patient radiation protection undergoing standard nuclear medicine procedures can be complex, since several factors must be considered: equipment type, radiopharmaceutical, the quantity of activity, DRLs, dosimetry, calibration of the equipment, quality control, and age-dependent procedure protocols [6]. Pediatric patients show a wide range of weights and heights [2, 8, 9]. Therefore, it is highly relevant to consider patient age, gender, body morphometry, and pharmacokinetics, along with all available image acquisition and processing techniques, to ensure an optimal procedure [2, 9]. Ideally, the absorbed doses to organs and tissues and their associated risks should be quantified individually for each patient [2].

In the last years, efforts have been undertaken by the European Association of Nuclear Medicine (EANM) and, in particular, by the EANM dosimetry committee to identify areas for dose optimization in pediatric diagnostic nuclear medicine, e.g., in 2008 [11]. EANM published a weight-dependent pediatric dosage card, followed by an update in 2014 [12], with particular emphasis on the pharmaceuticals used in children and adolescents. However, there are still data gaps concerning the assessment of the stochastic radiation risk in diagnostic pediatric nuclear medicine, as has been stated by a consultancy meeting report to the IAEA [2]:

Lack of standardized image acquisition and dosimetry protocols for new agents;

General lack of biokinetic data for pediatric patients for all radiopharmaceuticals, balancing image quality and, patient risk;

Need for considering patient morphometry beyond age or weight in pediatric dosage guidelines.

One of the gaps identified concerns *^{99m}Tc-MAG3 renal scans* are currently among the most frequent diagnostic procedures for pediatrics [4]. The only published data on ^{99m}Tc-MAG3 biokinetics and dosimetry are more than 26 years old and were carried out on four subjects only [13, 14].

The majority of the patients undergoing planar dynamic ^{99m}Tc-MAG3 scintigraphy are newborns (age: from 0 to 12 months) and toddlers (age: from 12 to 36 months), considered as "*high-risk group"* due to the radiation exposure at a young age [2, 8]. This fact combined with the general lack of dosimetry and biokinetic information makes this group of patients important to be evaluated. Moreover, planar ^{99m}Tc-MAG3 scans in newborns or toddlers typically cover the entire body of the patient which is very useful for image quantification and dosimetry [15]. Therefore, ^{99m}Tc-MAG3 scans for pediatrics were selected as a main nuclear medicine procedure to be assessed in the present retrospective analysis, in which collection of patients' morphological data and retrospective image quantification was performed to reassess the patients' biokinetics for dosimetry calculations.

Furthermore, a procedure-related radiation-associated cancer risk estimation using age-and-gender-specific risk factors was performed. More specifically, the following tasks were carried out:

- Demographic information on nuclear medicine (NM) diagnostic procedures performed in pediatric patients in order to identify the most frequent procedure.
- Phantom experiments for performing a retrospective imaging-based quantification of ^{99m}Tc-MAG3 scans in infants and toddlers with normal and abnormal renal function by using a depth- and size-dependent attenuation correction.
- Based on the image quantification the following assessments were performed:
  - Patient-specific time-activity curve (TACs) were estimated;
  - Patient-specific time-integrated activity coefficients (TIACs) were assessed;
  - Patient-specific absorbed and effective doses were calculated;
  - The procedure- and patient-specific radiation risk was estimated.

Moreover, based on a retrospective analysis of published dosimetry data a weight-dependent table for the EANM dosage card for *^{68}Ga-DOTA-Peptides* and *^{68}Ga-Pentixafor PET/CT scans* was developed

2. BASIC PRINCIPLES OF RADIATION EXPOSURE AND RISK

2.1. Ionizing Radiation

Ionizing radiation originates from particle adjustment processes in the atomic shells composed by electrons (Fig. 2.1) or in the atomic nucleus which is composed of neutrons and protons (Fig. 2.1) [6, 16, 17]. It can also arise from particles interacting with a “target” atom [6, 16, 17].

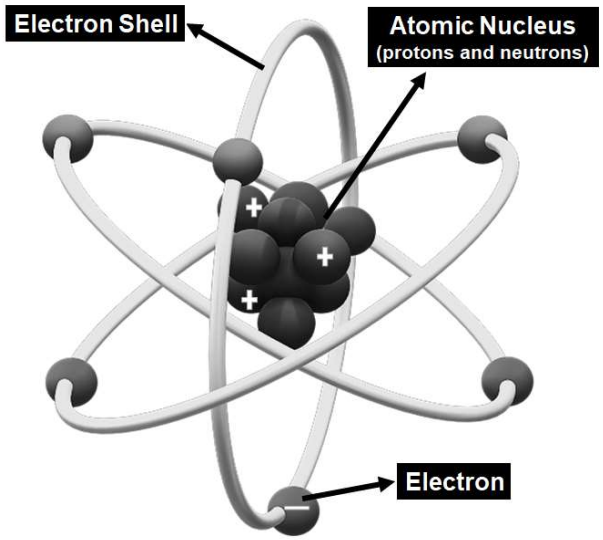

FIGURE 2.1. Schematic atomic structure. Components: nucleus and electron shell. Figure reproduced based on the source: https://simple.wikipedia.org/wiki/Atom (Copyright: Public domain).

Regarding medical diagnosis or treatment, the most important particles are positrons and electrons (Fig 2.2), either originating from the atomic nucleus or from the atomic shell [6, 16, 17]. If the particles originate from the radioactive beta decay of a nucleus, they are called beta particles.

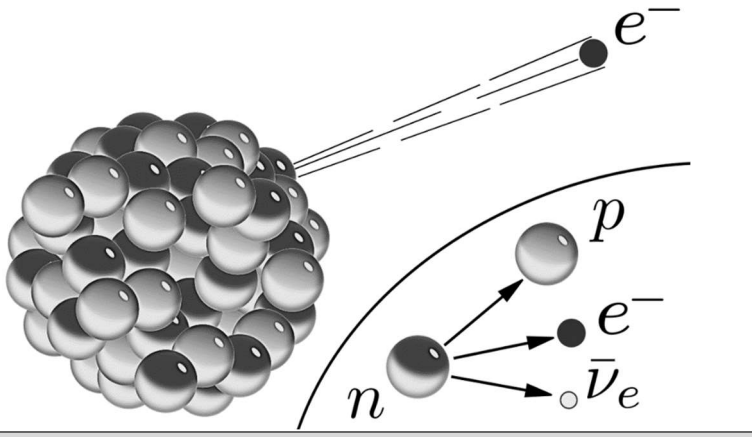

FIGURE 2.2. Representation of a beta particles emission. Figure reproduced based on the source: https://commons.wikimedia.org/wiki/File:Beta-minus_Decay.svg (Copyright: Public domain).

The process of positron formation consists of a proton (p) disintegrating into a neutron (n), a positron (e) and, a neutrino (ν_e) (Fig.2.2). In contrast, electron formation (Fig.2.2) occurs from a neutron (n) disintegrating into a proton (p), an electron (e^-), and an antineutrino (ν_e^-) [6, 16, 17].

The maximum range of beta particles used for nuclear medicine diagnostics or therapy is in the order of a few centimeters in tissue and thus can lead to substantial radiation exposure [6, 17].

Other sources of ionizing radiation in nuclear medicine are gamma rays (γ) and x-rays. Gamma rays are mainly emitted by atomic nucleus decays, resulting in particle emission. After the discharge, the remaining nucleus components are typically an excited condition. Therefore, to reach stability, the nucleus emits the excess energy as an electromagnetic wave. Gamma rays are produced in the atomic nucleus whereas x-rays are emitted from the atomic electron shells. The physical processes that produce x-rays primarily occur when an electron in an excited condition emits an electromagnetic wave for stabilizing the energy levels. X-rays can also be produced by *electron capture*, a process that occurs when the atomic nucleus is in an excited state, and an electron from the intern shell is absorbed by the nucleus. Consequently, the reallocation process of the electrons remaining in the atomic shell causes x-ray emission. In general, the photon energy of gamma rays is higher in comparison to x-rays [6, 16, 17].

2.2. Radionuclides

In general, radioactive nuclides or radionuclides used for medical purposes are produced in nuclear reactors, cyclotrons or particle accelerators [6, 17, 18].

The relationship between the number *N* of atomic nucleus decays at a given time point *t* depends on the initial number of atoms (N_0) and is described by the decay equation 2.A [19, 20].

EQUATION 2.A. DECAY

$$N(t) = N_0\, e^{-\lambda t}.$$

N = Number of the atomic nucleus decays at time point t

λ = Decay constant (unit: s^{-1})

N_0 = Initial number of atoms

The decay process is probabilistic; the decay constant λ is specific for each radioactive element (s^{-1}) [19, 20].

The time interval required for a radionuclide reaching half the number of its radioactive atoms is called *half-life* $T_{1/2}$ (unit: s) (Eq. 2.B) [19, 20].

EQUATION 2.B. HALF-LIFE

$$T_{1/2} = \frac{\ln(2)}{\lambda}.$$

The radioactive decay function can then be expressed as [6, 16, 17]:

EQUATION 2.C. DECAY II

$$N = N_0 \cdot e^{-\lambda t} = N_0 \cdot e^{-\frac{\ln(2)}{T_{1/2}} \cdot t}.$$

Activity (A) is *a* radiation *measurement quantity,* which quantifies the radioactive atomic nucleus decays per unit time (Eq.2.D) [7, 16, 17, 19, 20]. The SI unit of activity is

Becquerel (s^{-1}). A is defined as the total number of particles in a sample N multiplied by the decay constant λ:

EQUATION 2.D. ACTIVITY

$$A\,(t) = \lambda \cdot N(t).$$

Therefore, the activity of a sample can be expressed as [6, 16, 17]:

$$A(t) = \lambda N(t) = \lambda \cdot N_0 e^{-\lambda t}.$$

Furthermore, the activity at t = 0 can be expressed as [6, 16, 17]:

$$A_0 = \lambda \cdot N_0.$$

resulting in:

$$A(t) = A_0 e^{-\lambda}\ .$$

The main classes of radionuclides used in nuclear medicine are those with beta decay (β+; β–) and/or gamma decay (pure gamma decay and electron capture) [16, 19, 20].

2.3. Radiopharmaceuticals

Radiopharmaceuticals are a chemical combination of a radionuclide with a pharmaceutical (drug), which are typically applied for nuclear medicine diagnostics or therapy [6, 16, 21]. Nuclear medicine and molecular imaging are developing fast with the continuous development of new radiopharmaceuticals and technological improvements [17, 21, 22].

In the present study, the radiotracers ^{18}F-FDG, ^{68}Ga-DOTA-Peptides, ^{68}Ga-Pentixafor, ^{99m}Tc-DMSA, and ^{99m}Tc-MAG3 will be dealt with.

The ^{18}F-fluoro-2-deoxy-D-glucose (FDG) is one of the main compounds used in *Positron Emission Tomography combined with Computed Tomography – PET/CT* [12823, 24]. PET/CT is a hybrid imaging technique that combines a positron emission (two photons of 511 keV) detector with a computed tomography scan [18, 23, 24]. ^{18}F-FDG is used in diagnostic imaging for characterization of glucose metabolism [18, 25].

The introduction of ^{68}Ga-labeled PET ligands has revolutionized the diagnostic algorithm in well-differentiated neuroendocrine tumors for both adult and pediatric patients [26, 27]. ^{68}Ga-DOTA-peptides provide superior imaging of primary tumors, lymph node and organ metastases including bone lesions compared to conventional diagnostic imaging modalities (CT, MRI and bone scintigraphy) [26, 27]. Another promising recently developed radiopharmaceutical for in-vivo imaging of Chemokine receptor four expressions (CXCR4) is the ^{68}Ga labeled PET tracer Pentixafor [27, 28]. Pentixafor allows the proof of CXCR4 expression which is a potential therapeutic target of patients with hematological tumors such as multiple myeloma, lymphoma, and leukemia. Accordingly, Pentixafor represents a potential for children applicable in vivo biomarker [27, 29].

^{99m}Tc-dimercaptosuccinic acid (DMSA) is used in nuclear medicine imaging (in vivo) for evaluation of renal morphology and structure [9, 30]. ^{99m}Tc-DMSA has a quick physical half-life of ^{99m}Tc (Table 2.1), a biological half-life of ~3.5 hours, as ~50% of the component is fixed in the renal cortex [9, 30].

^{99m}Tc-mercaptoacetyltriglycine (MAG3) is utilized to perform planar imaging in vivo for investigating renal system function. Therefore, ^{99m}Tc-MAG3 scans are often indicated for renal function examinations in children and adults [8, 9, 18, 31]. It is commonly prescribed for diagnostic studies in infants because of the minimum recommended age (1 month), the short physical half-life of ^{99m}Tc (Table 2.1), a biological half-life of ~4 hours, a high extraction rate of the radiopharmaceutical (60% in the first filtration), and the high kidney uptake (97%), providing a good image quality even for infants [9, 27]. Therefore, renal scans with ^{99m}Tc-MAG3 are among the most frequently performed urinary tract exams in infants and toddlers [9, 18, 32].

TABLE 2.1. Some radionuclides used in nuclear medicine for diagnostic purposes.

Radionuclide	Half-life ($T_{½}$)	Decay Type	Energy	Applications
^{18}F	110 min	β+ (99.8 %)	0.6 MeV	PET/CT
^{68}Ga	67.6 min	β+ (87.7%)	0.8 MeV	PET/CT
		γ (3.2%)	1.08 keV	
^{99m}Tc	6.01h	γ	141 keV	Planar; SPECT/CT

Data Sources: CERN- European Council for Nuclear Research (Document Server) (https://cds.cern.ch/record/1309915/files/978-3-642-025860_BookBackMatter.pdf); LNHB – Laboratoire National Henri Becquerel (http://www.nucleide.org/DDEP_WG/DDEPdata.htm)

Usually, the leading causes of kidney diseases are congenital disabilities, hereditary disorders, infection, nephrotic syndrome systemic diseases, trauma, urine blockage or reflux [33]. Congenital disability already happens in the formation period of babies. These defects are abnormalities of kidney size, structure or kidneys' position [33]. The defects that affect small children consist in renal agenesis (children that are born with only one kidney), renal dysplasia (children that are born with both kidneys, however with unilateral function) and, ectopic kidney (kidney position is different from the usual anatomical position) [33]. Hereditary diseases are passed from the parents to the child through the genes, for example, polycystic kidneys [33]. An infection in the renal system can result in kidney failure [33]. The nephrotic syndrome is a cluster of symptoms that indicate kidney damage as, albuminuria, hyperlipidemia and, edema in legs, feet or ankles [33]. Systemic diseases such as lupus and diabetes involve different organs or even the whole body, including the renal system [33]. Traumas as dehydration, bleeding, burns, injury or surgery can lead to kidney diseases since they have a strong influence on increasing or decreasing blood pressure [33]. Urine blockage or reflux happens when there is a blockage between the kidneys and urethra or ureter. In these conditions, the urine flows from the bladder back to kidneys causing damage [33]. Children in the range age range of 0 to 4-years-old in most of the cases present of congenital disabilities and hereditary diseases causing kidney failure [33].

2.4. Radiation Interaction

Positrons and electrons interact either with the electrons in the shell of an atom or, in case of close approximation, with the atomic nucleus. [6, 16, 20].

In contrast, electromagnetic radiation interacts indirectly with atoms as the process of ionization first requires the production of charged particles [16, 20]. These processes can cause either atomic or molecular excitation, ionization, or activation [16, 20]. Atomic or molecular excitation happens when electrons are dislocated from their original shell position emitting an excess of electromagnetic radiation (light or x-ray). Ionization occurs when electrons are removed from the electron shell, resulting in a free electron with high energy, in positive ions or in free radicals (if breakage of chemical bonds occurs) [16, 20]. Excitation and ionization are essential processes for most radiation types [16, 20]. Activation consists of nuclear reactions that result in radiation emissions, and that occur for particular radiation types under specific conditions [16, 20].

The primary photon interaction types of photons of radionuclides used in nuclear medicine are the *photoelectric effect*, the *Compton effect*, *pair production, and annihilation photons* [6, 16, 17].

The photoelectric effect occurs most frequently for photons with low energy and elements with a high atomic number (Z) [6, 16, 17]. It is defined as an interaction between a photon and an electron in the inner shell of an atom, leading to a free electron with kinetic energy, which is the energy of the photon minus the linkage energy of the electron. The photon is completely absorbed. The probability for this effect to happen increases with Z and decreases if the photon energy increases. For example, photoelectric effect occurs for energy ranges below 0.6 MeV for lead and 0.06 MeV for aluminum [6, 16, 17].

The Compton effect occurs when an incident photon transfers part of its energy to an electron (with low binding energy). During this process, the direction of the photon is changed, and the photon loses part of its energy [6, 16, 17].

Pair production occurs when the trajectory of an incident photon with an energy equal to or higher than 1.022 MeV passes closely by the atomic nucleus [6, 16, 17]. Due to strong attraction arising from the nuclear electric field, the incident photon interacts with the nucleus being absorbed [6, 16, 17]. This interaction results in the formation and emission of an

electron-positron pair ($2mc^2$ = 1.022 MeV), which this reaction is represented in equation 2.E [6, 16, 17].

EQUATION 2.E. ELECTRON-POSITRON

$$\gamma \rightarrow e^- + e^+ + E_k \ .$$

When a positron (e^+) slows down and interacts with an electron (e^-), e.g., in an atomic shell, two antiparallel photons of 511 keV will be emitted. This process is called pair annihilation (eq. 2F) [6, 16, 17].

EQUATION 2.F. PAIR ANNIHILATION

$$e^- + e^+ \ \rightarrow \ \gamma + \gamma.$$

Incident photons are partly or entirely absorbed by a specific material mainly by the previously described interaction processes [6, 16, 17].

In case of a narrow photon beam, the attenuation process is described by the following formula:

EQUATION 2.G. ATTENUATION

$$I(x) = I_0 \cdot e^{-\mu x}.$$

I represents the beam intensity at thickness x, while the incident radiation beam is represented by I_0. The factor μ is called the attenuation coefficient (unit: m^{-1}). It describes the probability of the material attenuating the radiation, taking into account the different interaction effects. As shown in Fig 2.3, increasing material thickness leads to a higher attenuation (exponential) of the incoming beam [6, 16, 17, 34]. The attenuation coefficient μ depends not only on the incident radiation energy and material thickness (x), and density (ρ), but also on the material type, and its physical state (solid, liquid, gaseous) [6, 16, 17, 34]. Therefore, specific attenuation coefficients for many materials have been established [19, 34].

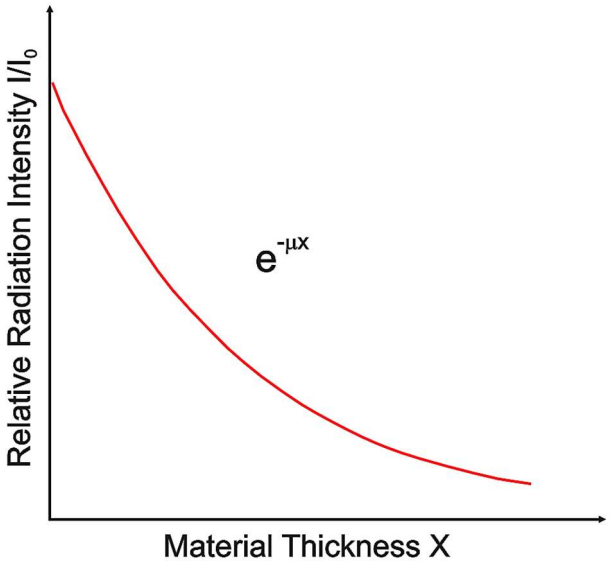

FIGURE 2.3. Radiation attenuation as a function of the material thickness. This figure was donated by the authors of the citation [16] who also allowed the edition of it. Original available on https://inis.iaea.org/collection/NCLCollectionStore/_Public/45/073/45073465.pdf

2.5. Imaging in Nuclear Medicine

The primary imaging devices in nuclear medicine are the gamma camera and the positron emission tomograph [5].

The gamma camera consists of four essential components: the collimator (defines the spatial resolution of the images); detector (with photomultipliers and analog-to-digital converters to analyze the photons (γ) interactions); computer system (it registers counts to the 2D image matrix); gantry (gives physical support for the detector heads and controls the movement of the gamma camera and the patient bed) [5]. Usually, the detector consists of a large area NaI (Tl) crystal with up to 100 coupled photomultiplier tubes (PMTs) [5]. Moreover, the detectors are mostly composed of scintillation due to their high stopping power, have a high efficiency of converting radiation into visible light [5].

Planar imaging studies are mainly classified into two categories static and dynamics [5]. Planar static imaging provides a static image of the distribution of the radionuclide during image acquisition [5]. In planar dynamic imaging, the images are acquired as a set of frames over time allowing to observe the compound distributing through the organs/body [18]. The duration of the image frames can be changed according to the study purpose [5].

There are some essential factors which influence the image acquisition processes such as the collimator (determines resolution and sensitivity), the number of counts (increases with the amount of injected activity and/or imaging time; increased count rates lead to better counting statistics), patient positioning (the image orientation can be altered according to the patient position), and camera position (in order to improve the spatial resolution the camera should be as close as possible to the patient).

The positron emission tomography (PET) is based on the detection of pairs of annihilation photons emitted by the tracers in the patient body [5]. About 1,000 scintillating crystals with up to 1,000 PMTs commonly compose the positron detectors areas [5].

PET in combination with CT or magnetic resonance imaging (MRI) scanners – so-called hybrid imaging systems – provide a sophisticated method for imaging. These examinations present high quality by combining morphological images with metabolism [5].

2.6. Dosimetry

Radiation dosimetry is essentially applied in the fields of radiation protection and medical physics; it consists basically, as the assessment of the ionizing radiation in an area, object/material or organs/body. The dosimetry assessment can be performed by means of measurement techniques and specific calculations methods. The radiation quantities and respective units were established by international organs such as the International Commission on Radiation Units and Measurements (ICRU) responsible for the operational quantities [7, 16, 17, 19]. Furthermore, the International Commission on Radiological Protection (ICRP), makes recommendations related to the limits of exposure [7, 16, 17, 19].

2.6.1. Absorbed Dose

The fundamental dosimetry quantity *is* the *absorbed dose (D)*. It is defined as the amount of absorbed energy per tissue mass. The absorbed dose (D) can be expressed as the ratio of the average absorbed energy (dε) deposited in a specific tissue point and the material mass (d*m*) (Eq. 2.H) [7, 16, 17, 19, 20, 35].

EQUATION 2.H. ABSORBED DOSE

$$D = \frac{d\varepsilon}{dm}$$

SI unit: J.kg^{-1} = Gray (Gy)

2.6.2. Effective Dose

The quantity *effective dose* is generally applied for estimating the risk level of biological effects for a population/group. Therefore, the effective dose can also be utilized as a standard parameter for the optimization of radiation exposure control purposes. The effective dose was introduced first in ICRP publication 60 [7, 16, 17, 19, 20, 35].

This radiation protection quantity combines information about radiation exposure, described by the measurable quantity absorbed dose, with organ-specific weighting factors that describe the contribution of each organ/tissue to the stochastic radiation risk (Table 2.2) [7, 16, 17, 19, 20, 35].

In ICRP 60 the effective dose is calculated as the sum of the absorbed doses in the tissue/organs of distinct radiation types by means of the tissue/organs weighting factors and radiation weighting factors (Eq. 2.I) [7, 16, 17, 19, 20, 35]. According to the radiation weighting factors w_r established by the ICRP publication 60 and [5-7] confirmed by ICRP publication 103 [5], 1 is the value for x-rays, gamma-rays (γ), electrons (e^-), and beta-particles (β). For the sake of unifying the whole body exposure, for a specific radiation type the tissue/organ absorbed dose for specific radiation should be multiplied by the respective radiation weighting factor [7, 16, 17, 19, 20, 35].

The calculation of the Effective dose E is given by equation 2.I:

EQUATION 2.I. EFFECTIVE DOSE

$$E = \sum_T \mathrm{w}_T \sum_R w_R \, \mathrm{D}_{T,R} = \sum_T \mathrm{w}_T \, \mathrm{H}_T$$

SI unit: $J.kg^{-1}$ = sievert (Sv)

H_T is the equivalent dose absorbed by tissue/ organ obtained by multiplying the organ absorbed doses with w_R; w_T is the tissue weighting factor which represents the variable radiosensitivity specific for the different body tissues/organs; $\overline{D}_{T,R}$ is the mass-average radiation-type dependent absorbed dose in tissue(T) [5, 7, 16, 17, 19, 20, 35].

TABLE 2.2. Tissue-weighting Factors.		
Tissue Weighting Factors		
Tissue or Organ	**ICRP 60**	**ICRP 103**
	W_T	W_T
Bone Surfaces	0.01	0.01
Bladder	0.05	0.04
Breast	0.05	0.12
Brain	–	0.01
Colon	0.12	0.12
Gonads	0.2	0.08
Liver	0.05	0.04
Lungs	0.12	0.12
Oesophagus	0.01	0.04
Red bone marrow	0.12	0.12
Salivary glands	–	0.01
Skin	0.01	0.01
Stomach	0.12	0.12
Thyroid	0.05	0.04
[+]Remainder	0.05	0.12
Total ($\sum T\ W_T$)	1.0	1.0
ICRP 60	**[+]Remainder:** adrenal glands, brain, kidneys, muscle, pancreas, small intestine, spleen, thymus, upper large intestine, uterus (female)	
ICRP 103	**[+]Remainder:** adrenal glands, extrathoracic airways, gallbladder, heart, lymphatic nodes, oral mucosa, pancreas, prostate (male), skeletal muscle, small intestine, spleen, thymus and, uterus (female), cervix (female).	
Data Sources [4]: ICRP publications 60 and 103.		

Tissues weighting factors (W_T) can be resumed in a cluster of values with a range between 0.01 and 0.12 which can symbolize a certain risk level (e.g.: low: W_T= 0.01; moderate: W_T= 0.04; high: w_T= 0.12) [5]. Comparing the ICRP publication 60 and publication 103 tissues weighting factors, there are some differences between those values (Table 2.2). The W_T for breast and remainder increased in the publication 103 by approximately a factor of two; in contrast, gonads had the W_T decreased by around a factor of two [5]. These variations can be related to the fact that ICRP 60 had as reference phantoms mathematical models while ICRP 103 had computational models based on tomography images from the human body [5]. Furthermore, the tissues weighting factors from 103 were estimated by means of a revised age-and sex-average which means that the resulting effective doses are rounded values for applying to a general population [5]. The effective dose concept/quantity

is essential for the deployment of the principles of radiation protection in several areas [5]. Therefore, ICRP 103 clearly demands the use of male and female reference voxel phantoms, described by ICRP publication 110 and consequently, the determination of the equivalent doses to the organs and tissues of the reference male and the reference female separately [14]. According to ICRP 103, only the latest ICRP voxel phantoms should be used for the calculations of ED [5, 14].

ICRP 128 [18], the latest publication of the ICRP on absorbed doses and effective dose coefficients for radiopharmaceuticals still applies the tissue weighting factors given in ICRP 60 [5]. For the sake of compatibility, all comparisons and analyses in this work were made using the ICRP 60 tissue weighting factors, partly also because the values of nuclide-specific absorbed fractions for the adult phantom prescribed by ICRP 103 have not yet been published [5].

The effective dose concept can be applied to quantify the stochastic risk estimation of an exposed population group such as workers or patients [5, 7, 15]. According to ICRP, it can be applied in diagnostic exams to estimate the health detriment for a general group of exposed individuals, without considering ages and gender [5, 7, 15]. Based on the effective dose values, the risk levels of different procedures can be compared and optimized whenever it seems reasonable or necessary [5, 7, 15]. However, the ICRP formalism is not applicable for performing individual risk estimation of radiation-induced effects [5, 7, 15].

2.6.3. Administered Activity Weight-Based Formalism

Children and teenagers present an extensive range of sizes and weight, making an assessment of the activity to be administered for a certain radiopharmaceutical is challenging. In the past, the activity dosage was scaled by two different methods, either based on the body weight or the body surface [6]. As expected these methods presented discrepancies when compared to each other [6].

More recently, the EANM published the EANM *Dosage Card*, which acknowledged that the use of a single scale is not indicated for all radiopharmaceuticals [6, 12, 36]. In the Dosage Card, the radiopharmaceuticals were classified into three classes with dissimilar scaling factors for each class. A weight -dependent scaling factor is provided for each radiopharmaceutical that was set to determine a weight-independent effective dose [12, 36]. This formalism was introduced and described by Jacobs et al. 2005 [36]. It was developed describing the effective dose as a function of body weight for 95 radiopharmaceuticals using a single parameter [36]. From these data three clusters A, B, and C could be identified; cluster A contains tracers for renal studies, cluster B the remaining tracers, and cluster C the iodine

labeled tracers [36]. In addition, the EANM dosage Card derived from this publication provides the minimum recommended activity [12, 36].

2.7. Absorbed dose calculation in Nuclear Medicine

The internal dose calculation of organs/tissues consists of a complex methodology as it has to consider many factors such as the physical properties of the respective radiopharmaceutical as well as patient pharmacokinetics and physiology [14, 20]. In summary, the internal dose is calculated based on the following key information: radiopharmaceutical distribution in space and time; amount of administered activity; phantom measurements for calibration purposes; computational models that simulates organs' morphometry and organ-to-organ distances; patient-specific body morphometry data information (acquired from quantitative imaging processes) [14, 20].

To describe the pharmacokinetics of the radiopharmaceutical inside the body, the biological half-life (T_b) must be considered in addition to the physical half-life (T_{phys}) to estimate

the time interval of an organ's clearance for a specified substance [19]. It can be expressed by the following simplified equation for a single excretion rate [19]:

EQUATION 2.J. BIOLOGICAL HALF-LIFE

$$X(t) = X_0 e^{-\lambda_b t}$$

Where $X_{(t)}$ is the amount of the substance at the time; X0 represents the initial amount of substance; λb is the biological clearance (constant: $\ln(2)/T_b$); T_b biological half-life for substance removal [20].

EQUATION 2.L. EFFECTIVE CLEARANCE

$$EC_e = \lambda_b + \lambda_{phys}$$

The effective clearance constant (EC_e) represents the relation between the radioactive physical decay constant (λ_{phys}) and biological clearance constant (λ_b) per time unit (Eq. 2.I) [20].

EQUATION 2.M. EFFECTIVE HALF-LIFE

$$T_e = \frac{T_b \cdot T_{phys}}{T_b + T_{phys}}$$

Tb=biological half-life
Tphys=physical half-life

The effective half-life (T_e: ln(2)/λ_e) is the actual time for half of the amount of activity to be removed from the organism [20].

EQUATION 2.N. TIME-INTEGRATED ACTIVITY

$$\tilde{A} = \int_0^\infty A_h(t)dt$$

The time-integrated activity $\tilde{A}$ (unit: Bq.s) is defined as the time integral of the activity ($A_h(t)$) (unit: MBq) in a source organ h as a function of time t (time-activity curve) [20, 37]. $\tilde{A}$ normalized to the injected activity *A0* is called the time-integrated activity coefficient (TIAC) [20, 37].

The Medical Internal Radiation Dose (MIRD) formalism established a model in which the internal absorbed dose can be assessed according to a combination of biokinetics and physical and geometrical properties of a source organ *h* and a target organ *k* (Eq. 2.O) [20, 37]. For describing the absorbed dose D_k in a target organ *k*, all contributions from all organs and tissues need to be considered.

EQUATION 2.O. ABSORBED DOSE

$$D_k = \sum_h \tilde{A}_h \, S_{(k \leftarrow h)}$$

$\tilde{A}_h$ is the time-integrated activity, $S_{(k \leftarrow h)}$ is the S-value or absorbed dose rate per unit activity (Gy/Bq/s), *k* represents a target location and h a source location (possible application for multiple sources) [20, 37].

EQUATION 2.P. S-VALUE DEFINITION

$$S(k \leftarrow h) = \sum_i n_i \, E_i \, \phi_i(k \leftarrow h) \, / m$$

The S-values formalism (Eq. 2.P) represents the mean absorbed dose rate per activity. *ni* represents the number of transitions with energy *Ei* emitted per nuclear transition; *Ei* is the energy per transition *i* (unit: MeV); ϕi represents the fraction of energy absorbed in the target; m is the mass of the target region (unit: kg); *k* is proportionality constant (unit: Gy.kg/MBq/s/MeV). Considering radioactive decay, the sum has to be taken over all transitions *i* [20, 37].

The Radiation Dose Assessment Resource – RADAR also introduced a system for internal dose calculations based on the MIRD formalism [20], which is mathematically equivalent to the S-value equation from MIRD formalism [20, 38, 39]. RADAR published the OLINDA/EXM personal computer software for absorbed dose calculations with different input settings including several radionuclides, of simulators for adults, children, pregnant women, organs, and tissues [20, 38, 39].

2.8. Radiation Risk

2.8.1. Biological Effects of Radiation

The biologic effects of radiation are classified into two types, deterministic (short-term) and stochastic (long-term). The important deterministic effects (a significant number of damaged cells) occur in high levels of radiation exposure, has a threshold value of radiation quantity to set in and, it takes a short period (days) to manifest in the organism (tissue pathology) [16, 17]. In contrast, the stochastic effect has no defined threshold level of radiation exposure. Therefore, the occurrence of stochastic effects is random [16, 17, 35]. In addition, stochastic effects (somatic cells) can take decades to manifest in the organism and, for this reason, is very difficult to be detected [16, 17, 35]. In order to improve the accuracy of the radiation-related stochastic effect estimation, epidemiologic studies comparing exposure to non-exposure populations have been performed for many years [35]. However, there are still no sufficient epidemiologic data to determine precisely a threshold for stochastic effects mainly for electron and photon radiation [16, 17, 35].

In the range of low doses, the role of internal dosimetry in diagnostic nuclear medicine is essential to provide the basis for quantification of the stochastic radiation risk. Once this risk is quantified, it can be used to optimize the amount of administered activity maximizing image quality while minimizing patient risk. This optimization process is of particular importance for pediatric patients since children are three times more sensitive to radiation in comparison to adults [2, 5, 6, 8, 35, 40], owing to their enhanced organ radiosensitivity and years over which stochastic effects may become manifest [2, 9, 35].

The correlation between radiation exposure in low doses and biological effects may depend on factors as absorbed dose, exposure time, latency time after the exposure to occur an effect [2, 8, 16, 35]. Figure 2.4 illustrates the linear extrapolation model based on lifespan studies. Considering low doses, it is assumed that there is no threshold dose value for biological effects; however, the “low dose region” presents some sources of uncertainties [16,

35]. The complexity of estimating effects resulting from radiation exposure is related to the difficulty to provide data in the low-dose region as denoted by the circle in Fig. 2.4 [16, 35].

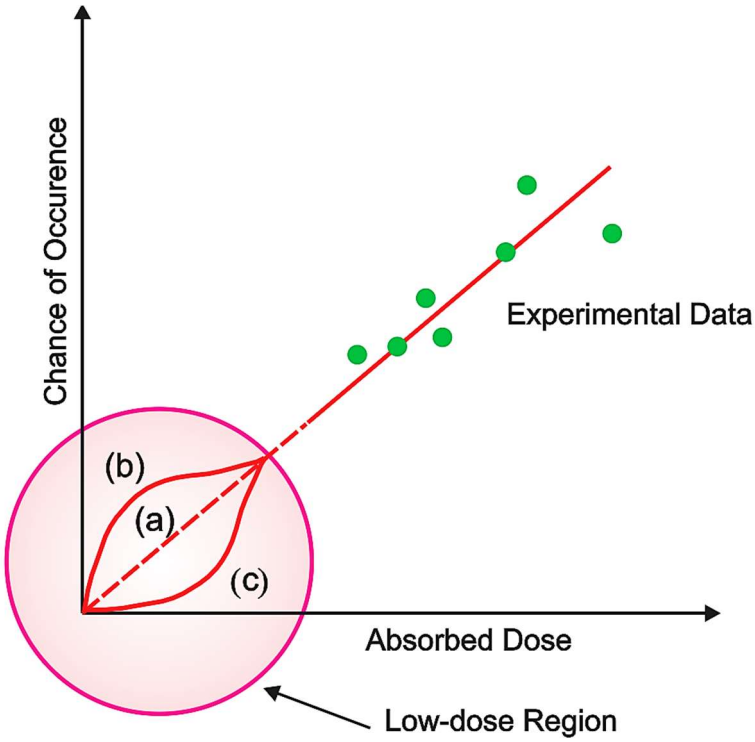

FIGURE 2.4. Linear extrapolation model [16, 35, 41]. **a:** correlation of dose-biologic effect. **b:** not counted possible factors that increase the probability of occurrence of effects in low doses. **c:** unknown thresholds or factors which reduce the incidence of effects. Experimental data: data of lifespan studies on atomic bomb survivors. The authors of citation [16] permitted the edition and incorporation of this figure. Original available on https://inis.iaea.org/collection/NCLCollectionStore/_Public/45/073/45073465.pdf

Based on a cohort of atomic bomb survivors, the study of Ozasa et al. [41] showed that the risk of higher mortality caused by late effects of radiation exposure is increased during lifespan [15, 35, 41]. The rates of cancer deaths increased in proportion to age and dose of radiation [15, 41]. In this cohort, the individuals who were exposed at younger ages presented a higher risk for different cancer sites [15, 41]. In contrast, the risk decreases for those who were exposed at older ages [15, 41-43].

Due to the young age, pediatric patients could potentially be classified as a group with a higher probability of developing late radiation effects compared to adults [8]. Therefore, exposure to ionizing radiation at young ages will, most likely, increase the cancer risk [44]. Furthermore, the radiation risk in children, especially the small ones (newborns and toddlers) can be related not only to their long lifespan but also to the higher radiosensitivity [35]. The immunologic system is responsible for detecting defective cells, for repairing them or for eliminating them. Small children have an immature immunologic system [45] and, for this reason, this fact may represent a minor risk associated with defective cell no detected or mis-repaired (mutation)[35]. Albeit, the stochastic nature of cancer make it a complex disease that depends on multiple factors to arise such as age, gender, genetic predisposition, lifestyle and, it can take a few years (examples: leukemia, thyroid, kidney cancer) or decades to develop (examples: colon, liver cancer) [5, 8, 33].

2.8.2. Quantifying the radiation risk

The *overall population risk* consists of the risk of the occurrence of cancer diseases which everyone partakes of (Fig. 2.5). Furthermore, the *lifetime attributable risk (LAR)* is, in the case of ionizing radiation, defined as the additional risk from radiation exposure during a lifetime. LAR is an important concept since it measures how much the radiation exposure contributes to increasing the risk for cancer diseases to happen, allowing more accurate dose optimizations for specific groups in order to decrease and/or to keep it low [35, 46].

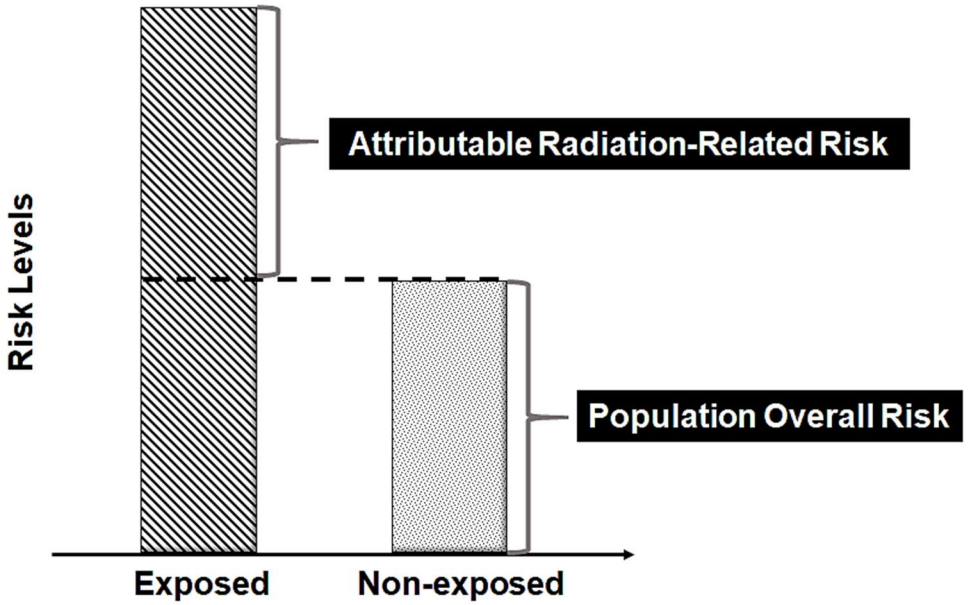

FIGURE 2.5. Lifetime attributable risk (LAR) baseline for cancer diseases. Figure reproduced based on information present in the citation [35].

The attributable risk is also named as e*xcess risk (ER)* that represents the risk attributed to radiation exposure only (Fig. 2.5) [35, 46]. It is important to highlight that radiation exposure can increase the risk of stochastic effects. However, this does not mean that they will occur since some individuals exposed to, e.g., to environmental carcinogens might develop cancer and some others might not; the same can be considered for the non-exposed individuals (Table 2.3) [35].

Basically, ER can be estimated by the difference between the cancer incidence upon the group of exposed and non-exposed individuals (Eq. 2Q). The rate of *occurrence* and *non-occurrence* of cancer in each group is represented by the variables: ***a*** (occurrence) and ***b*** (non-occurrence) for the exposed group; ***c*** (occurrence) and ***d*** (non-occurrence) for the non-exposed group (Table 2.3) [35].

EQUATION 2.Q. EXCESS RISK

$$ER = a/(a+b) - c/(c+d)$$

TABLE 2.3. Excess Risk (ER) and respective variables.

ER = Disease Incidence of Exposed Group ─ Disease Incidence of Non-exposed Group

Group	Occurrence	Nonoccurrence	Total
Exposed	A	b	a+b
Non-Exposed	C	d	c+d

Table reproduced based on information present in the citation [35]

ER can be used to assess the proportion of the risk incidence as percentage risk (chances in 100,000 persons) of cancer development and/or death by an individual specifically related to radiation exposure; by means of the ratio between ER and the cancer incidence among the exposed group (Eq. 2.R) [35, 46]. Based on the data of the Gonzalez et al. study [46], the cancer risk arising from the ionizing radiation remains elevated for a person even 50 years after exposure.

EQUATION 2.R. EXCESS RISK PERCENT

$$\boldsymbol{ER}\% = \frac{a/(a+b) - c/(c+d)}{a/(a+b)} \cdot 100$$

3. MATERIALS AND METHODS

3.1. Experiments - Retrospective Image Quantification

As specific data on dosimetry for children for many radiopharmaceuticals are missing, ^{99m}Tc-MAG3, one of the most commonly used compounds in pediatric nuclear medicine, was chosen for evaluating the biokinetics, dosimetry, and associated cancer risk. As a calibration (more specifically: an attenuation correction) had not been performed in the clinical setting, a retrospective calibration of the gamma camera had to be performed to enable an assessment of patient-specific organ activities for further estimation of the organ doses.

The calibration measurements were performed on the same gamma camera that had previously been used for patient acquisitions (e.cam Single, Siemens Healthcare) [15, 47]. The goal was to derive a calibration factor for planar gamma camera acquisitions by considering the sizes and depths of the individual patient kidneys (Table A1). For this purpose, two one-compartment manufacturered kidney phantoms were used. They had previously been designed according to MIRD pamphlet 19 [48] and fabricated with a 3D printer as described by Tran-Gia et al. [47] to simulate different kidney sizes (newborn: 8.6 ml; 1-year-old: 23.4 ml) (Fig. 3.1). For imaging, both kidneys were filled with ^{99m}Tc solution (newborn: 1.10 MBq/ml; 1-year-old: 0.98 MBq/ml) [15]. The phantoms were mounted in a body phantom (NEMA-NU2-2012, PTW-Freiburg) using a dedicated, 3D-printed and depth-adjustable attachment system which is also presented in [15, 47] (Fig. 3.2). To simulate different kidney depths inside a patient acquisitions were repeated with the kidney inserts mounted at variable positions inside the body phantom (distances of 8.2 cm, 11.7 cm, and 15.2 cm from the patient bed) [15].

FIGURE 3.1. 3D-Printed 1-year-old and newborn kidney phantoms [15].

After filling the remaining compartment of the phantom with water (Fig. 3.2), static planar images (duration: 600 s) were acquired for each depth position and phantom (Fig. 3.3) [15]. Besides the acquisitions of the kidney phantom placed inside the water-filled torso phantom, an additional acquisition was performed with the kidney phantom placed directly on the patient bed (Fig. 3.4) to simulate a depth of 0 cm (i.e., approximately zero attenuation) [15].

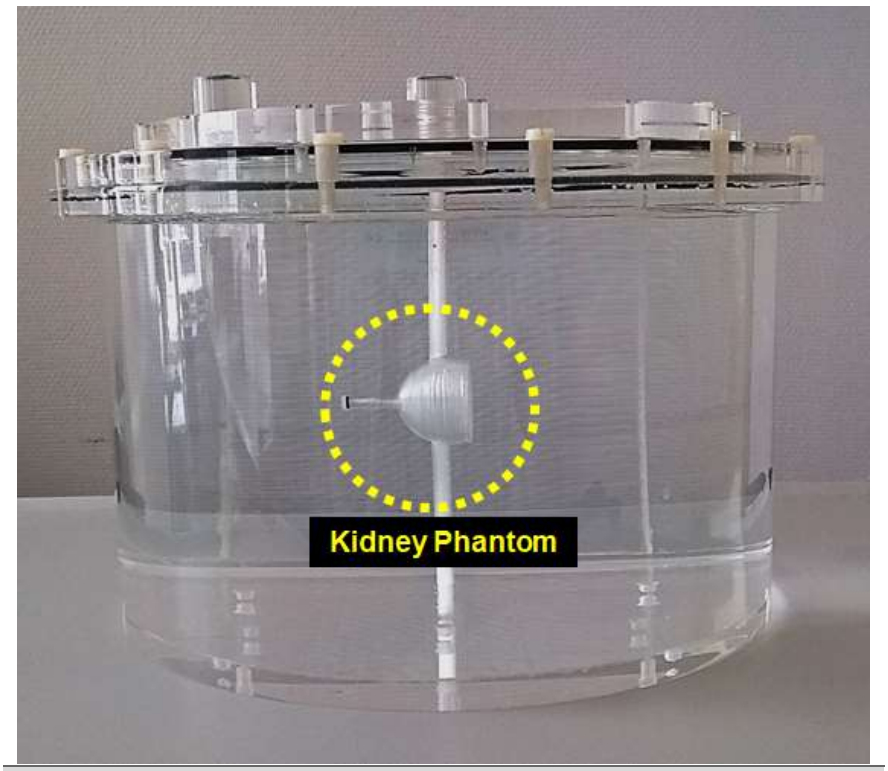

FIGURE 3.2. Phantom experiment. In this setup, kidney insert (newborn) is centrally mounted in the torso phantom [15].

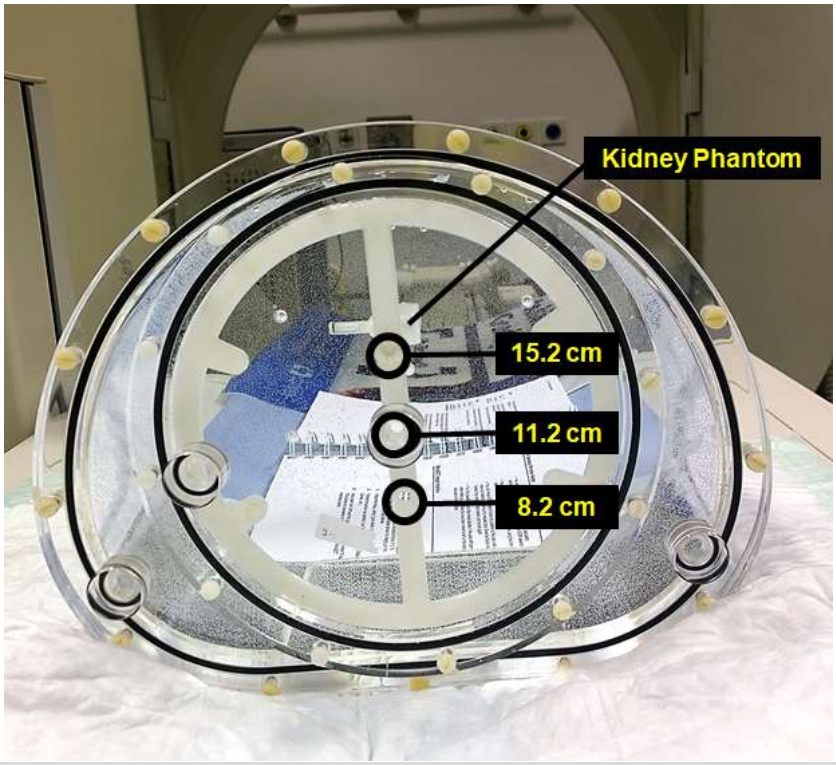

FIGURE 3.3. Phantom experiment. In this setup, the kidney insert is mounted in the highest position of the manufactured attachment system with three different depth positions 8.2 cm, 11.7 cm, and 15.2 cm [15].

FIGURE 3.4. Phantom experiment. Kidney phantom placed directly on the gamma camera bed (depth position: 0 cm).

All post-processing was performed with vendor-specific software (e.soft, Siemens Healthcare). For each measurement, regions-of-interest (ROIs) were drawn around the phantom insert and in the background (Fig. 3.5) [15].

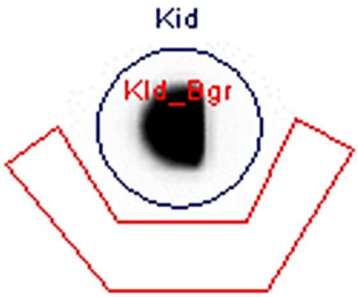

FIGURE 3.5. Post-processing. Exemplary ROI positioning for the kidney phantom (1 y) placed directly on the bed ("Kid": dark blue) and the background ("Kid_Bgr": red) [15].

Before any further calculations, the background subtraction was performed to correct for background activity, noise, and scatter from areas above and below the volume of interest. As the background and phantom ROIs were different in size ($Area_{Pha} \neq Area_{Bgr}$), a ROI normalization had to be applied to the counts in the background ROI ($Counts_{Bgr}$) [15]:

EQUATION 3.A. ROI NORMALIZATION

$$Counts_{Bgr \rightarrow Phantom}(d) = Counts_{Bgr}(d) \cdot \frac{Area_{Phantom}}{Area_{Bgr}}$$

Here, the parameter *d* represents the depth of the phantom (distance kidney ↔ patient bed). Based on the background counts normalized to the size of the phantom ($Counts_{Bgr \rightarrow Phantom}$), a depth-dependent calibration factor cf_{volume} (unit: cps/MBq or counts-per-second-per-MBq) [15] was calculated as:

EQUATION 3.B. DEPTH-DEPENDENT CALIBRATION FACTOR

$$cf_{volume}(d) = \frac{Counts_{Phantom}\,(d) - Counts_{Bgr \rightarrow Phant}\quad (d)}{Activity * \Delta t}$$

Here, *Activity* represents the decay-corrected activity, and Δt stands for the total acquisition duration.

Next, the depth-dependent calibration factors $cf_{volume}(d)$ were divided by the calibration factor at depth zero $cf_{volume}(d_0)$ to obtain a unitless attenuation factor for a kidney-shaped organ of either age group (newborns and 1-year-old) [15]:

EQUATION 3.C. ATTENUATION CORRECTION FACTOR

$$Attenuation\ Correction\ Factor_{volume}\ (d) = \frac{cf_{volume}(d)}{cf_{volume}(d_0 = 0\ cm)}$$

The depth-dependent attenuation correction function was approximated by a second-degree polynomial curve (y= ax^2+bx+c) [15]. It was separately fitted to the newborn and the 1-year-old data to enable an age- and depth-dependent attenuation correction for each patient [15].

3.2. Patient Demographics

To overcome the lack of data on diagnostic procedures in pediatric nuclear medicine (PEDNM) and, if necessary, establish improvements, demographic information was obtained in a retrospective evaluation of patient data. The following two points were analyzed:

- The frequency of pediatric nuclear medicine exams.
- Administered activities and effective dose levels.

Data were collected directly from the database of the Department of Nuclear Medicine of the University Hospital of Würzburg (Klinik und Poliklinik für Nuklearmedizin, Universitätsklinikum Würzburg - UKW). The gathered information included exam type, date of exam, age (months or years), weight (kg), height (cm), gender (male or female) and amount of injected activity (MBq). Diagnostic procedures with higher relevance were ^{18}F-FDG whole body PET/CT scans, ^{99m}Tc-DMSA renal scintigraphy scans and ^{99m}Tc-MAG3 renal scintigraphy scans, which were selected for a detailed analysis of the patients' biokinetics and dosimetry (database: 2012 to 2017) (Fig. 3.6).

The results of the evaluation of the administered activities and dose levels were compared to national and international recommendations. National recommendations were based on the German Federal Office for Radiation Protection (Bundesamt für Strahlenschutz – BfS) [BfS2012] [49]. International recommendations were based on the European Association of Nuclear Medicine (EANM) (EANM 2008 Dosage Card [EANM2008]), EANM/SNMMI 2014 Harmonization Document [EANM2014]) [11, 12] and the American Society of Nuclear Medicine and Molecular Imaging (SNMMI) (North America Consensus Guideline [NACG]) [50].

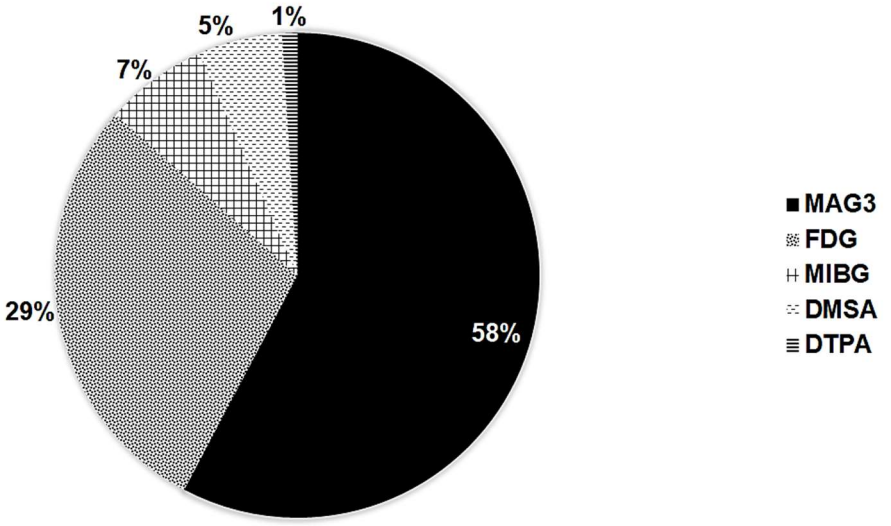

FIGURE 3.6. Pie chart of the main pediatric nuclear medicine scans performed at UKW between 2012 and 2015. ^{18}F-FDG PET/CT: 143 Scans (Age range: 2-17 y); ^{99m}Tc-MAG3: 287 scans (Age range: 0-17 y); ^{99m}Tc-DMSA: 28 scans (Age range: 0-17 y); ^{123}I-MIBG and ^{131}I-MIBG: 34 Scans (Age range: 2-17 y); ^{99m}Tc-DTPA: 5 scans (Age range: 0-17 y). Data source: UKW database from 2012 to 2015.

For the dosimetry and risk analysis data from 20 consecutive patients were analyzed. The preparation of the patients (including oral hydration with 10 ml/kg or by breastfeeding 30 min before injection) was performed according to the EANM guidelines for standard and diuretic renograms in children [9]. Furosemide (1 mg/kg in infants, 0.5 mg/kg in children above the age of 1 y) was injected intravenously following an F+20 protocol (diuretic is injected about 20 min after the radiopharmaceutical) in all but two patients who showed almost complete tracer excretion 20 min after ^{99m}Tc-MAG3 administration [9]. For a radiation-related absorbed dose and risk analysis, the patients were separated into two groups based on their age: 27 newborns (1.6-12.0 months) and four 1-year-olds (13.0-20.0 months) [15]. As this retrospective analysis only included data acquired within the clinical routine, our local ethics committee waived the need for further approval [15].

At our institution, ^{99m}Tc-MAG3 scans are typically performed on a single-head gamma camera (E.Cam Signature, Siemens Healthcare) equipped with a low-energy high-resolution (LEHR) collimator. The injected activities are patient-specifically calculated based on the Pediatric Dosage Card 2014 of the EANM [11, 12]. The acquisition protocol is a planar dynamic acquisition of 132 images centered on the patients' kidneys, started at the bolus injection, and lasting 35 min [9]. The dynamic data are distributed in the following three phases (described in Figure 3.7) [9]:

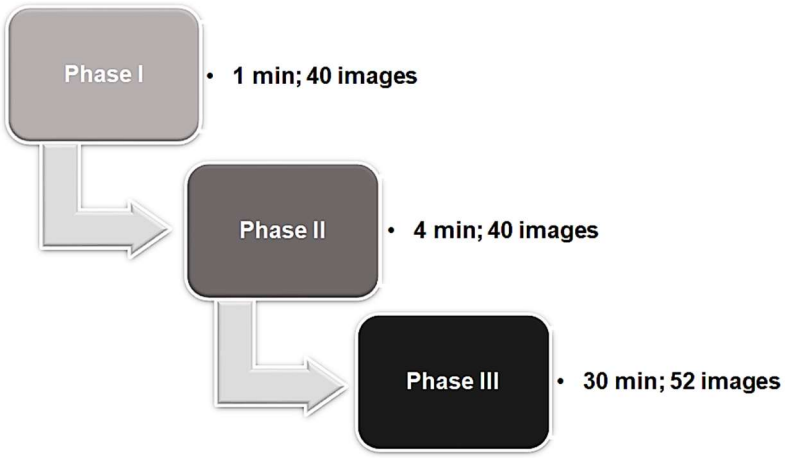

FIGURE 3.7. Organigram of the dynamic ^{99m}Tc-MAG3 scans' protocol showing the information of time duration and number of images classified by time.

Among the 34 ^{99m}Tc-MAG3 patients there were 20 with *normal renal function - NRF* (with good wash-out [Fig. 3.8: Patient P04]) and 14 patients *with abnormal renal function - ARF* (with *unilateral abnormal renal function - UARF* and *bilateral abnormal renal function - BARF* [Fig. 3.8: Patient P23 and Patient P30]). Referral criteria for ^{99m}Tc-MAG3 scintigraphy included sonographic suspicion of either urinary tract dilation or obstructive uropathy [15].

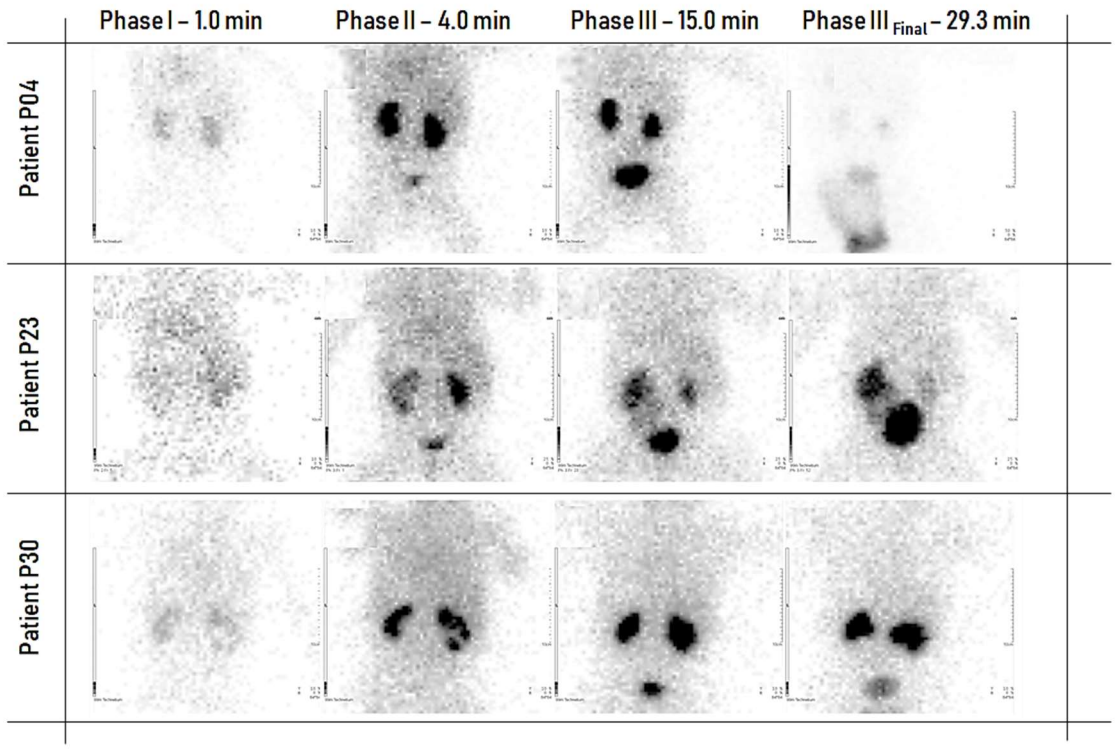

FIGURE 3.8. Examples of pediatric ^{99m}Tc-MAG3 scintigraphy. **Patient P04:** 4.0-month-old male with normal renal function (NFR). **Patient P23:** 1.5-month-old male with unilateral abnormal renal function (UARF). **Patient P30:** 5.0-month-old male with bilateral abnormal renal function (BARF). **Phase I:** blood flow, 1 min after the bolus injection. **Phase II:** clearance and uptake (4 min). **Phase III:** uptake and excretion (15 min). **Phase III$_{Final}$:** final stage of voiding (~30 min).

Phase I (Fig. 3.7: Patients P04, P23, and P30): Blood flow (pre-renal) stage after the injection of the activity in the patient body [9].

Phase II (Fig. 3.7: Patients P04, P23, and P30) and *Phase III* (Fig. 3.7: Patients P04, P23, and P30): Stages of renal uptake, kidney excretion, and bladder voiding [9].

The individual sizes and depths of each patient's organs were taken from ultrasound data previously acquired on the UKW system database (provided by M. Lassmann). Besides the reports of the nuclear medicine physicians, we retrospectively collected information directly from the ^{99m}Tc-MAG3 scans images. We analyzed the patients' renal function using the organ-specific time-activity curves, the maximum uptake time point (T_{max}), and the kidney excretion [15].

3.3. Biokinetics

One of the prerequisites for patient-specific dosimetry is the quantification of the individual organ activities as a function of time after radiopharmaceutical administration. This time-activity curve is subsequently integrated for obtaining the TIAC (see chapter 2.7). For obtaining time-activity curves for the considered patients, an ROI analysis was performed for the 34 patients undergoing the ^{99m} TC-MAG3 scans. This analysis consists of drawn ROIs around the kidneys (LK: Left kidney and RK: Right kidney) and the bladder (BL), with an additional ROI placed beside each organ to estimate the background (Fig. 3.9). Additionally, a whole body (WB) ROI was drawn covering the entire field-of-view. After background-correction (subtraction of the counts in the background ROI normalized to the area of the organ ROI as described by Eq. 3.A, the results were the background-corrected counts in the ROI as a function of time in all examined organs.

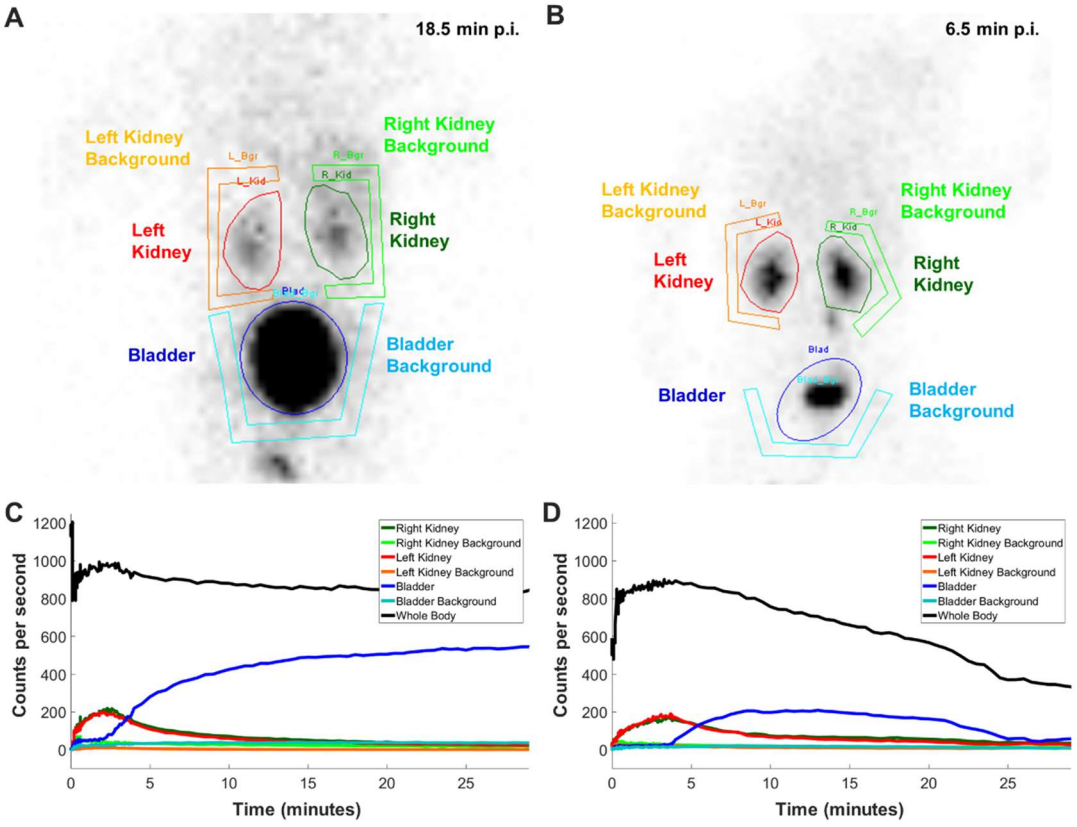

FIGURE 3.9. ROI analysis of patients P20 (left, 20-month-old female) and P10 (right, 5-month-old female). A-B: ROIs and background in kidneys (red: left kidney, green: right kidney) and bladder (blue) for multiple time points. The whole body ROI covers the entire field-of-view and is not depicted. C-D: number of counts as a function of time for all ROIs [15].

The conversion from counts to activity was performed based on pre-determined ultrasound-based patient data (kidney and bladder volumes, kidney depth). First, the patients' kidney-depth data (Table A1) was inserted into both attenuation correction functions to obtain depth-corrected attenuation factors for newborn and 1-year-old volumes (Table A1) [15].

Subsequently, the calibration factor for the patient-specific kidney volume was linearly interpolated based on these volume-cf pairs. Finally, kidney time-activity curves (TAC) were obtained by dividing the number of counts in each temporal frame by the resulting attenuation correction factor and the acquisition time [15].

The bladder TAC was determined similarly, with the exception that no depth could be extracted from the ultrasound data. Instead, a depth of 5 cm was used for all bladders. The assumption that the kidney geometry is comparable to the approximately spherical geometry of the bladder is based on a study by Tran-Gia et al. [47], in which only a negligible difference between the MIRD-based kidneys and a spherical model of similar volume was observed [15].

The whole body time-activity curves (TAC) were obtained under the assumption that the total number of counts corresponded to the total administered activity. This assumption typically holds for pediatric patients, as a large part of the body is included in the camera field-of-view. The coverage sufficiently represents the normalized whole body biokinetics. The patient-specific time-integrated activity coefficients (TIAC) were obtained by time integration of the organ-specific time-activity curves (TAC) for kidneys, bladder, and whole body. During the renal scans (described in chapter 3.2 Patient Demographics), 132 images were acquired starting at the bolus injection over a period of 35 min [9].

While the organ-specific time-activity curves were integrated up to the last time point for each patient, only physical decay was assumed after the last time point. A combination of a sum of trapezoidal integrations (Eq. 3.D) for time-points t_2 and t_1 (data points a_1 [t_1] and a_2[t_2]) before the curve maximum and a bi-exponential function after the T_{max} (Eq. 3.E) was applied for all time-activity curves [15].

EQUATION 3.D. TRAPEZOIDAL INTEGRAL

$$TIAC_{12} = \frac{a_1+a_2}{2} \cdot (t_2 - t_1)$$

While the bi-exponential functions were fitted in OriginPro 2016 (ADDITIVE GmbH), integrals were calculated using Microsoft Office 365 Excel version 2016 (Microsoft Corporation).

EQUATION 3.E. BI-EXPONENTIAL FIT FUNCTION

$$A_h(t) = a_1 \cdot e^{-(\lambda_{b1}+\lambda_{phys})\cdot t} + a_2 \cdot e^{-(\lambda_{b2}+\lambda_{phys})\cdot t}$$

In some cases of patients with severe renal abnormal function, very late uptake and points in which the configuration was not suitable for a fitting curve, only the trapezoidal method was applied for TIAC estimation [15].

3.4. Dosimetry

3.4.1. Absorbed Doses

The absorbed dose coefficients (mGy/MBq) were estimated using the software OLINDA/EXM that is based on pre-determined absorbed dose coefficients Monte-Carlo simulated absorbed dose coefficients for a set of numerical phantoms. Available phantoms are adult (73.7 kg), 15-year-old (56.8 kg), 10-year-old (33.2 kg), 5-year-old (19.8 kg), 1-year-old (9.72 kg), and newborn (3.60 kg). These phantoms were designed by Cristy and Eckerman in the 1980s. 3, 6 and 9-month pregnancy phantoms were added by Stabin et al. in 1995 [38, 51].

The absorbed dose coefficients (mGy/MBq) were estimated by entering the patient-specific TIAC values as input into the OLINDA/EXM software [38]. The output was the organ absorbed dose coefficients (mGy/MBq) for the newborn and the 1-year-old numerical phantoms [38].

The organ absorbed doses (mGy) were calculated by weight-based linear interpolation of the absorbed dose coefficient values of the numerical phantom weights (newborn: 3.60 kg; 1-year-old: 9.72 kg) [38]. The coefficient was multiplied by the patient-specific administered activity (MBq). It is important to emphasize that the absorbed doses (mGy) were calculated only for the ^{99m}Tc-MAG3 patients as these data were used for the subsequent risk estimation.

3.4.2. Effective Doses

3.4.2.1. Effective Doses Estimation for the NM Procedures

For standardizing the results, the patients' age- and weight-dependent effective doses were derived from the corresponding ICRP effective dose coefficient tables [52, 53].

The effective dose coefficients (mSv/MBq) as function of the phantom weight (1-year-old: 10 kg; 5-years-old: 19 kg; 10-years-old: 32 kg; 15-years-old: 56 kg, and adult: 73 kg [38]), were approximated by a power curve ($y=ax^b$), which was separately fitted for each compound. Here, x represents the patient-specific weight (kg). Subsequently, the patient-specific effective dose (mSv) was assessed by multiplying the results of the fitted function from each compound by the respective procedure's patient-specific administered activity (MBq).

3.4.2.2. Administered Activity Weight-Based Formalism

The *Baseline Activity* and *Multiple* values for ^{18}F (FDG), and ^{99m}Tc (MAG3 and DMSA) radiotracers were published in previous studies [10, 11]. Consequentially, the administered activity (MBq) values for these compounds are, in a clinical setting, calculated (Eq. 3.F) based on the EANM Pediatric Dosage Card formalism [10, 11, 43]. However, for ^{68}Ga-labeled compounds, there were no available standard values to calculate the administered activities [10, 11, 27]. Therefore, based on the concept of keeping the effective dose constant for a pediatric population (as introduced by the EANM dosage card), a study was undertaken for determining weight-dependent activities for ^{68}Ga-labeled compounds. Consequently, the weight-independent effective dose model proposed by the EANM Pediatric Dosage Card [10] was applied, in order to suggest the ^{68}Ga baseline Activity value and corresponding biokinetics class for calculating the administered activities [27]. To do so previously published weight-based effective dose coefficients (mSv/MBq) were rescaled according to the formalism described by Jacobs et al. [10, 43] applying available data on biokinetics (Table A.4) and assuming weight-independent count rates. Thus, we obtained the normalization factor “a” of effective dose and the corresponding coefficient of determination R^2 for each dataset by comparing these values to those previously published by Jacobs et al. [36]. In this way, the radiopharmaceutical class of ^{68}Ga-labeled peptides (“multiples”) was determined. The baseline activity factor for ^{68}Ga was based on an upper limit of the administered activity of 185 MBq for an adult [27, 36]. When combining the baseline activity value and the ^{68}Ga-labeled peptides class information, the recommended administered activity for pediatric diagnostic exams is calculated by using EANM Dosage Card and the corresponding weight-dependent multiples (Equation 3.F) [12, 27, 36]:

EQUATION 3.F. EANM FORMALISM

$$A_{administered}[MBq] = Baseline\ Activity \cdot Multiple$$

3.4.2.3. Effective doses estimation for ^{99m}Tc-MAG3 Pediatric Patients

The method to estimate the effective dose coefficients (mSv/MBq) for ^{99m}Tc-MAG3 renal patients was similar to the one for NM procedures described before. The difference lies in the *Effective Dose Factor* which was calculated individually for each patient. The effective dose coefficients (mSv/MBq) were estimated by means of the newborn and the 1-year-old mathematical phantom [38]. The effective doses (mSv) were calculated by using the effective dose coefficient values (mSv/MBq) approximated by a power curve ($y = ax^b$).

3.5. Radiation Risk

3.5.1. Risk Estimation

The risk estimation for pediatric patients was performed with the Radiation Risk Assessment Tool (RadRAT) (Fig. 3.10) [46]. This online platform (Fig. 3.10) is provided by the U.S. NCI - National Cancer Institute (Division of Cancer Epidemiology and Genetics) [46]. The RadRAT was developed based on risk models included in the 2006 report of the National Academies of Sciences' BEIR VII Committee regarding radiation health effects, named Health Risks from Exposure to Low Levels of Ionizing Radiation [46]. By utilizing the RadRAT, it is possible to perform estimations of radiation-related cancer induction risk by estimating the lifetime attributable risk (LAR).

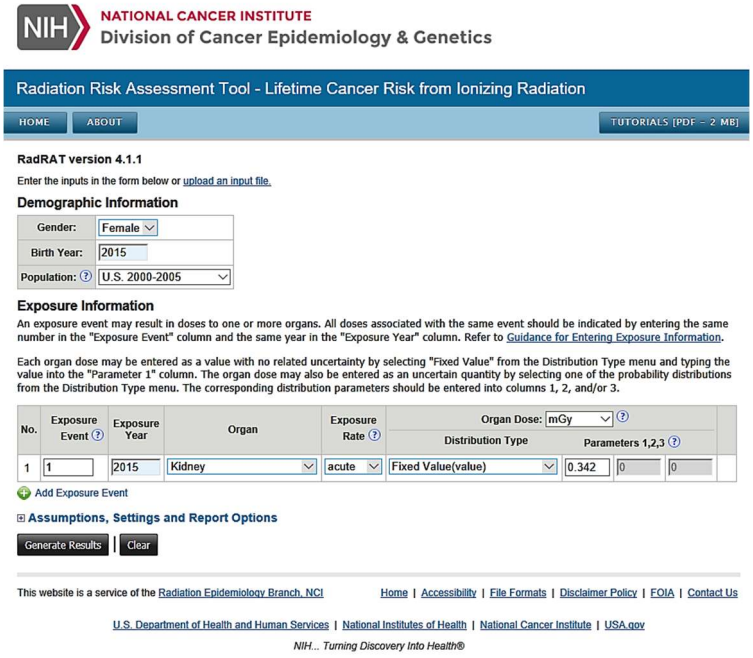

FIGURE 3.10. Screenshot of the Radiation Risk Assessment Tool (RadRAT) online platform. Need data input: Demographic information (Gender, Birth year, Population); Exposure information (Exposure event, Exposure year, Exposure rate, Organ dose, Distribution type and Parameters) [52]. Figure acquired as a screenshot of the Radiation Risk Assessment Tool (RadRAT) online platform: https://radiationcalculators.cancer.gov/radrat/model/inputs/

The tool enables predicting the effect of low-level ionizing radiation (absorbed doses <100 mGy) for individuals based on their age, gender, year of exposure, uniform and/or non-uniform dose and organ-specific absorbed dose [15, 46, 54].

RadRAT is an interactive software which enables a user-specified history of exposures for several organs [46]. Besides the excess risk, RadRAT also performs a future risk projection for cancer occurrence, defined as the risk estimated for an individual from the present time until the end of the expected lifetime [46]. The risk projections by RadRAT were calculated individually for the 34 ^{99m}Tc-MAG3 pediatric patients. The following Table 3.1 shows the entered data used to run the risk estimation for our patients:

TABLE 3.1. Input patient data and defined tool settings utilized to execute the risk estimation on the RadRAT online platform.

Input data	Patient-specific Information	RadRAT Settings [46]
Demographic Information	▪ Gender ▪ Age	▪ Population group (U.S. 2000-2005)
Exposure Information	▪ Exposure year ▪ Organ-specific absorbed doses (mGy)	▪ Exposure rate (acute) ▪ Dose distribution type (fixed value)
Exposed Organs	▪ Brain, ▪ Breast (female) ▪ Colon ▪ Gallbladder ▪ Kidneys ▪ Liver ▪ Lungs ▪ Ovaries (female) ▪ Pancreas ▪ Red bone marrow ▪ Stomach ▪ Thyroid ▪ Urinary bladder ▪ Uterus (female)	

The resulting output is given as "*excess lifetime risk (ELR)*" and "*excess future risk (EFR)*" (chance in 100,000 persons).

Despite a high uncertainty in the individual risk estimation (90%), this information might assist in the establishment of more accurate recommendations for this high-risk group of pediatric patients for keeping the balance between sufficient image quality at the lowest-possible patient radiation exposure [15, 46].

3.5.2. Radiation Risk Analysis

A *Radiation Risk Analysis (RRA)* was performed based on the method of *deductive reasoning* (Fig. 3.11) utilized for categorizing and analyzing information associated with patient-specific radiation-related risk. RRA was set based on the causality concept (cause-effect). The "causes" were classified as *independent variables* (*Patient, Exposure).* The "effects" or factors that could be affected by the "cause" were defined as *dependent variables* (*Risk).*

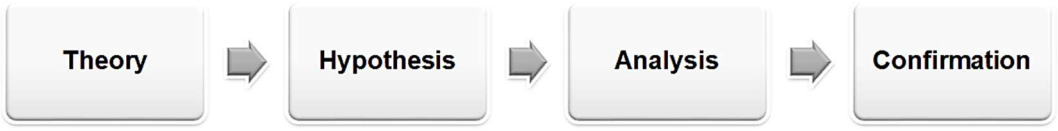

FIGURE 3.11. Deductive reasoning basic structure.

In general, the critical risk factors related to the somatic stochastic effects to be considered are [35, 54, 55]:

- Age at exposure
- Gender
- Exposed volume
- Dose
- Organ /Tissue
- Host susceptibility (immunodeficiency, genetic predisposition, etc.)
- Individual biological factors (e.g., tissue's rate of cell division)

Among the elements of influence previously cited, only a few were chosen to perform several statistic comparisons in the RRA. The choice was based on their importance and on data that were measurable: *Age at exposure* is a fundamental factor since the studied group has a specific age range besides the long lifespan that may increase the risk [35, 55]. *Organ/Tissue* is an essential factor since there are different organs/tissues with higher or lower radiosensitivity [5, 35, 55].

The *absorbed dose* is a crucial factor in assessing the individual/group risk, as, theoretically, at low levels of radiation, the risk increases or decreases with the absorbed dose [35, 55]. *Gender* must be considered because of the gender-specific changes of radiosensitivity and organs-at-risk [35, 55].

According to this classification, the results of the patient demography survey, biokinetics, dosimetry, and risk calculations were applied as *crucial data* to the RRA as depicted in Figure 3.12. Furthermore, these data were converted to *attributes* which were categorized according to the suitable variable (patient, exposure, and risk). The primary purpose of the attributes is to provide "straightforward answers" to the maximum number of possibilities that could be related to increasing or decreasing the patient risk (based on the studied patient group). The attributes were composed of several "*non-mutual factors*" which represented the straightforward answers (Fig. 3.12). Consequentially, the attributes were compared to each other to observe which of them presented a higher influence on patient risk. In addition, statistical significance testing was performed on the attributes and respective "non-mutual factors."

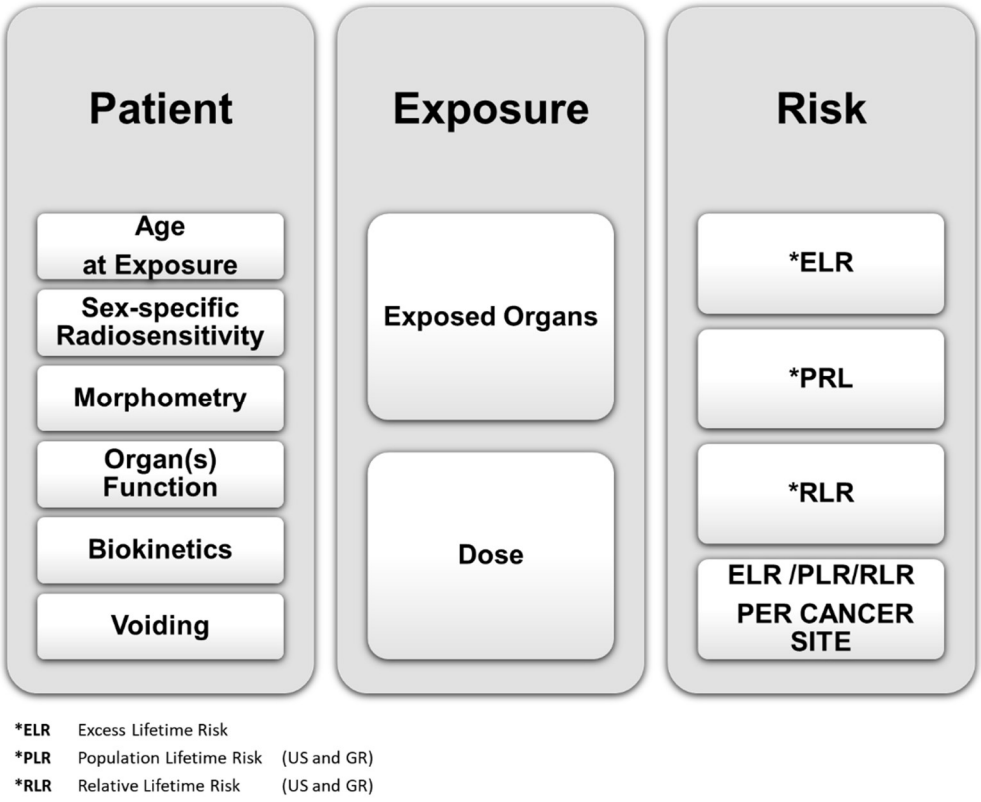

FIGURE 3.12. The basic structure of the Radiation Risk Analysis correlation between the three variables Patient, Radiation Exposure and, Radiation Risk as well as the related attributes. The reference population used for comparing the lifetime risk values were from the United States of America (US) and Germany (GR).

At present, not much data are available on dosimetry in pediatric populations [14]. For this reason, as a standard reference, the biokinetics and dosimetry data of ^{99m}Tc-MAG3 published in ICRP 128 were used [18]. In order to obtain the risk values for the standard reference persons, we performed a dose calculation based on the absorbed dose coefficients (mGy/MBq) and the phantom data (adult: 73 kg; 1-year-old: 10 kg) as provided by the ICRP [7, 18]. The administered activity was estimated by using the EANM Dosage Card [12] and the phantom weights (Eq. 3F). The resulting doses (mGy) were entered into the RadRAT tool for performing the corresponding risk estimation. For the sake of comparison, the risk was estimated for the same list of 11 exposed organs for male and female patients (sub-chapter: 3.5.1 Risk Estimation), except for the gender-specific organs of females.

In addition to the patient-specific lifetime risk, data of the overall *Population Lifetime Risk (PLR*) was gathered for comparison purposes. PLR consist of the lifespan risk for developing cancer diseases that all individuals are exposed to. The percentage risk for males and females of the German and U.S. population was collected. The cancer risk information for the German population was taken from a Robert Koch Institute (RKI) publication (database: 2012) [56]. The cancer risk information for the North American population was collected from the US National Cancer Institute's Surveillance Epidemiology and End Results (SEER) of the American Cancer Society (database: 2010 to 2012) [15, 57].

In general, it was essential to understand the proportion that the estimated ELR represents in comparison to the general population; therefore, the *Relative Lifetime Risk (RLR)* was calculated, to evaluate the magnitude of the patient-specific ELR in relation to the overall population lifetime risk (PLR) (Eq. 3.G). Based on this, RLR can be described as the "relative" risk percentage resulted from the ratio between the PLR and ELR (Eq. 3.G).

EQUATION 3.G. RELATIVE LIFETIME RISK

$$RLR = \frac{PLR}{ELR} \cdot 100{,}000$$

3.6. Software

The main programs used for the calculations and analyses performed in this thesis are specified in Table 3.2:

TABLE 3.2. Software used in this work.

Software	Application	Specifications	Vendor/Developer
SyngoMI	Image post-processing Image	Siemens Healthcare. Version VA60C (2008)	Siemens Healthcare
OLINDA/EXM Organ Level Internal Dose Assessment [38]	Absorbed and effective dose coefficient calculations	Version (s) 1.1 (2007)	Vanderbilt University
OriginLab	TAC and TIAC curve-fitting Statistical tests Graphs	Version(s) 8.0 and 2016	OriginLab Corporation
Office 365	Calibration calculations TIAC Integrals calculations Absorbed and effective dose calculations Statistical calculations and tests Graphs, figures, and tables	Version(s) 2011 and 2016	Microsoft Corporation
RadRAT Online Risk Calculator [46]	Radiation-related risk projections	Version 4.1.1 (2015)	Division of Cancer Epidemiology and Genetics - National Cancer Institute

4. RESULTS AND DISCUSSION

This retrospective analysis in infants with *normal renal function (NRF)* and *abnormal renal function (ARF)* undergoing ^{99m}Tc-MAG3 is the first comprehensive analysis on biokinetics, dosimetry and radiation-related risk in a large group of patients.

All values in this section will be given as mean plus/minus one standard deviation (SD) except otherwise specified.

To allow a direct comparison to the published data given in ICRP Report 128 [18] and in Stabin et al. [13], we decided to use the Christy-Eckerman stylized phantoms provided by OLINDA/EXM for the analysis, as the effective doses provided by ICRP 128 are still calculated with the ICRP 60 tissue weighting factors [7]. Although new hybrid phantoms for pediatric patients have been developed by the University of Florida group and have been applied by Sgouros et al. in their study on DSMA absorbed doses [15, 58], we believe that, for a retrospective organ dose assessment as it is performed in this analysis in a limited number of source organs (kidneys [KD]: left kidney [KL] and right kidney [RK]; bladder [BL]; whole- body [WB]), the accuracy of the dose calculation with OLINDA/EXM is sufficient as basis for risk estimates [15].

4.1. Experiments - Retrospective Image Quantification

For retrospective image quantification, age-specific 3D-printed phantoms were manufactured, and calibration measurements were performed [15]. The depth- and size-dependent attenuation correction curves are shown in Figure 4.1. Separate second-degree polynomials were fitted separately for the newborn and the 1-year-old kidney [15]. Depth-dependent attenuation correction factors (Fig. 4.1) for the newborn phantom were 1.00 (0 cm), 2.21 (8.2 cm), 4.53 (11.7 cm), and 7.70 (15.2 cm); for the 1-year-old phantom, they were 1.00 (0 cm), 1.94 (8.2 cm), 3.68 (11.7 cm), and 5.98 (15.2 cm).

As expected, the attenuation increases with the distance (Figure 4.1). It can also be seen in Figure 4.1 that the attenuation is comparable for small depths < 5 cm (no difference for 0 cm) [15]. The attenuation of the newborn kidney phantom is higher than that of the 1-year-old phantom if the depth is increased (differences of 14% for 8.2 cm, 18% for 11.7 cm, and 22% for 15.2 cm) [15].

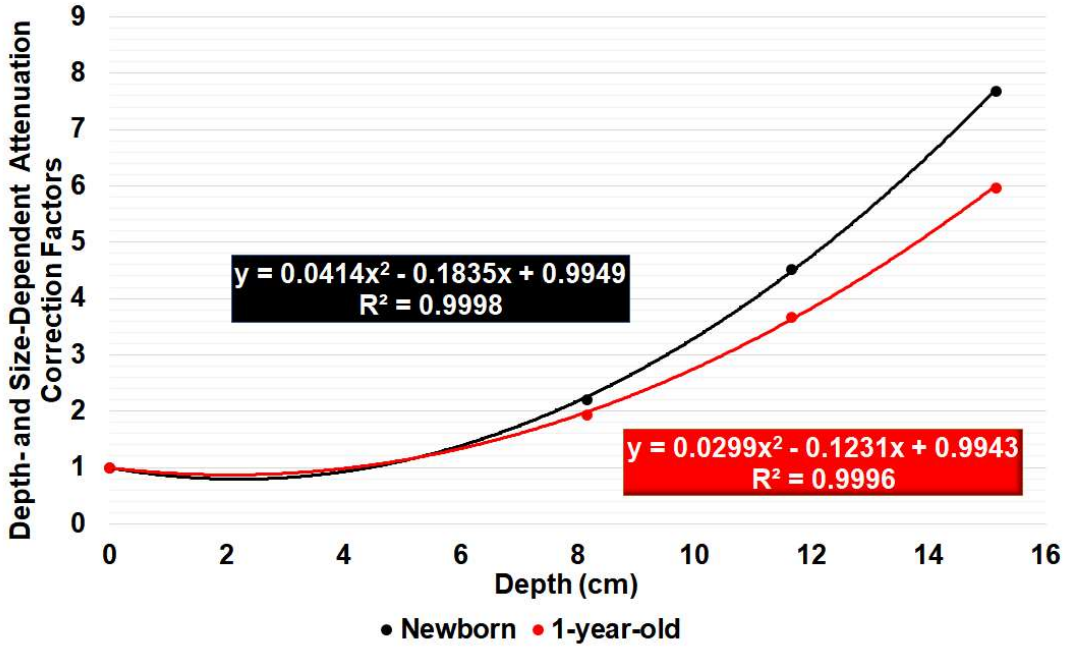

FIGURE 4.1. 3D-Printed 1-year-old and newborn kidney phantoms. Depth-dependent attenuation correction factors (absolute values) obtained in the phantom experiment (Eq. 3C). **Black:** newborn. **Red:**1-year-old.

The calibration of planar gamma camera scans based on the homogeneously filled kidney phantoms may represent a source of uncertainty, as it is only an approximation of the real kidney anatomy (cortex, medulla, and collecting system) which typically has inhomogeneous activity distributions. Despite these impairments, this method enables a way of retrospectively assessing the attenuation planar imaging exams, which can be applied for further estimations of biokinetics and other dosimetry applications.

4.2. Patient Demographics

The respective patients' radiation exposure and associated risks are obviously the main research subject. Therefore, data from pediatric patients scanned in our department were collected for the period between 2012 and 2017 in order to assess the frequency of exams, patients' information and exposure information.

In the period between 2012 and 2014, 88 exams of ^{18}F-FDG PET/CT were performed in 44 patients (14 males and 20 females; 21 aged between 4 months and 10 years; 23 between 11 years and 17 years). The administered activity ranged from 29 MBq to 345 MBq; the mean deviation of the administered activities (Fig. 4.2) from the values suggested by EANM2008 was –12.9%, 33.0% for NACG, 39.0% for EANM2014, and –11.4% for BfS2012.

A total of 242 renal scans were included (from 2012 to 2014), consisting of 216 ^{99m}Tc-MAG3 scans (177 patients; ages: 168 between 27 days and 10 years, 14 between 11 years and 17 years; gender: 106 males, 76 females) and 26 ^{99m}Tc-DMSA scans (24 patients). This analysis showed that most of the patients were very young, with a total of 129 patients younger than 2 years. The administered activities ranged from 11 MBq to 146 MBq; the mean deviation of the administered activities (Fig. 4.2) for ^{99m}Tc-MAG3 was –6.3% (EANM2008), 51.4% (NACG), –3.7% (EANM2014), and –16.6% (BfS2012). The corresponding values for ^{99m}Tc-DSMA were 24.0% (EANM2008), 7.0% (NACG) [50], and –3.2% (EANM2014). No values for ^{99m}Tc-DMSA are recommended in BFS2012 [49].

The administered activities of the ^{18}F-FDG PET/CT scans showed a good agreement with EANM2008 and BfS2012, while more significant differences were observed in comparison to NACG and EANM2014, because of the slightly higher recommended activities. All renal scans (^{99m}Tc-MAG3 and ^{99m}Tc-DMSA), were in good agreement with the EANM recommendations.

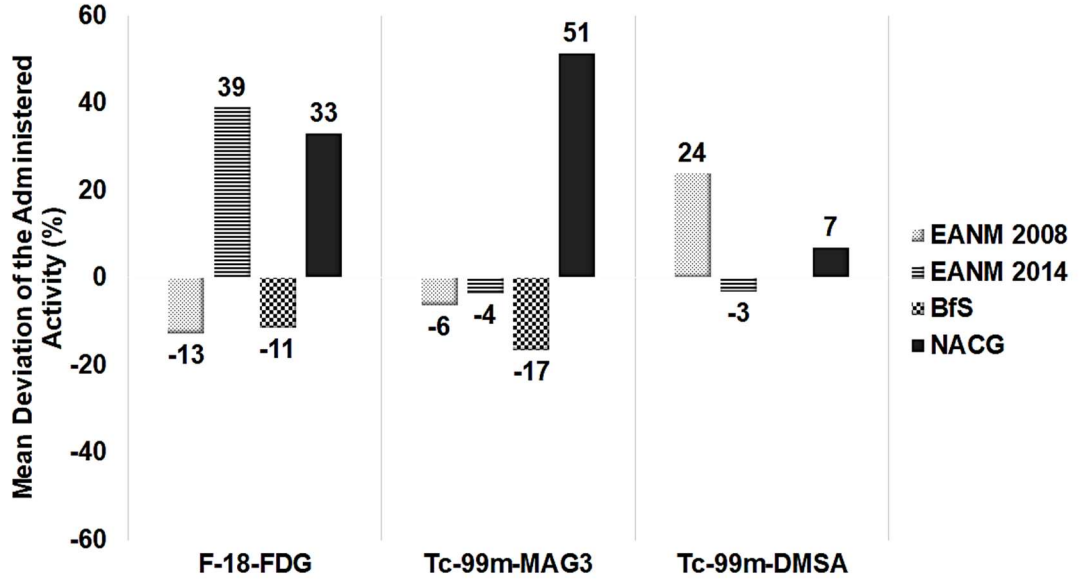

FIGURE 4.2. Mean deviation (%) of the administered activity (MBq) to the patients in comparison to the recommended administered activity by EANM Dosage Card 2008 (EANM2008), EANM/SNMMI 2014, Bundesamt für Strahlenschutz (BfS) and National American Consensus Guidelines (NACG).

Based on the previous assessment a total of 34 pediatric patients with ^{99m}Tc-MAG3 scans were selected for a detailed investigation. The collected information consists in gender: 25 males; 9 females; age: 1.3-20.0 months (mean±SD: 6.0±4.1 months); weight: 4.0-12.0 kg (mean±SD: 7.2±2.0 kg); body size: 30.0-89.0 cm (mean±SD: 66.0±10.6 cm); injected activity: 12.0-24.0 MBq (mean±SD: 17.2±2.4 MBq). On average, the activity administered to our patients was 12.2% lower than the injected activity values recommended in the EANM Dosage Card 2014 [12].

Table A1 (Annex) shows the patient-specific organs sizes (kidneys and bladder, all data provided by M. Lassmann). The depth in all patients (with NRF and ARF) was between 1.6 cm and 3.2 cm (mean±SD: 2.4±0.4 cm) for the RK; 1.7 cm and 3.0 cm (mean±SD: 2.4±0.3 cm) for the LK. In comparison to the renal depth values presented in the study of Scott et al. (mean±SD: 2.2±0.3 cm [RK]; 2.1±0.2 cm [LK]) [59], our patients had a difference of 7.3% (RK) and 10.7% (LK). Related to the kidney volumes for all patients, a range of 12.0-60.0 ml (mean±SD: 25.4±9.4 ml) was observed for the RK and 9.0-46.0 ml (mean±SD: 21.5±7.3 ml) for the LK.

The NRF patient group (Table 4.1) consisted of 14 males and 6 females with ages 1.6-20.0 months (mean±SD: 7.0±4.6 months), weight 5-12 kg (mean±SD: 7.8±1.9 kg), body size 60-89 cm (mean±SD: 69.5±7.8 cm), and injected activity 12-24 MBq (mean±SD: 17.9±2.6 MBq). 4 patients had injected activities between 12 MBq and 15 MBq, 14 patients between 16 MBq and 20 MBq, and 2 patients between 21 MBq and 24 MBq. The activity administered

to our patients was 22% lower than the injected activity values recommended in the EANM Dosage Card 2014 [12].

Furthermore, the organ dimensions of the patients with NRF classified by age groups are as follows:

Newborns organ depth: RK: 1.6-3.2 cm (mean±SD: 2.5±0.4 cm); LK: 1.7-2.8 cm (mean±SD: 2.4±0.3 cm). Newborns organ volume: RK: 14.0-32.0 ml (mean±SD: 22.1±5.5 ml); LK: 11.4-29.0 ml (mean±SD: 20.1±4.5 ml); BL: 5.0-52.5 ml (mean±SD: 30.8±15.3 ml).

1-year-olds organ depth: RK: 1.7-2.2 cm (mean±SD: 1.9±0.2 cm); LK: 1.8-2.8 cm (mean±SD: 2.4±0.4 cm). 1-year-olds organ volume: RK: 20.0-60.0 ml (mean±SD: 36.7±17.0 ml); LK: 21.0-46.0 (mean±SD: 34.0±10.2 ml); BL: 60.0-92.5 (mean±SD: 72.5±14.3 ml).

The organ sizes may be influenced by the age and gender associated with the individual body or organ morphology of each patient [59].

Normality tests (Shapiro-Wilk) were performed to evaluate how the organ sizes are distributed (interpretation: a normality test does not reject a normal distribution of values if the p-values are higher than the reference level of 0.05).

The patients with NRF showed a normal distribution of the kidney depth values; newborns p-values: 0.23 (RK), 0.32 (LK); 1-year-olds p-values: 0.36 (RK), 0.32 (LK). Regarding the volumes, the newborns showed a non-normal distribution for RK (p-value of 0.02). This result can be related to an asymmetric distribution of the values caused by a minority of values which are higher than the mean value. Conversely, there were normal distributions for the volumes of the LK (p-value: 0.93) and BL (p-value: 0.11). In the 1-year-old group, a normal distribution of the organ volumes for RK (p-value: 0.46), LK (p-value: 0.87) and BL (p-value: 0.27) was observed.

TABLE 4.1. Patients with normal renal function clustered by age groups with patients' information on age, gender, weight, body size, and injected activity.

Age group	Patient	Gender	Age (month)	Body Size (cm)	Weight (kg)	Injected Activity (MBq)
Newborn (1.6-11.0 months; M: 13; F: 4)	P01	M	1.6	62	5.0	12
	P02	M	2.0	60	5.0	15
	P03	M	3.0	62	6.3	18
	P04	F	3.0	59	5.0	14
	P05	M	4.0	63	6.0	18
	P06	M	4.0	65	7.0	15
	P07	M	5.0	67	7.0	19
	P08	F	5.0	72	8.0	16
	P09	M	5.0	66	8.0	16
	P10	F	5.0	66	7.0	19
	P11	M	6.0	72	9.5	20
	P12	M	7.0	68	7.0	17
	P13	M	7.0	65	8.0	19
	P14	M	7.0	76	10.0	18
	P15	M	8.0	70	9.0	19
	P16	F	9.0	72	8.0	20
	P17	M	11.0	74	8.0	21
	MEAN±SD		5.4±2.4	67.0±4.9	7.3±1.5	17.4±2.4
1-year-old (13.0-20.0 months; M: 1; F: 2)	P18	M	13	87	11.0	20
	P19	F	14	74	9.0	18
	P20	F	20	89	12.0	24
	MEAN±SD		15.7±3.1	83.3±6.6	10.7±1.2	20.7±2.5
All	MEAN±SD		6.98±4.5	69.5±7.8	7.8±1.9	17.9±2.6
M = Males; F = Females						

A total of 14 patients with ARF (Table 4.2) was analyzed (11 males; 3 females) with an age range of 1.3-2.0 months (mean±SD: 4.6±3.1 months); weight: 4.0-10.0 kg (mean±SD: 6.7±2.0); body size: 30.0-75.0 cm (mean±SD: 60.0±11.6 cm); injected activity: 13.7-21.0 MBq (mean±SD: 16.4±2.0 MBq). 2 in 14 patients had injected activities between 13 and 14 MBq, 7 in 14 patients between 15 and 16 MBq and 5 in 14 between 17 and 21 MBq (Table 4.2).

The patients with ARF had the following organ sizes (clustered per age group): newborn organ depth: RK: 1.6-3.2 cm (mean±SD: 2.4±0.4 cm), LK: 1.7-3.0 cm (mean±SD: 2.4±0.3 cm); organ volume range: RK: 12.0-41.0 ml (mean±SD: 23.5±7.2 ml), LK: 9.0-31.0 ml

(mean±SD; 20.2±5.7 ml); BL: 3.0-52.5 ml (mean±SD: 21.6±15.9 ml). In the ARF patient group, there was only one 1-year-old patient (P34). All organ sizes are shown in Table A1 (Annex).

The organ depth values of the newborn patients with abnormal function were normally distributed (p-values: 0.17 [RK]; 0.32 [LK]); similarly, their organ volumes were normally distributed (p-values: 0.91 [RK]; 0.18 [LK]; 0.06 [BL]).

TABLE 4.2. Patients with abnormal renal function clustered by age group with patients' information on age, gender, weight, body size, and injected activity.

Age group	Patient	Gender	Age (month)	Body Size (cm)	Weight (kg)	Injected Activity (MBq)
Newborn (1.3-8.0 months; M: 10; F: 3)	P21	F	1.3	54.0	4.0	16.0
	P22	F	1.3	30.0	5.0	15.0
	P23	M	1.5	50.0	5.0	14.0
	P24	M	1.5	54.0	5.0	15.0
	P25	M	2.0	60.0	6.6	16.0
	P26	M	3.0	68.0	7.0	17.0
	P27	F	5.0	63.0	6.4	16.0
	P28	M	5.0	65.0	7.6	13.7
	P29	M	5.0	59.0	10.0	21.0
	P30	M	5.0	53.0	4.0	17.9
	P31	M	6.0	65.0	7.0	16.3
	P32	M	8.0	72.0	10.0	19.0
	P33	M	8.0	75.0	9.0	15.4
	MEAN±SD		4.0±2.4	59.1±11.1	6.7±1.9	16.3±1.9
1-year-old (12.0 months; M)	P31	M	12.0	72	8	17.0
All	MEAN±SD		4.6±3.1	60.0±11.2	6.8±1.9	16.4±1.9

M = Males; F = Females

In contrast to adults, excretion cannot be controlled or contained by newborns and toddlers [15]. Moreover, the human bladder can present a variety of sizes during the urine excretion processes [60]. Considering these facts, the volume distribution of patients with ARF can be associated with the bladder voiding as patients with kidney dysfunction such as urine blockage can show a tendency towards no voiding. Furthermore, 65% of the patients with NRF showed bladder excretion, while only 28% of the patients with abnormal function presented excretion. A statistical test (one-way ANOVA) was performed to compare and test if these groups were significantly different. According to this test, the incidence of voiding in the group of patients with NRF and ARF is not significantly different (p-value: 0.55) at a level of 0.05.

The clustered patient and exposure data provided sufficient information to reach the essential steps of the present study. The organ sizes were a crucial part of the calibration methods and consequently of the retrospective image quantification (sub-chapter 4.1); a process that allows further assessments of the patients' biokinetics and dosimetry.

4.3. Biokinetics

4.3.1. Time-Activity Curves

To analyze the patients' biokinetics, it was pertinent to comprehend the general characteristics and main differences between the NRF and the ARF group. The time-activity curve (TAC) provides key information about the patients' renal function; the maximum uptake time (T_{max}) about the flow through the kidneys and excretion. The TAC and T_{max} were determined based on the data collected from the retrospective image quantification.

The patients with NRF presented kidney-specific TACs with the shape of an early peak followed by a rapid descending phase, as it is typically shown for renal systems with normal excretion and good wash-out (Figure 4.3).

TABLE 4.3. The range of maximum uptake times for the 20 patients with NRF clustered by kidney side.

Organ	No. of Patients	Range of T_{max} (minutes)
RK	13	2 - 4
	5	5 - 10
	2	13 - 17
LK	9	2 - 4
	8	5 - 9
	3	15 - 17

RK = Right kidney; **LK** = Left Kidney

According to Table 4.3, the data of the NRF patients can, in general, be considered similar with regards to T_{max}. There was a tendency towards later T_{max} for the left kidney in all patients (~20 min). This factor can relate to the patient's age range since the renal system of newborns and toddlers is still under development. Also, many patients showed kidney excretion in Phase III of the acquisition scheme (between minutes 4 and 30) and the counts per second (cps) showed values close to zero for the last time points.

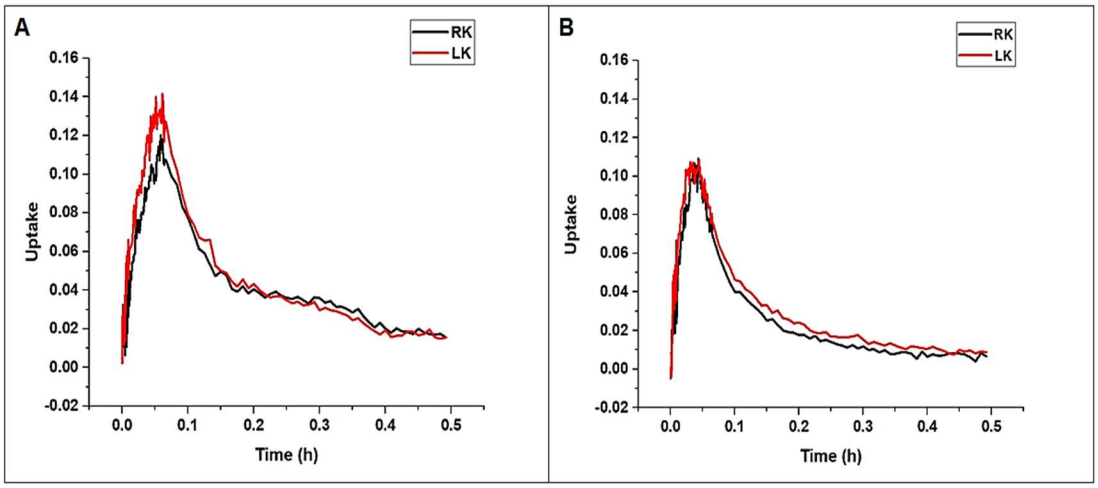

FIGURE 4.3. Exemplary patients' time-activity curves with a normal renal function for the right and left kidney (RK; LK). **A:** P10: 5.0 months (female); **B:** P20: 20.0 months (female).

Regarding the 14 infants with *ARF*, 6 patients had unilateral kidney failure. As an example, the patient P31 (Fig. 4.4 A) showed a typical TAC for NRF in the right kidney (solid black line in Fig 4.4 A, T_{max}: 5 min). In contrast, the left kidney (T_{max}: 18 min) showed a TAC shaped by a long ascendant curve without the early peak, and almost no descending curve over the time (solid red line in Fig. 4.44 A). This shape with an absence of regular kidney washout is typical for an abnormal kidney function, leading to the number of counts (cps) is not decreasing over time. 8 of 14 patients with ARF showed bilateral kidney failure. An example of a characteristic TAC occurring for RK and LK dysfunction is given in Figure 4.4 B; patient P23 presented T_{max} at 22 min in RK and 8 min for LK (Figure 4.4 B).

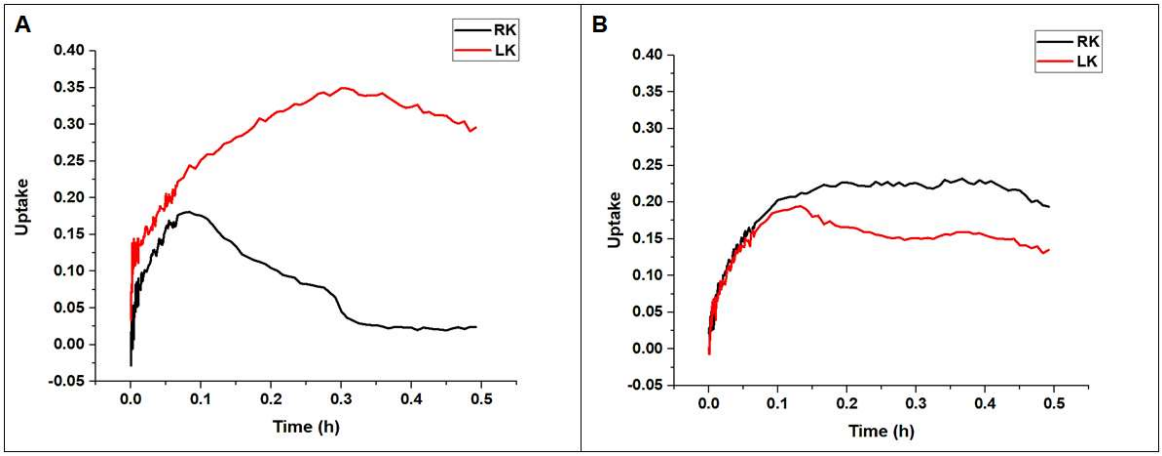

FIGURE 4.4. Exemplary patients' time-activity curves with an abnormal renal function for the right and left kidneys. **A:** P31: 6.0 months (male), with unilateral abnormal renal function (UARF). **B:** P23: 8.0 months (male), with bilateral abnormal renal function (BARF).

In comparison to the patients with NRF, most of the patients with ARF showed late T_{max} values (Table 4.4).

TABLE 4.4. The range of the maximum uptake times for the 14 patients with ARF clustered by kidney side.

Organ	No. of Patients	Range of T_{max} (minutes)
RK	2	0 - 4
	5	5 - 12
	5	15 - 20
	2	21 - 30
LK	2	0 - 4
	3	5 - 12
	5	15 - 20
	4	21 - 30

RK = Right kidney; **LK** = Left Kidney

Overall, the patients presented different organ-specific time-activity curve shapes and T_{max} values when evaluated individually. Nevertheless, it was possible to observe similar characteristics according to the renal function (normal or abnormal) by means of the TAC shape and the T_{max} values clustered by intervals.

4.3.2. Time-Integrated Activity Coefficients

After observing the patients' TAC and T_{max} characteristics according to the renal function, the following section will be dealing with the integration of TAC. The time-integrated activity curves (TIAC) represent an estimated number of disintegrations inside of the organ over time (h).

Figures 4.5 (patient with NRF) and 4.6 (patient with ARF) exemplify the TIAC fitting and integration process (Eq.3.E) for right kidney (RK), left kidney (LK), and whole body.

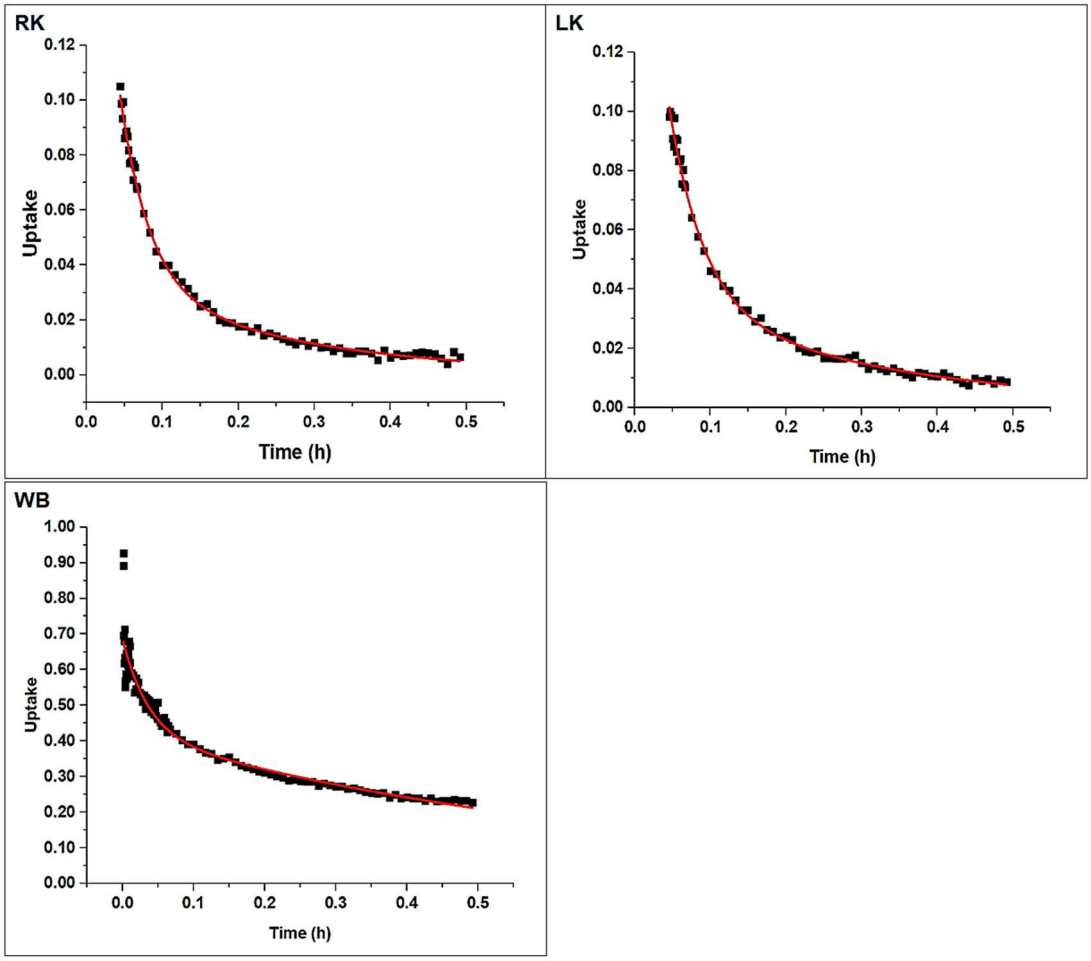

FIGURE 4.5. Black dots: Patient-specific data points for right kidney (T_{max} 0.043 h), left kidney (T_{max} 0.045 h), and whole body (WB) of the patient P20 (20.0 months, female, NRF). Red line: Fitted curve (bi-exponential function).

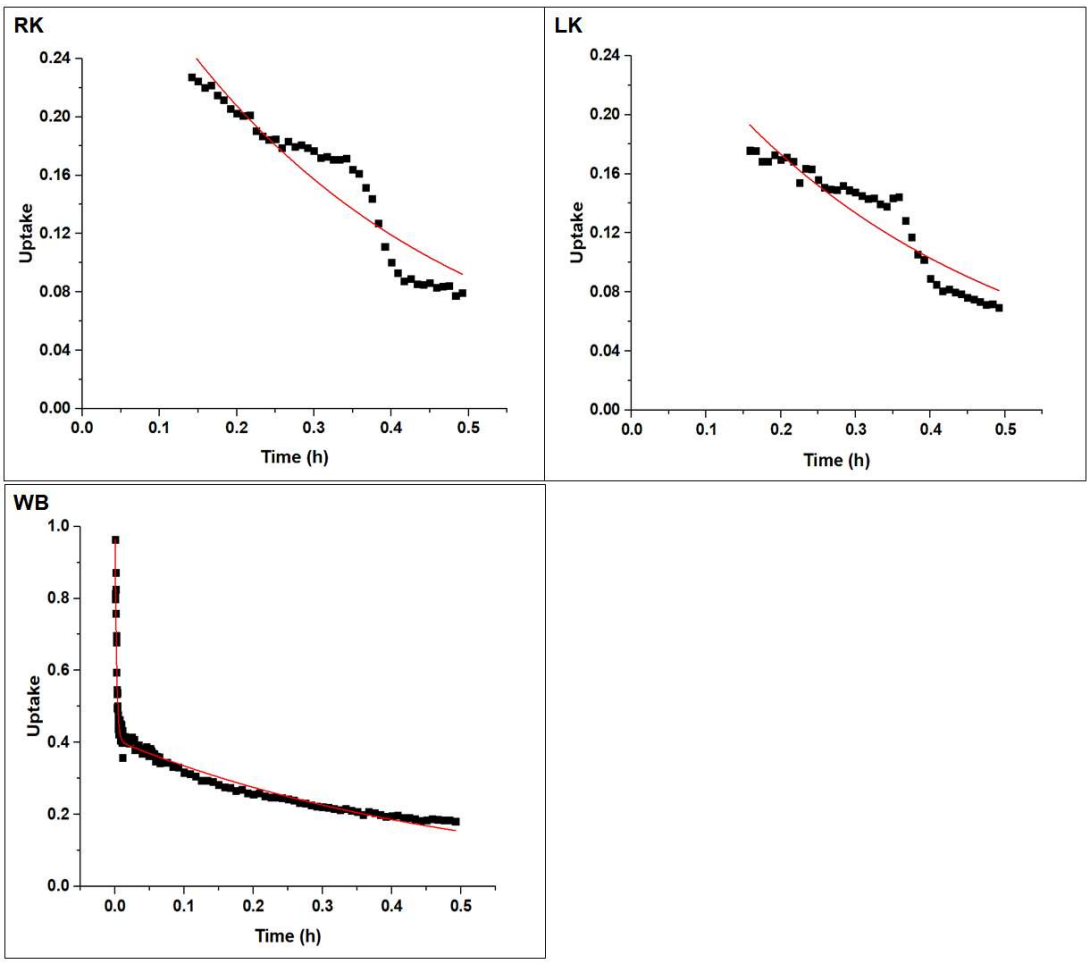

FIGURE 4.6. Black dots: Patient-specific data points for right kidney (T_{max} 0.13 h), left kidney (T_{max} 0.15 h), and whole body (WB) of patient P29 (5.0 months, male, BARF). Red line: Fitted curve (bi-exponential function).

The TIAC values of the patient with NRF are given in Table 4.5. This patients group presented the following range of TIAC values between 0.03 h and 0.44 h (mean±SD: 0.11±0.09 h) for the kidneys; 0.05 h to 2.99 h (mean±SD: 1.04±0.96 h) for the bladder; 0.17 h to 3.88 h (mean±SD: 1.35±1.30 h) for the whole body. When comparing the patients by age groups, the mean TIAC values for the newborns in comparison to the 1-year-olds were 47% higher for the kidneys, 50% lower for the bladder, and 80% higher for the whole body. However, according to one-way ANOVA tests comparing the TIAC values between the newborn and the 1-year-old group (p-values: 0.84 for the kidneys, 2.32 for the bladder, 2.30 for the whole body), there was no significant difference (reference level: $p > 0.05$).

Although none of the patients suffered from severe kidney function impairment, large inter-patient variations were observed. A normality test (Shapiro-Wilk) was performed to evaluate how the TIAC values were distributed. For the newborn group, the normality test showed a non-normal distribution of the TIAC values (p-values: 7.85E-05 for the kidneys, 3.33E-02 for the bladder, 5.44E-04 for the whole body). In contrast, the 1-year-old group presented a normal distribution of the values (p-values: 0.57 for kidneys, 0.19 for bladder, 0.93 for the whole body).

In comparison to the ICRP 128 values for the 1-year-old group with NRF (kidneys: 0.065 h; bladder: 1.6 h; whole body: 0.23 h) [18], the mean TIAC values in our group of patients were 38% higher for the kidneys, 35% lower for the bladder, and 83% higher for the whole body.

TABLE 4.5. Organ-specific time-integrated activity coefficients (TIACs) in hours for patients with normal renal function (clustered into age groups).

Age group	Patient	Gender	TIAC (h)		
			Kidneys	Bladder	Whole Body
Newborn (1.6-11.0 months; M: 13; F: 4)	P01	M	0.17	0.42	1.32
	P02	M	0.11	0.30	0.70
	P03	M	0.16	1.30	0.71
	P04	F	0.06	0.21	0.59
	P05	M	0.07	0.31	3.88
	P06	M	0.07	0.38	3.57
	P07	M	0.07	2.94	0.61
	P08	F	0.08	2.92	0.75
	P09	M	0.03	1.97	0.35
	P10	F	0.05	0.58	0.43
	P11	M	0.07	0.21	1.55
	P12	M	0.19	1.39	0.57
	P13	M	0.05	0.06	0.50
	P14	M	0.15	1.34	3.66
	P15	M	0.09	0.05	0.35
	P16	F	0.44	0.93	3.12
	P17	M	0.07	0.14	3.35
	MEAN±SD		0.11±0.09	0.91±0.92	1.35±1.32
1-year-old (13.0-20.0 months; M: 1; F: 2)	P18	M	0.05	1.11	0.17
	P19	F	0.10	1.32	0.43
	P20	F	0.03	2.99	0.31
	MEAN±SD		0.06±0.03	1.81±0.84	0.31±0.11
All	MEAN±SD		0.11±0.09	1.04±0.96	1.35±1.30
ICRP 128 [18] (1-year-old)			0.065	1.6	0.23

M = Males; F = Females

The TIAC values of the patients with ARF (Table 4.6) were between 0.12 h and 3.02 h (mean±SD: 1.06±0.90 h) for the kidneys; 0.06 h and 4.15 h (mean±SD: 1.45±1.26 h) for the bladder; 0.21 h and 3.75 h (mean±SD: 1.33±1.09 h) for the whole body. Similar results were found regarding the TIAC values distribution in comparison to the NRF patients. Inter-patient variation was present in the data; therefore, the normality test presented a normal distribution for the kidneys (p-value: 0.05) and non-normal distributions for the bladder (p-value: 0.02) and the whole body (p-value: 0.01).

In total, there were 8 patients with *unilateral abnormal renal function (UARF)* and 6 with *bilateral abnormal renal function (BARF)* (Table 4.6). The TIACs for the patients with unilateral renal abnormal function (UARF) were in the range between 0.1 h and 1.6 h (mean±SD: 0.5±0.4 h) for the kidneys; 0.1 h and 3.9 h (mean±SD: 1.4±1.2 h) for the bladder; 0.3 h and 3.7 h (mean±SD: 1.1±1.5 h) for the whole body. Related to the patients with BARF the TIAC values for the kidneys were 0.9 h to 3.0 h (mean±SD: 1.9±0.7 h); 0.5 h to 4.2 h (mean±SD: 1.5±1.3 h) for the bladder; 0.2 h to 3.7 h (mean±SD: 1.1±1.1 h) for the whole body. Comparing the TIAC values of the BARF patient group to the UARF, the percentage differences were 76% for the kidneys, 4% for the bladder and –31% for the whole body. These results may reflect renal function abnormalities. The patients with UARF had lower kidneys' TIACs (mean) in comparison to the ones with BARF, which is caused by a relatively faster biokinetics since one of the kidneys typically has normal excretion/washout. In contrast, the patients with BARF presented no kidney excretion/washout; consequently, activity retained in the kidneys for these patients (Fig. 3.8.-Image 3).

There were TIAC values with normal and non-normal distributions in both groups (reference level: 0.05): the UARF patients showed p-values of 0.001 for the kidneys, 0.32 for the bladder, and 0.29 for the whole body; the BARF patients presented p-values of 0.89 for the kidneys, 0.02 for the bladder, and 0.03 for the whole body. A statistical test (Wilcoxon Signed Rank Test was performed for non-parametric samples to evaluate if the TIACs of the UARF patients and BARF patients were statistically different. The results showed that the TIAC values are not statistically different for the kidneys (p-value: 0.06) and bladder (p-value: 0.84). Conversely, the test presented that the groups are significantly different comparing the whole body TIACs (p-value: 0.03). This difference can be related to the slow/null renal excretion and, consequently, higher TIAC (h) (kidneys and bladder) for the BARF group compared to the UARF.

Comparing the mean TIAC values of the non-normal patients to the reference TIAC values from ICRP [18], the UARF patients showed a percentage difference of 93% for the kidneys, 43% for the bladder and –65% for the whole body. Regarding patients with BARF, the differences were 85% for the kidneys, 26% for the bladder and –24% for the whole body. These systematic discrepancies can be related to the fact that the biokinetics data presented by ICRP 128 [18] were estimated based on mathematical models and phantoms with simple geometric forms that have no precise body/organ morphometry [14]. In addition, the compared ICRP standard values of the biokinetics in children were assessed by means of extrapolation methods based biokinetics in adults [14], a process that could lead to an underestimation of the values.

TABLE 4.6. Organ-specific time-integrated activity coefficients (TIACs) in hours for patients with abnormal renal function (clustered into age groups).

Age group	Patient	Gender	Renal Abnormality Type	TIAC (h)		
				Kidneys	Bladder	Whole Body
Newborn (1.3-8.0 months; M: 10; F: 3)	P21	F	Bilateral	0.90	2.01	0.80
	P22	F	Unilateral	1.57	2.43	0.89
	P23	M	Unilateral	0.17	0.66	2.37
	P24	M	Bilateral	2.46	0.71	0.75
	P25	M	Unilateral	0.38	0.35	0.66
	P26	M	Unilateral	0.37	1.40	1.70
	P27	F	Unilateral	0.16	0.54	1.72
	P28	M	Unilateral	0.32	2.06	3.75
	P29	M	Bilateral	1.42	4.15	0.21
	P30	M	Bilateral	1.81	0.47	0.57
	P31	M	Unilateral	0.52	3.95	0.80
	P32	M	Bilateral	3.02	0.75	0.62
	P33	M	Unilateral	0.12	0.06	0.31
	MEAN±SD			1.02±0.92	1.50±1.29	1.17±0.95
1-year-old (12.0 months; M)	P34	M	Bilateral	1.59	0.82	3.42
All	MEAN±SD			1.06±0.90	1.45±1.26	1.33±1.09
ICRP 128 [18] (1-year-old)		-	Unilateral	0.033	0.82	4.4
			Bilateral	0.28	1.1	1.4

M = Males; F = Females

4.4. Dosimetry

4.4.1. Absorbed Doses

The values for the organ absorbed dose coefficients (mGy/MBq), and effective dose coefficients (mSv/MBq) were estimated based on the patient-specific TIACs.

The patients with NRF are shown in Table A.2. The absorbed dose ranges were: 0.004-0.131 mGy/MBq (mean±SD: 0.035±0.029 mGy/MBq) for the kidneys; 0.01-0.93 mGy/MBq (mean±SD: 0.27±0.26 mGy/MBq) for the bladder; 0.001-0.019 (mean±SD: 0.008±0.005 mGy/MBq) for the remainder.

Comparing the results for the dose coefficients per age group, the newborns showed higher mean values. The percentage differences were 69% for the kidneys, 10% for the bladder, and 59% for the remainder. To observe if the mean absorbed dose coefficients of the two age groups were statistically different, a one-way ANOVA was performed. Based on this test, the groups were not significantly different with p-values of 0.14 for the kidney dose coefficients, 0.86 for the bladder dose coefficients, and 0.55 for the remainder dose coefficients.

The mean absorbed dose coefficients of the patients (NRF) were compared to the absorbed dose coefficient values from ICRP (publication 128 [17]). The patients presented higher dose coefficients for kidneys and remainder with differences of 58% and 54%, respectively; in contrast, the absorbed dose coefficients were lower for the bladder (–16%).

Compared to the pediatric patient ^{99m}Tc-MAG3 patient data presented by Stabin et al. [12], the absorbed dose coefficients observed in our patients were lower for the newborns and higher for the 1-year-old patients. The kidney absorbed dose coefficients were 17% lower for the newborns and 25% higher for the 1-year-old group, while they were 22% lower for newborns and 76% higher for 1-year-old patients in the bladder. Lastly, the dose coefficient of the remainder was 7% lower for newborns and 63% higher for 1-year-old patients. This can be related to the difference in the number of patients: While we included 20 pediatric patients, Stabin et al. included only two pediatric patients in the age range considered [13].

The results for the organ absorbed dose coefficients for the patients with ARF (Table A.3) were: 0.03-1.04 mGy/MBq (mean±SD: 0.40±0.34 mGy/MBq) for the kidneys; 0.01-1.25 mGy/MBq (mean±SD: 0.46±0.37 mGy/MBq) for the bladder; 0.001-0.024 mGy/MBq (mean±SD: 0.015±0.006 mGy/MBq) for the remainder. The mean values for the patients with UARF indicated a percentage difference of –73% for the kidneys in comparison to the patients with BARF. This difference was expected since the patients with UARF typically retain less activity (in one of the kidneys) and, consequently, there is a lower time of radiation exposure in the organ. Contrariwise, the BARF patients had the majority of the activity concentrated in

both kidneys. The group of patients with UARF presented absorbed dose coefficients which were 13% higher for the bladder and –26% lower for the remainder in comparison to BARF; these results may also be related to their renal function: according to the exam images and quantification, the UARF patients presented a more efficient urine flow, increasing the absorbed dose to the bladder. Albeit the percentage differences, the mean absorbed dose coefficients of the patients with unilateral and bilateral abnormal functions were not statistically different for the kidneys (p-value: 0.18), for the bladder (p-value: 1.00), and for the remainder (p-value: 0.18).

Furthermore, comparing the results of the patients with ARF to the dose coefficient values from ICRP 128 [18], the differences were: UARF patients: 77% for the kidneys, 65% for the bladder, and 38% for the remainder; BARF patients: 91% for the kidneys, 46% for the bladder, and 65% for the remainder.

With regards to the absorbed doses (mGy), the patient group with NRF showed values between 0.1 mGy and 2.6 mGy for the kidneys and between 0.2 mGy and 17.7 mGy for the bladder. In Table 4.7 the absorbed dose is clustered by age groups. Comparing the mean values of the newborn to the 1-year-old patients, the percentage differences were 69% for the kidneys and -6% for the bladder. The two age groups are not statistically different (p-values: 0.18 for the kidneys absorbed doses, and 0.78 for the bladder absorbed doses).

TABLE 4.7. Absorbed doses (mGy) and effective doses (mSv) for the patients with normal renal function clustered by age groups (mean±SD).

Age Group	Absorbed Dose (mGy)		Effective Dose (mSv)
	Kidneys	Bladder	
Newborn (1.3-8.0 months; M: 13; F: 4)	0.69±0.55	4.79±4.70	0.36±0.25
1-year-old (13.0-20.0 months; M: 1; F: 2)	0.23±0.15	5.08±1.50	0.48±0.23
All	0.62±0.53	4.84±4.37	0.38±0.25

M = Males; F = Females

The patient absorbed doses were also compared to data of an intravenous urography (IVU) study: Almen et al. showed an average absorbed dose per exposure of 0.68 mGy (range: 0.48-1.10 mGy) for pediatric patients aged between 0 and 1 years [63]. In comparison, the ^{99m}Tc-MAG3 scans presented here resulted in a 9% lower kidney absorbed dose of 0.62 mGy averaged over 20 patients (range: 0.10-2.62 mGy).

Table 4.8 lists the mean absorbed doses (mGy) for the ARF patients; the values were in the range of 0.4-15.3 mGy for the kidneys and 0.2-20.4 mGy for the bladder.

TABLE 4.8. Absorbed doses (mGy) and effective doses (mSv) for the patients with abnormal renal function clustered by age groups (mean±SD).

Age Group	Absorbed Dose (mGy)		Effective Dose (mSv)
	Kidneys	Bladder	
Newborn (1.3-8.0 months; M: 10; F: 3)	6.51±5.72	7.85±6.22	0.64±0.41
1-year-old (12.0 months; M)	7.67	4.03	0.48
All	6.59±5.52	7.57±6.08	0.62±0.40

M = Males; F = Females

The patients with ARF, clustered by renal abnormality type, presented the following ranges of the absorbed doses: UARF patients: 0.4-10.1 mGy (mean±SD: 2.8±3.0 mGy) for the kidneys and 0.2-20.4 mGy (mean±SD: 7.6±6.5 mGy) for the bladder; BARF patients: 5.5-15.7 mGy (mean±SD: 11.6±4.0 mGy) for the kidneys and 2.7-16.0 mGy (mean±SD: 7.6±5.5 mGy) for the bladder. The BARF patients showed mean absorbed doses which were 75% higher for the kidneys in comparison to the UARF patients; the differences for the kidneys can be explained by the differences in the patient-specific administered activity (MBq) (BARF: 13% higher administered activity).

One of the dose assessment shortcomings can be associated with the uncertainty arising from the calibration process and the subsequent patient-specific correction. Nonetheless, in this age group, the variability concerning morphology is rather low. Furthermore, as it is a retrospective analysis with images taken at suboptimal time points for dosimetry, the reported absorbed doses might be overestimated due to the approximation of only physical decay after the last time-point.

In conclusion, the function was the main factor that affected the absorbed doses. In general, ARF patients, presented higher values than NRF patients, which can be explained by activity accumulating in the ARF patients' organs for a time longer, leading to higher radiation exposure.

4.4.2. Effective Doses

Besides the absorbed doses, it is essential to evaluate the effective doses, a concept which basically represents the detriment caused by radiation exposure. Therefore, effective doses were calculated for some common NM procedures applied to pediatric patients in order to evaluate the exposure levels in these procedures. Furthermore, effective doses were also estimated for the group of the 34 ^{99m}Tc-MAG3 scanned patients which had been studied in more detail, to observe the factors of influence such as e.g. renal function, age, and gender.

4.4.2.1. Effective Doses Estimation for NM Procedures

The weight-dependent functions for the *effective dose coefficients*, which were determined by the fitting process (Fig. 4.7), are presented in the following section:

^{18}F-FDG: $y=0.610x^{-0.808}$, $R^2=0.99$;

^{99m}Tc-MAG3: $y=0.075x^{-0.553}$, $R^2=0.92$;

^{99m}Tc-DMSA: $y=0.203x^{-0.747}$, $R^2=0.99$.

The corresponding effective doses for the ^{18}F-FDG PET/CT scans ranged from 3.0 mSv to 7.1 mSv (mean±SD: 4.2±0.8 mSv). The corresponding effective doses were between 0.2 mSv and 1.0 mSv (mean±SD: 0.5±0.1 mSv) for the ^{99m}Tc-MAG3 scans and 0.5 mSv to 1.6 mSv (mean±SD: 0.8±0.3 mSv) for ^{99m}Tc-DMSA. The corresponding effective doses are sufficiently low to conclude that no change in daily practice is needed.

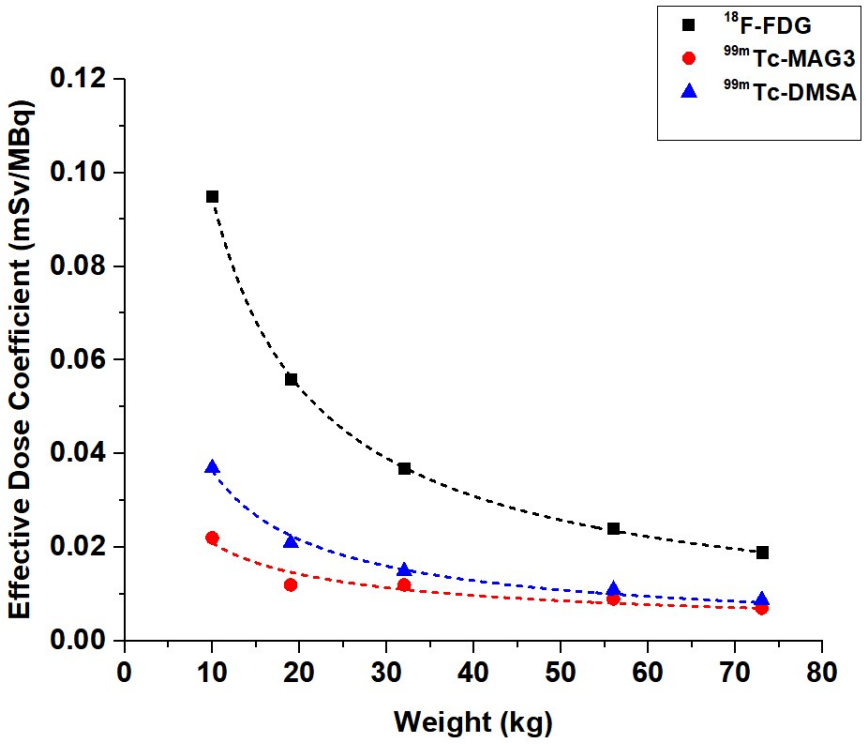

FIGURE 4.7. Effective dose coefficients [52, 53, 61] for different radiopharmaceuticals as a function of the phantom weight (1-year-old: 10 kg; 5-year-old: 19 kg; 10-year-old: 32 kg; 15-year-old: 56 kg, and adult: 73 kg [38]). **^{18}F-FDG** was applied for tumor diagnostics procedures with PET/CT. **^{99m}Tc-MAG3** and **^{99m}Tc-DMSA were** utilized in renal diagnostics procedures with planar imaging.

4.4.2.2. Administered activity weight-based Formalism

The corresponding TIACs were taken from published data for ^{68}Ga-DOTATATE [61], ^{68}Ga-DOTATOC [61, 62], and ^{68}Ga-Pentixafor [29]. The data are summarized in Table A4 (Annex). The resulting effective dose coefficients for the age-dependent phantoms provided by OLINDA/EXM are presented in Table 4.9 [11, 12]. The lowest and highest values are those of ^{68}Ga-Pentixafor [29] and ^{68}Ga-DOTATOC [62], respectively.

The results for all calculated normalization factors of the effective doses for *a* values and R^2 values were –0.9176 and 0.999 for ^{68}Ga-DOTATOC [62], –0.9438 and 0.999 for ^{68}Ga-DOTATATE [61], –0.9586 and 0.999 for ^{68}Ga-DOTATOC [61], and –1.0339 and 0.999 for ^{68}Ga-Pentixafor [29], respectively. These values all lie within the range of values for class “B” radiopharmaceuticals, suggesting that the ^{68}Ga labeled peptides also belong to class “B” [11, 12, 36]. As a result, the *baseline activity* (for calculation purposes only) for all compounds was set to 12.8 MBq. An activity of 14 MBq is recommended as minimum activity to be administered, in analogy to ^{18}F-fluoride (taken from the newest version of the EANM Dosage card [11, 12]).

Table 4.10 shows the values of recommended administered activities and respective effective doses for 3, 10, 20, 40, 60, and 68 kg patients [11, 12]. As expected, the corresponding effective doses were lowest for ^{68}Ga-Pentixafor [29] and highest for ^{68}Ga-DOTATOC [62]. The effective dose remains constant within 20% above a patient weight of 10kg.

TABLE 4.9. Effective dose coefficients (mSv/MBq) calculated using OLINDA/EXM.

Age	*Weight (kg)	Effective Dose Coefficient (mSv/MBq)			
		^{68}Ga-DOTATATE [60]	^{68}Ga-DOTATOC [60]	^{68}Ga-DOTATOC [61]	^{68}Ga-Pentixafor [28]
Adult	73.7	2.0E–02	1.9E-02	2.2E-02	1.6E-02
15-years-old	56.8	2.5E–02	2.6E–02	3.1E–02	2.0E–02
10-years-old	33.2	4.0E–02	4.1E–02	4.6E–02	3.2E–02
5-years-old	19.8	6.4E–02	6.6E–02	7.6E–02	5.1E–02
1-year-old	9.72	1.3E–01	1.3E–01	1.5E–01	1.0E–01
Newborn	3.6	3.5E–01	3.6E–01	3.8E–01	2.9E–01

*Phantom weight (kg) provided by OLINDA/EXM [38]

TABLE 4.10. Recommended administered activity and corresponding effective dose for six different patient weights.

Age	*Weight (kg)	Recommended Administered Activity (MBq)	Effective Dose (mSv)		
			^{68}Ga-DOTATATE [60]	^{68}Ga-DOTATOC **[61]	^{68}Ga-Pentixafor [28]
Adult	68	180	3.7	4.4	2.9
15-years-old	60	163	3.8	4.5	3.0
10-years-old	40	114	3.9	4.5	3.1
5-years-old	20	62	4.1	4.7	3.3
1-year-old	10	35	4.4	5.0	3.6
Newborn	3	14	5.5	6.2	4.7

*Maximum weight according to the EANM pediatric dosage card [11,12]
**For a conservative estimate, the higher values were chosen for DOTATOC, based on the data of Hartmann et al. [61]

4.4.2.3. Effective doses estimation for ^{99m}Tc-MAG3 Pediatric Patients

The values for the effective dose coefficients of the patients with NRF (Table A2 in the Annex) were: 0.002–0.063 mSv/MBq (mean±SD: 0.023±0.015 mSv/MBq).

The results for effective dose coefficients clustered by age groups ranged between 0.002 and 0.063 mSv/MBq (mean±SD: 0.024±0.016 mSv/MBq) for the newborns and between 0.011 and 0.021 mSv/MBq (mean±SD: 0.005±0.018 mSv/MBq) for the 1-year-olds. There was a normal distribution of the effective dose coefficients for the newborns (p-value: 0.18) and a non-normal distribution for the 1-year-olds (p-value: 0.03). The newborns presented higher mean effective dose coefficients (25%); these results (Table A2) may be related to the number of patients in each group. In addition, the newborn and 1-year-old mean ages are significantly different with a p-value of 9.63E–06 (one-way ANOVA test); the younger age of the newborns (mean±SD: 5.4±2.4 months) is a factor that can contribute to increasing the effective dose coefficients (radiation risk factor) in comparison to the 1-year-olds (mean±SD: 14.7±3.1 months). Nonetheless, the age groups have no significantly different effective dose coefficients means (p-value: 0.78).

The mean effective dose coefficient of the NRF patients was 5% higher in comparison to the values from ICRP 128 [18].

To estimate the ^{99m}Tc-MAG3 pediatric patients' effective doses the resulting effective dose factor (Fig 4.8) was multiplied by the patient-specific administered activity (MBq).

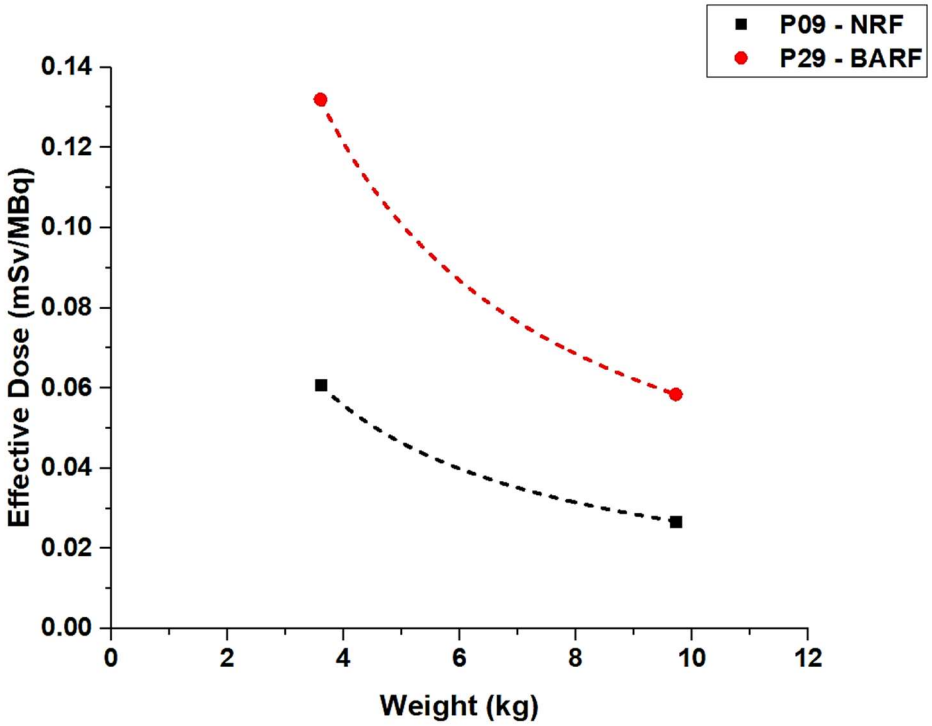

FIGURE 4.8. Effective dose coefficients (mSv/MBq) of the ^{99m}Tc-MAG3 patients as a function of phantoms weight (Newborn: 3.5 kg; 1-year-old: 10.0 kg [38]). **P09:** 5.0-month-old male with NRF; black curve: $y=0.1772x^{-0.823}$, $R^2=1$. **P29:** 5.0-month-old male with BARF; red curve: $y=0.3778x^{-0.821}$, $R^2=1$.

The effective doses (mSv) of the patients with NRF (Table 4.7) ranged between 0.04 mSv and 1.00 mSv (mean±SD: 0.38±0.25 mSv). Moreover, the newborns presented values between 0.04 mSv and 1.00 mSv (mean±SD: 0.36±0.25 mSv) and the 1-year-olds between 0.28 mSv and 0.81 mSv (mean±SD: 0.48±0.23 mSv). The effective dose values were normally distributed for both age groups; the p-values were 0.13 for the newborns and 0.27 for the 1-year-olds; there was no significant difference between the mean effective doses (p-value: 0.38).

The effective dose coefficients (mSv/MBq) for the patients with ARF (Table A3 in the Annex) ranged between 0.003 and 0.090 mSv/MBq (mean±SD: 0.045±0.025 mSv/MBq).

The effective dose coefficient intervals for the patients with UARF were between 0.003 mSv/MBq and 0.086 mSv/MBq (mean±SD: 0.040±0.027 mSv/MBq). Regarding the BARF patients, the effective doses were in a range between 0.03 mSv/MBq and 0.09 mSv/MBq (mean±SD: 0.05±0.02 mSv/MBq). The percentage difference between UARF and BARF mean effective dose coefficient was –25%; albeit the difference, the mean dose coefficients were not significantly different (p-value: 0.29).

Comparing the results for the patients with ARF to the effective dose coefficients values from ICRP 128 [18], the differences were 5% for the UARF and 64% for the BARF patients.

The ARF patients had effective doses (mSv) values (Table 4.8) between 0.04 mSv and 1.34 mSv (mean±SD: 0.62±0.40 mSv). The UARF patients presented values between 0.04 mSv and 1.18 mSv (mean±SD: 0.47±0.38 mSv), while the BARF patients presented values between 0.5 mSv and 1.3 mSv (mean±SD: 0.8±0.3 mSv). The BARF patients showed an effective dose 43% higher in comparison to the UARF patients, which might be influenced by the higher patient-specific administered activities (mean: UARF: 15.4±1.1 MBq; BARF: 18.0±2.0 MBq).

An estimate of the effective doses according to the weighting factors of ICRP 103 [5], could not be provided as the data of the underlying voxel-based ICRP phantom are yet to be published [5, 15].

4.5. Radiation Risk

4.5.1. Risk Analysis for the Patients with Normal Renal Function

The results of the excess lifetime risk (ELR) estimation for the patients with normal renal function (NRF) are given in Table 4.11; it lists the mean excess lifetime risk as well as the lower and upper bounds (limits) of the respective confidence intervals (CI) (95% uncertainty range) for the risk probability of all patients, clustered by age [15]. The group of newborn patients showed risk value ranges of 1.4-53.0 per 100,000 persons; the 1-year-old group had a risk value interval of 8.8-19.1 per 100,000 persons to develop cancer from radiation exposure.

TABLE 4.11. Age-dependent excess lifetime risk (chances in 100,000 persons) for the NRF patients (mean±SD).

Age Group	**Newborns** (1.6-11.0 months)	**1-year-olds** (13.0-20.0 months)	**All**
Excess Lifetime Risk (per 100,000)	16.8±13.9	14.7±5.3	16.5±12.6
Lower Bound	9.8	3.9	10.6
Upper Bound	24.0	26.0	22.4
Age (months)	5.4±2.4	15.7±3.1	7.0±4.5
CI 95% uncertainty range			

The newborn group had a non-normal distribution of the ELR values (p-value: 0.03). Figure 4.9 shows how the risk values are distributed for this age group. In summary, 11 in 17 patients (64%) had risk values between 1.4 and 20.4 per 100,000 persons, 4 in 17 patients (24%) showed risk values between 20.4 and 39.4 per 100,00 persons, and only 2 in 17 patients (12%) presented the highest risk values of 39.4 and 58.4 per 100,000. In contrast, the 1-year-old patients had a normal distribution of the ELR values (p-value: 0.50).

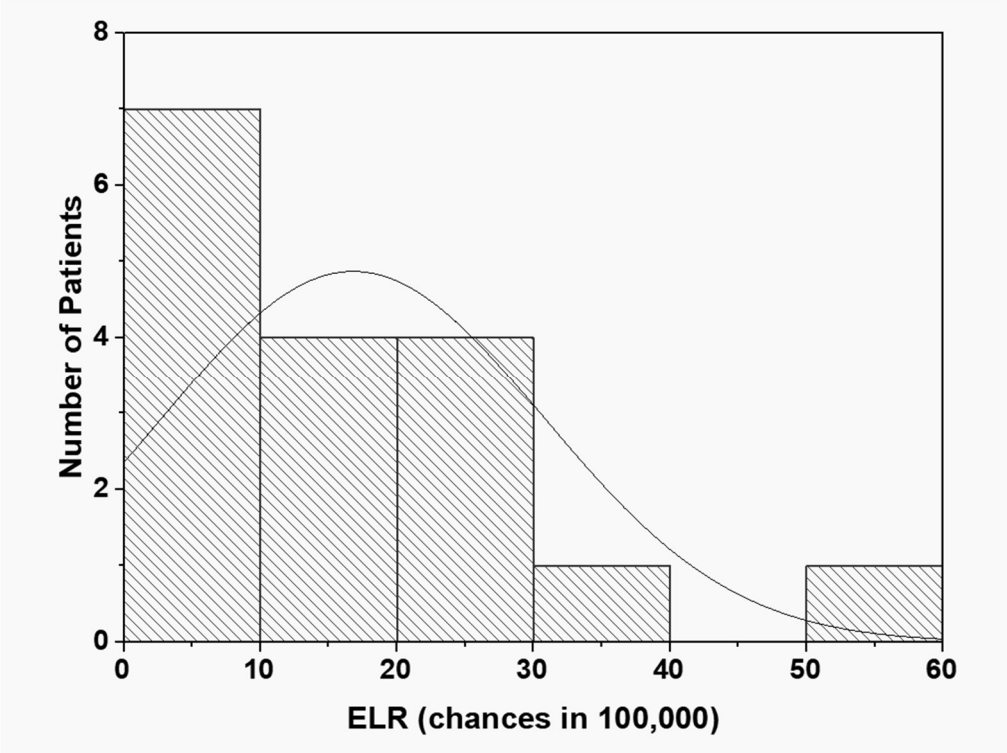

FIGURE 4.9. Non-normal distribution of the excess lifetime risk (chances in 100,000) for newborn patients with normal renal function.

The newborn patients had a mean risk for developing cancer from radiation exposure which was about 12% higher compared to that of the 1-year-old group. There is no significant difference (p-value: 0.75) between the ELR values of both age groups.

Gender-wise, the male patients showed a risk interval between 1.4 per 100,000 persons and 53.0 per 100,000 persons (mean±SD: 14.7±13.5 per 100,000 persons); the female patients had risk values of 6.0-39.4 per 100,000 persons (mean±SD: 20.7±11.4 per 100,000 persons) (Table 4.12).

TABLE 4.12. Gender-dependent excess lifetime risk (chances in 100,000 persons) for the NRF patients (mean±SD).

Gender Group	**Males** (14 patients)	**Females** (6 patients)
Excess Lifetime Risk (in 100,000)	14.7±13.5	20.7±11.4
Lower Bound	7.2	9.8
Upper Bound	22.2	31.6
Age (months)	6.0±3.1	9.3±6.0
CI 95% uncertainty range		

As stated before, the newborn group showed a non-normal distribution of the ELR values, and the majority of the newborn group was males (13 of 14 patients); therefore, as expected, the male group had a non-normally distributed dispersal of the risk values (p-value: 0.006): 10 in 14 patients (71%) had an ELR range of 1.4-21.4 per 100,000 persons; 3 in 14 patients (21%) had ELR values of 21.4-41.4 per 100,000 persons, and 1 in 14 patients (8%) presented an ELR value between 41.4 and 61.4 per 100,000 persons. In contrast, the ELR values of the female patient were normally distributed (p-value: 0.71).

Comparing the male and female patient ELR mean values, there were no significant differences (p-value: 0.41). However, it is worth to observe the discrepancies between these two groups, as they show tendencies which are in agreement with various publications [4, 20, 47]; although less in number, the female patients had a 29% larger risk in comparison with male patients. The incidence of cancer risk is about 35% higher for women, considering comparisons between several average age groups for women and men of the general population [4]. Nonetheless, this risk might vary with the gender-associated cancer type.

The ELR per cancer site values (clustered by gender groups) are stated in Table A5 (Annex). The main critical organs featuring higher risk values for the underlying patient group are the bladder (newborns: 12.9±12.6; 1-year-olds: 12.6±3.5), colon (newborns: 1.0±0.6; 1-year-olds: 0.7±0.2) and kidneys (newborns: 0.5±0.4; 1-year-olds: 0.1±0.1).

In Figures 4.10 and 4.11, the individual absorbed doses, and respective ELR values per 100,000 persons clustered by gender group are shown for the kidneys and bladder, respectively. As expected, the increased organ absorbed doses of both organs lead to a higher risk, independently of the age. Therefore, it can be confirmed that absorbed dose was a primary factor of influence on the ELR values for these two critical organs in the group of patients with NRF.

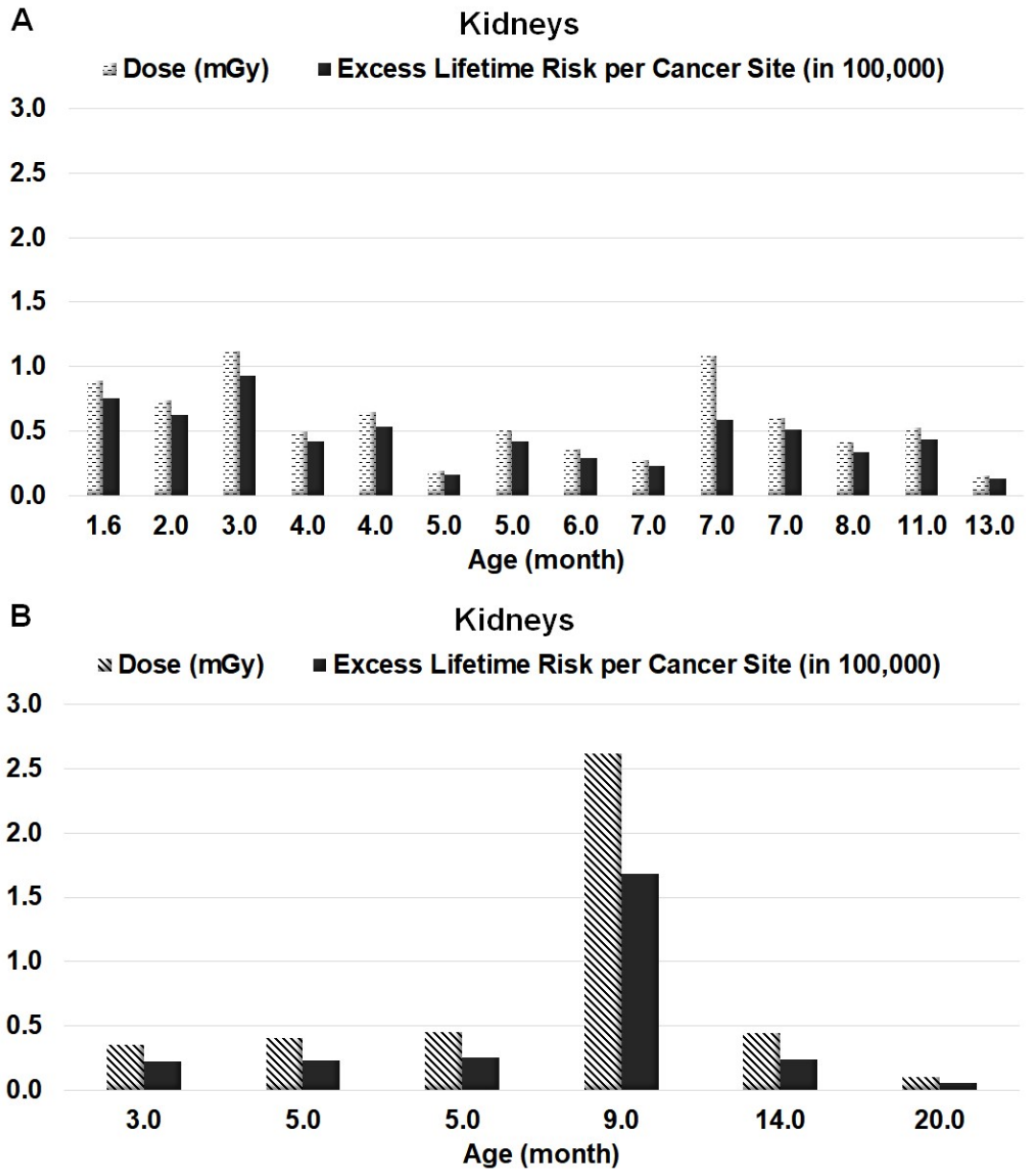

FIGURE 4.10. Kidney absorbed doses (mGy) and excess lifetime risk (chances in 100,000 persons) clustered by age (months). **A:** Male group with 14 patients aged between 2 and 13 months. **B:** Female group with 6 patients aged between 3 and 20 months [15].

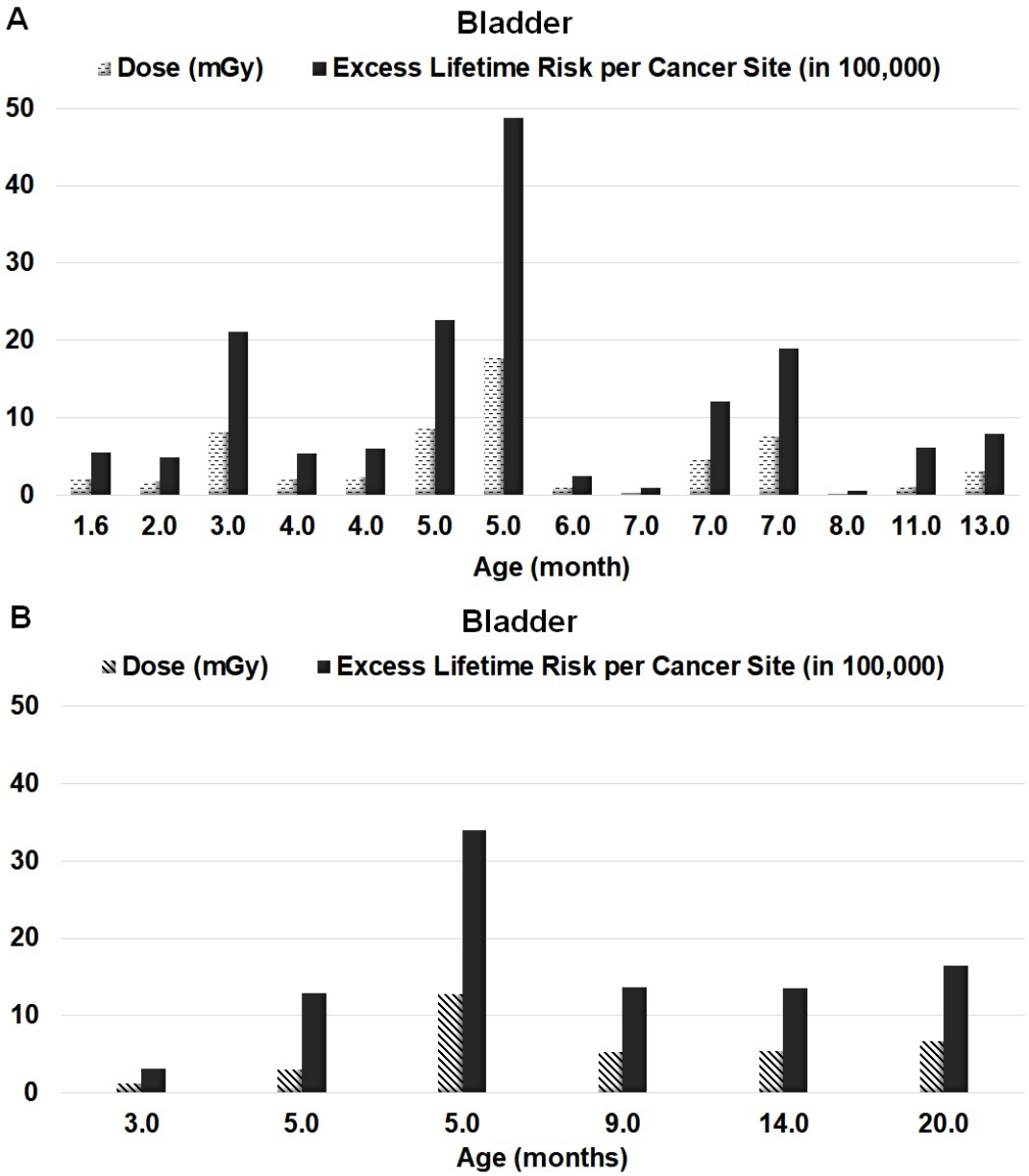

FIGURE 4.11. Bladder absorbed doses (mGy) and excess lifetime risk (chances in 100,000 persons) clustered by age (months). **A:** Male group with 14 patients aged between 2 and 13 months. **B:** Female group with 6 patients aged between 3 and 20 months [15].

The absorbed dose is the main factor of influence on the risk, although there are other factors that also have an impact on the risk. As an example, Figure 4.12 shows the influence of the factor “age” on the ELR per cancer site values; patient P3 (age: 3 months) had a kidney absorbed dose only 4% higher than that of patient P10 (age: 7 months). Nonetheless, the respective risk was considerably higher (37%) for patient P3. As both patients are male with NRF, age can be considered a factor of influence on the risk.

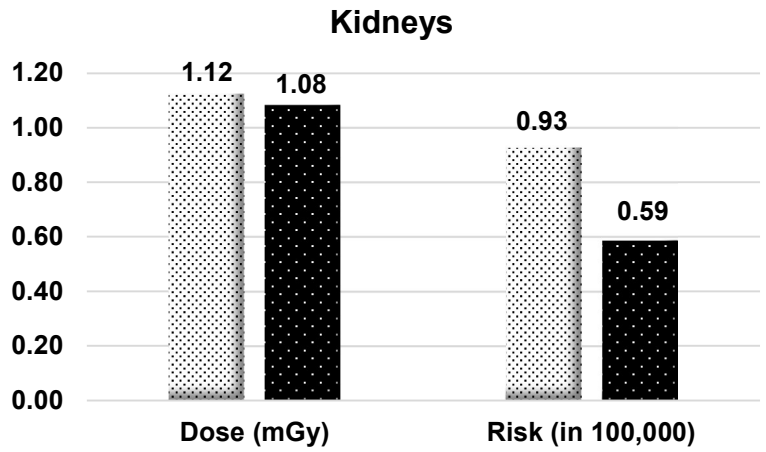

FIGURE 4.12. Kidney absorbed doses (mGy) and excess lifetime risk (chances in 100,000 persons) of patients P3 (3-month-old male, white bars) and P10 (7-month-old, male, black bars).

Figure 4.13 shows an example of the parameter “gender’s” influence on the risk. It compares male and female organ absorbed doses (mGy) of kidneys and thyroid against the ELR (per 100,000 persons). In figure 4.13: A, the female patients showed a larger absorbed dose (22%) in the kidneys compared to male patients, although the respective ELR was only 2% higher for the male patients. This example showed a tendency for “higher” ELR of kidney cancer in males. In figure 4.13: B, the discrepancy between male and female patients was even more evident considering the ELR values for thyroid cancer. The male patients had a 36% higher absorbed dose (mGy) in the thyroid in comparison to the females. However, female patients showed a higher ELR of 70%.

Except for the bladder, all other included organs showed a maximum ELR of 1 per 100,000 persons. The critical organs (highest risk values) were bladder, colon, thyroid, lungs, kidneys, and bone marrow. In comparison, Ozasa et al. [41] presented similar results: besides the organs stated above, breast (female), esophagus, gallbladder, and liver were reported as organs with the highest excess lifetime risk per cancer site. Conversely, rectum, uterus (female), prostate (male), and kidneys (parenchyma) presented no significant excess risk [41].

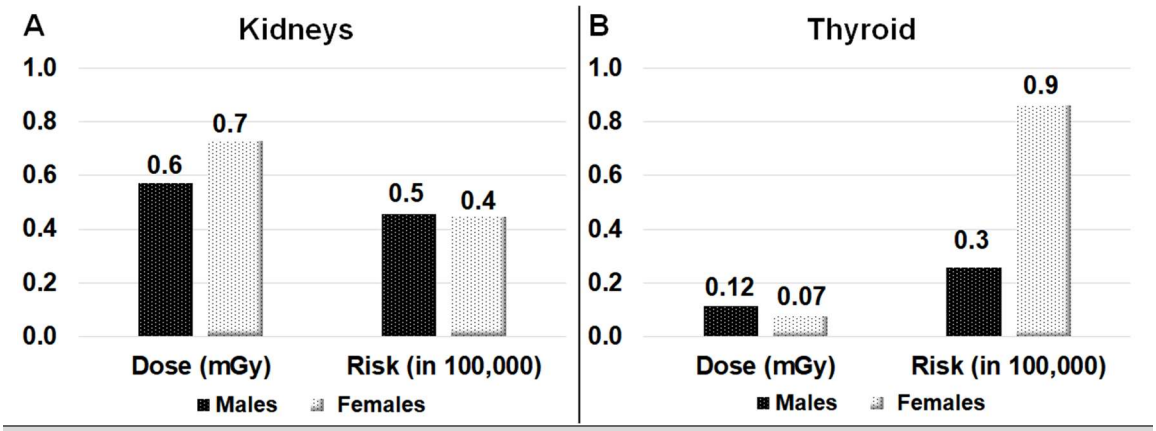

FIGURE 4.13. Organ absorbed doses (mGy) of the male and female patient groups and respective excess lifetime risk (chances in 100,000 persons) **A:** Kidneys. **B:** Thyroid [15].

In addition to the patient data, the ELR (per 100,000 persons) and the ELR per cancer site (per 100,000 persons) (Table A6 in the Annex) were estimated based on the absorbed dose coefficients (mGy/MBq) published by the ICRP [18]. The data information was collected for the adults and the toddlers (1-year-old) with NRF undergoing ^{99m}Tc-MAG3 scans. The resulting values were clustered and analyzed per age and gender. In comparison to the patient data, there was a similar "tendency" of the results (considering the age as a factor of influence on the risk). Collating the ELR from toddlers to adults with the same exposure, toddlers showed a higher risk for both males and females. The ELRs for toddlers was 20.5 per 100,000 persons (CI: 90%; LB:6.9; UB: 45.1) for the males [18] and 21.1 per 100,000 persons (CI: 90%; LB: 7.8; UB: 41.6) for the females [18]. The adults presented ELRs of 8.1 per 100,000 persons (CI: 90%; LB: 2.2; UB: 18.8) for males [18] and 8.1 per 100,000 persons (CI: 90%; LB: 2.6; UB: 17.0) for females [18]. Based on these results, a tendency towards an increased radiation-associated risk for individuals exposed at younger ages is shown (Fig. 4.14).

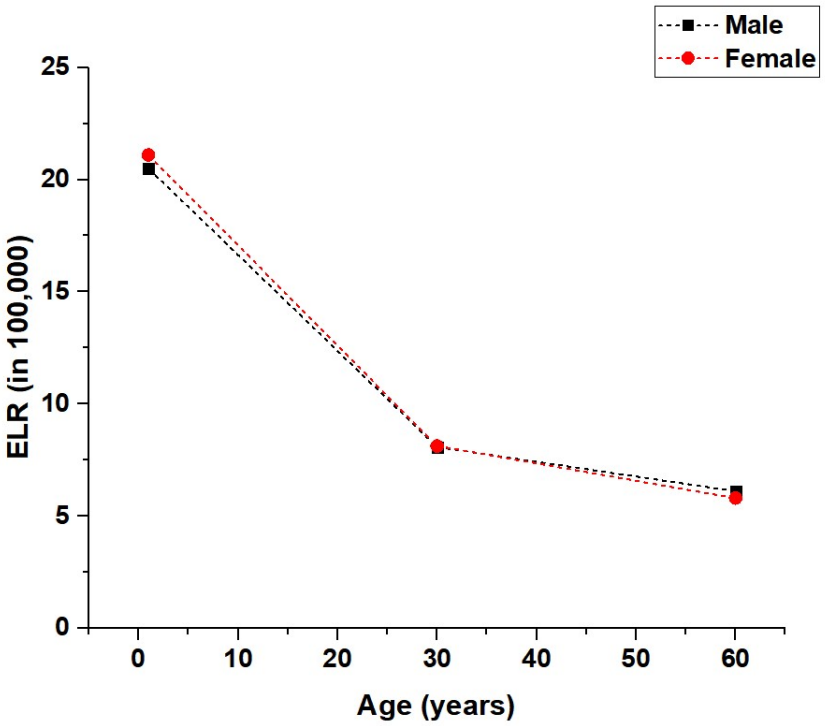

FIGURE 4.14. Risk projections based on ICRP dose information (^{99m}Tc-MAG3) [18] for males and females. ELR (chances in 100,000) as a function of the age (years).

The estimated risk values based on the absorbed dose values by ICRP [18] presented a propensity towards higher ELR (per 100,000 persons) for females compared to males (ICRP [18]: 1-year-old: 3%; adult: 0.5%). This could be associated with the radiosensitivity of gender-specific organs (Table A6) and age, as older ages showed a lower disparity between genders (Fig. 4.14). The male and female patients had an ELR (per 100,000 persons) that was –28.4% and –2.0% lower, respectively, in comparison to the ELR when using the ICRP data.

Besides the previous comparisons, it is essential to understand how meaningful the probability of developing cancer during the lifespan from radiation exposure (ELR) in relation to the likelihood of the general population for developing cancer (PLR) is. Based on information from the US National Cancer Institute's Surveillance Epidemiology and End Results (SEER) of the American Cancer Society (database: 2010 to 2012), the risk for developing cancer is 42% in males, and 38% in females [15, 57]. The overall PLR in males is 2,864 times higher than the mean excess lifetime risk of our patients. Compared to the female population, the mean excess lifetime risk of our patients is approximately 1,817 times lower for all cancer types [57]. Similar results are shown for comparison with the risk database (2012) from the Robert Koch Institute's (RKI) German Centre for Cancer Registry Data [56]. In Germany, the male population showed an overall lifetime risk of 50% for developing cancer [56], which is about 3,440 times higher than the mean excess risk for our male patients. The females have an overall PLR of 43% for developing cancer, which is approximately 2,084 times higher than the excess risk for our female patients [15]. According to these

comparisons, the overall additional risk for the patient group with NRF can be considered very low [15].

4.5.2. Risk Analysis for Patients with Abnormal Renal Function

Table 4.13 shows results of the excess lifetime risk (ELR), namely the lower and upper bounds (limits) of the respective CI for the risk probability of patients with abnormal renal function (ARF), clustered per age. As previously reported, there is only one 1-year-old patient in the ARF group (P34). Therefore, the values were reported individually for this patient as the RadRAT tool risk projection output (CI: 90% uncertainty range). For the sake of consistency with the prior chapters, except for the 1-year-old, the CI (95% of uncertainty range) and statistical tests (reference level: 0.05) remained as before for all the other groups (clustered by age, gender, and renal function).

The mean ELR (per 100,000 persons) for developing cancer from radiation exposure for the newborns ranged between 0.9 and 64.5 per 100,000 persons (mean±SD: 29.6±19.4 per 100,000 persons); the mean ELR (per 100,000 persons) for the 1-year-olds is shown in the Table 4.13.

TABLE 4.13 Age-dependent excess lifetime risk (chances in 100,000 persons) for the ARF patients (mean±SD).

Age Group	*Newborns (1.3-8.0 months)	+1-year-olds	*ALL
Excess Lifetime Risk (in 100,000)	29.2±18.7	22.9	29.1±18.8
Lower Bound	18.4	9.1	18.3
Upper Bound	41.4	44.1	39.9
Age (months)	4.0±2.4	12.0	7.0±4.5

*CI: 95% uncertainty range
+Output values of the RadRAT tool [46]

The newborn group showed normally-distributed ELR (per 100,000 persons) values (p-value: 0.93).

The ELR (per 100,000 person) for the male patients (Table 4.14) was between 0.9 and 64.5 per 100,000 persons (mean±SD: 25.9±17.1 per 100,000 persons); furthermore, the female patients (Table 4.14) showed ELR values (per 100,000 person) between 14.3 and 56.5 per 100,000 persons (mean±SD: 41.4±19.2 per 100,000 persons).

TABLE 4.14. Gender-dependent excess lifetime risk (chances in 100,000 persons) for the ARF patients (mean±SD).

Gender Group	**Males** (11 patients)	**Females** (3 patients)
Excess Lifetime Risk (in 100,000)	25.9±17.1	41.4±19.2
Lower Bound	14.4	–6.3
Upper Bound	37.3	89.0
Age (months)	4.5±2.3	2.5±1.7
CI: 95% uncertainty range		

TABLE 4.15. The excess lifetime risk (chances in 100,000 persons) for the ARF patients clustered by renal abnormality type (mean±SD).

Abnormal Renal Function	**Unilateral** (8 patients; M: 6; F: 2)	**Bilateral** (6 patients; M: 5; F: 1)
Excess Lifetime Risk (in 100,000)	25.6±20.6	34.0±14.4
Lower Bound	8.4	18.9
Upper Bound	42.8	49.1
Age (months)	4.0±2.4	6.4±3.2

CI: 95% uncertainty range
M = Males; F = Females

Gender-wise, the ARF patients showed a similar tendency as the NFR patients; the ARF patients' results showed a similar tendency. Although fewer in numbers, the females presented a 37% higher ELR (per 100,000 persons) in comparison to the male patients. The ELRs (per 100,000 persons) of male and female patients were normally distributed (p-values of 0.21 and 0.13, respectively). There was no significant difference (p-value: 0.22) between the risk of the gender groups.

Table A7 (Annex) shows the ELRs per cancer site (per 100,000 persons) clustered by gender are shown; the organs that presented higher risk values (ELR: ≥ 1 per 100,000 persons) were colon, bladder, kidneys and red bone marrow for the male ARF patients. Regarding the female ARF patients, the organs with ELR ≥ 1 (per 100,000 persons) were the stomach, colon, bladder, kidneys, thyroid, red bone marrow, ovaries, breast, and uterus (Table A7).

Figure 4.15 shows a comparison between the ARF patients' organ doses (mGy) and risk (per 100,000 persons) clustered by gender: Female patients had higher kidney doses (22%), but a lower risk (–3%) when compared to the male patients, confirming gender as an impact factor on the risk values. Nevertheless, the main element of influence on the risk for the kidneys of both male and female ARF patients was the absorbed dose (mGy).

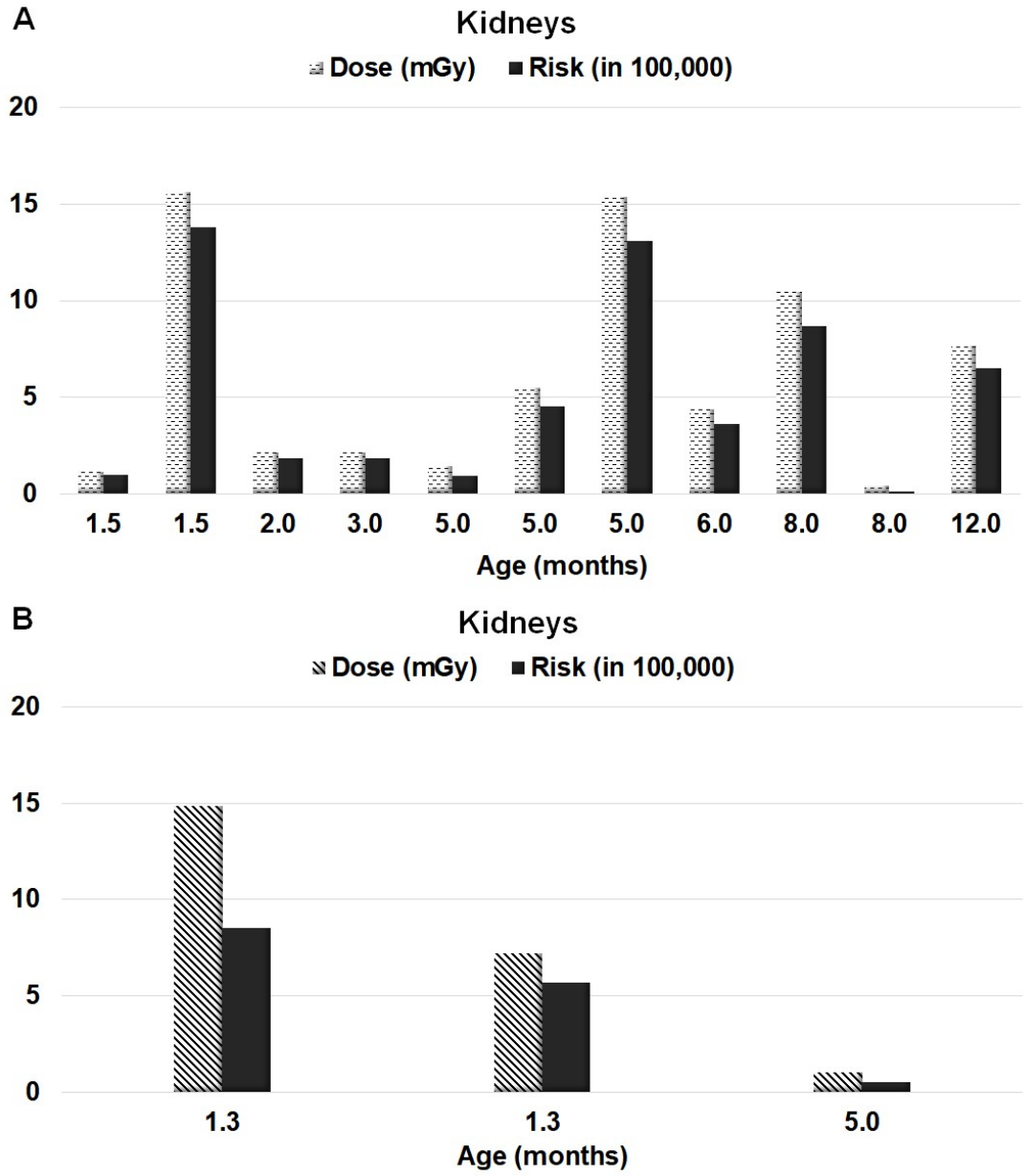

FIGURE 4.15. Bladders' absorbed doses (mGy) and excess lifetime risk (chances in 100,000 persons) clustered by age (months). **A:** Male group with 11 patients aged between 1.5 and 12.0 months. **B:** Female group with 3 patients aged between 1.3 and 5.0 months.

Furthermore, Figure 4.16 presents the bladder doses (mGy) and the respective ELR (per 100,000 persons) clustered by gender. Females had a higher bladder dose (38.4%) and risk (38.3%) than male patients. As for the kidneys, the dose was the main impact factor for the bladder ELR.

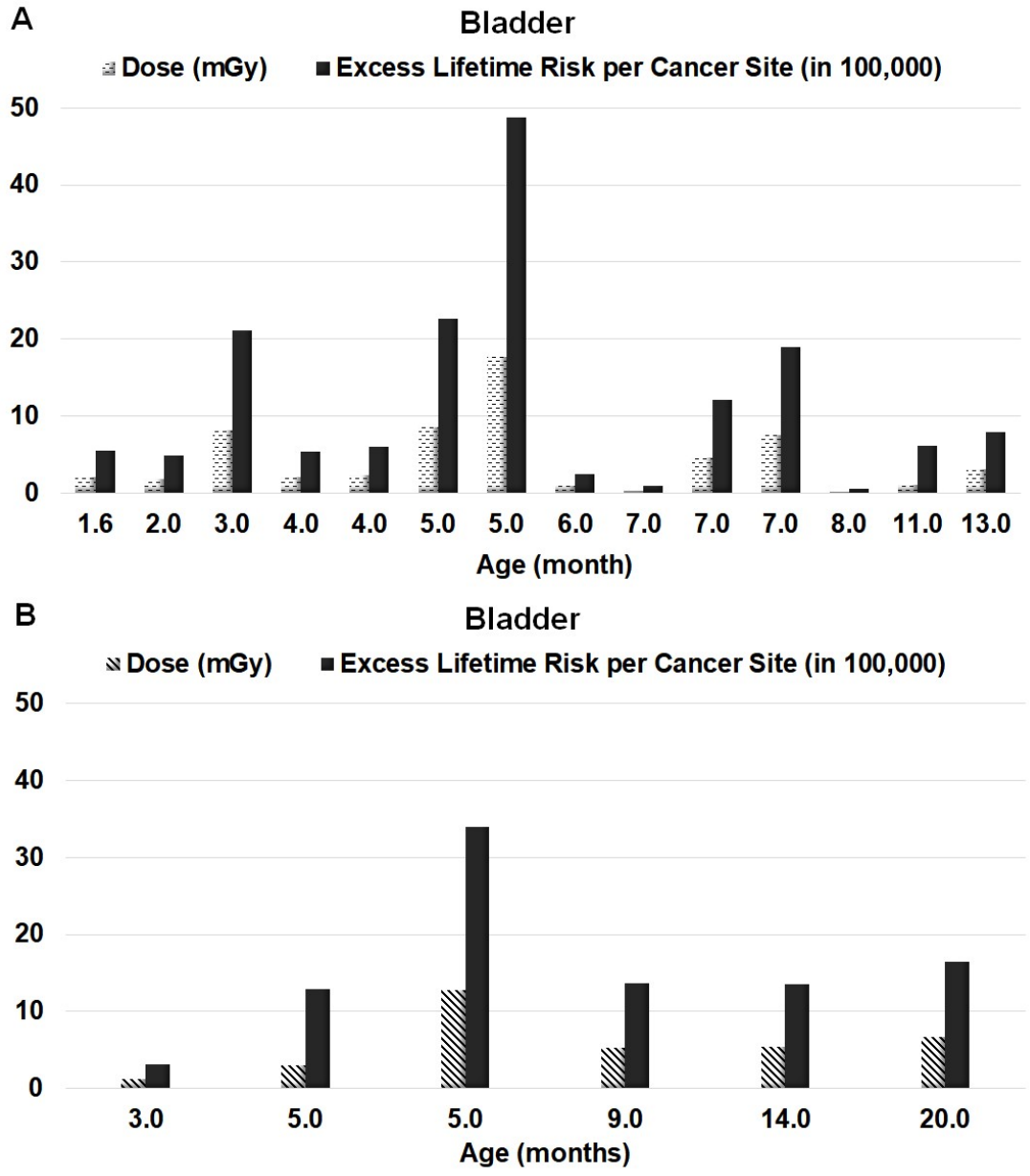

FIGURE 4.16. Bladders' absorbed doses (mGy) and excess lifetime risk (chances in 100,000 persons) clustered by age (months). **A:** Male group with 11 patients aged between 1.5 and 12 months. **B:** Female group with 3 patients aged between 1.3 and 5.0 months.

Based on the risk data provided by SEER [57], the overall PLR for U.S. males is approximately 1,621 times higher than the mean ELR (per 100,000 persons) of our male patient group; in comparison to the female population, the mean ELR (per 100,000 persons) of the female patients is about 908 times lower for all cancer types [57]. The results were similar for the German population [56]: The ELR for the male population was around 1,947 times higher compared to the ELR (per 100,000 persons) for our male patients. Regarding the females, the German PLR was about 1,042 higher than the ELR (per 100,000 persons) for our female patients [56].

Table 4.15 expresses the ELR (per 100,000 persons) for the patients with ARF clustered by the renal abnormality.

The BARF patients had a mean ELR (per 100,000 persons) which was about 25% higher than that of patients with UARF; this result was expected since the BARF patients, in addition to the slower biokinetic showed higher organ doses (mGy) (sub-chapter 4.4.1). The ELR was normally distributed for the patients with UARF and BARF with p-values of 0.21 and 0.19, respectively. According to a statistical test (T-test), there was no significant difference (p-value: 0.27) between the BARF and UARF groups' ELR.

The majority of ELR (per 100,000 persons) per cancer site was less than 1 per 100,000 persons for UARF and BARF patients, except for the following critical organs: colon (UARF: 1.2 per 100,000 persons; BARF: 1.5 per 100,000 persons), kidneys (UARF: 1.9 per 100,000 persons; BARF: 9.1 per 100,000 persons), bladder (UARF: 19.9 per 100,000 persons; BARF: 20.0 per 100,000 persons), ovaries (UARF: 1.2 per 100,000 persons; BARF: 1.5 per 100,000 persons). Figure 4.17 shows a comparison between kidneys' absorbed doses (mGy) and the respective ELR (per 100,000 persons); clearly, the main impact factor was the kidneys' absorbed dose (mGy). The influence of gender was also observed in Figure 4.17 (B). The youngest patient is female with a kidney dose of about 14.8 mGy, the second youngest patient in this group (BARF) is a male who has a similar age and kidney dose (15.6 mGy). However, the ELR value was about 38% higher for the male patient. This risk tendency is in

agreement with the overall PLR for males that have a 40% higher risk of developing cancer in comparison to the females [56, 57].

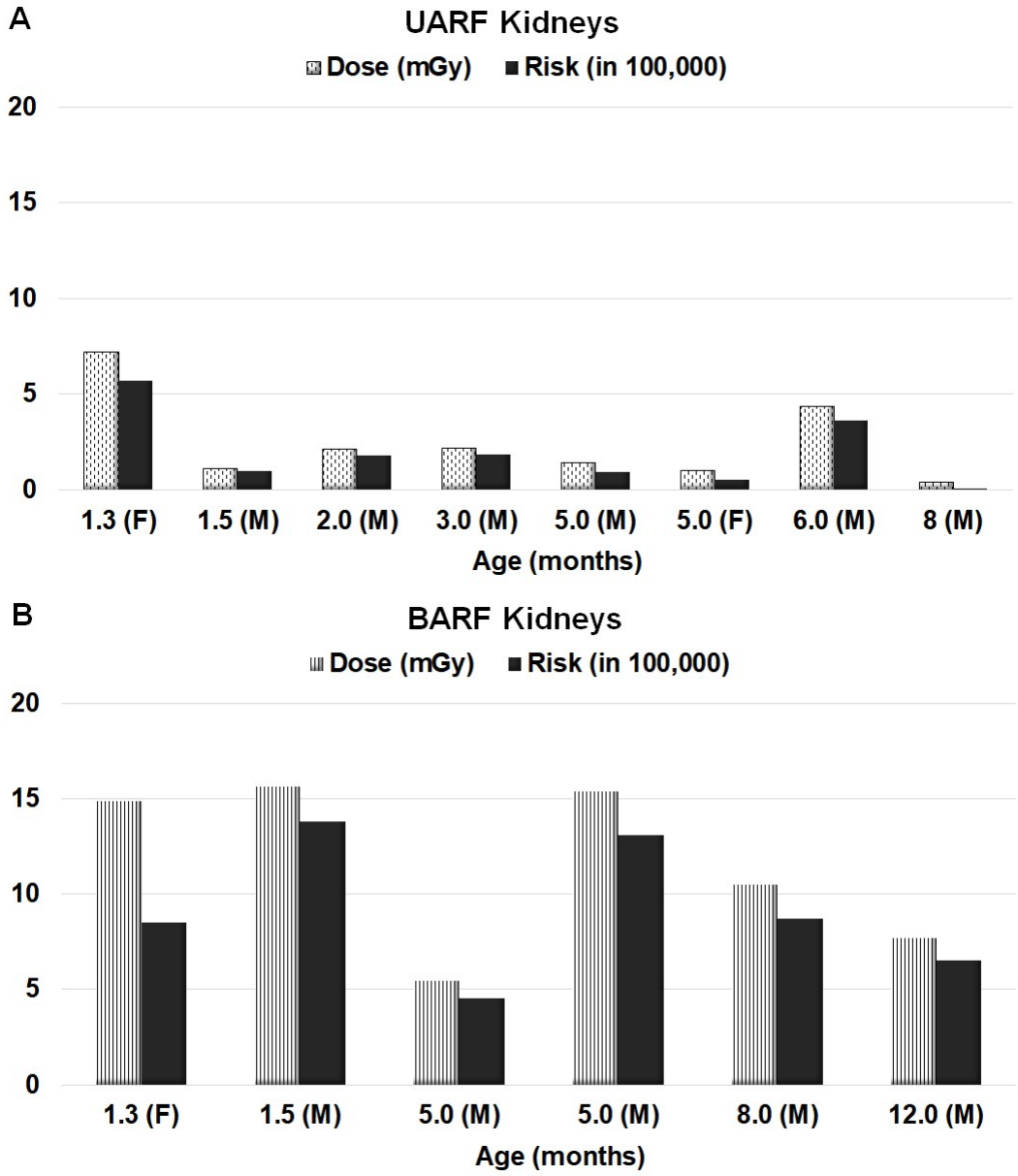

FIGURE 4.17. Kidney absorbed doses (mGy) and excess lifetime risk (chances in 100,000 persons) clustered by age (months) and gender (M: male; F: female). **A:** 8 UARF patients aged between 1.3 and 8 months. **B:** 6 BARF patients aged between 1.3 and 12.0 months.

Figure 4.18 shows the estimated risk values calculated based on ICRP absorbed dose data [18] for unilateral renal blockage. There was a tendency towards higher ELR (per 100,000 persons) for males compared to females (1-year-old: 12%; 30-year-old adult: 17%; 60-year-old adult: 14%). This tendency may be related to the combination of renal abnormality with a gender-related risk which is higher for males [56, 57].

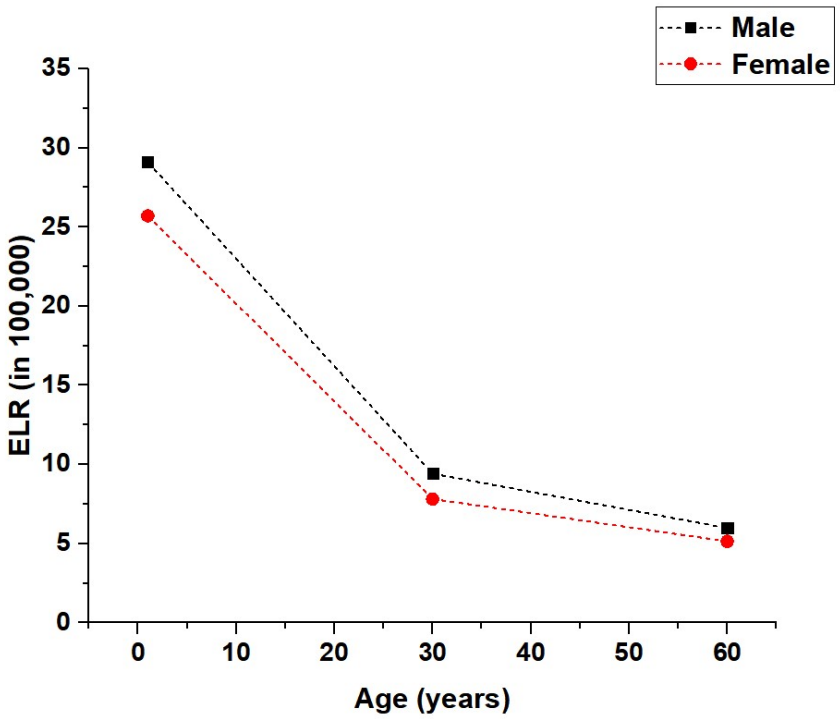

FIGURE 4.18. Risk projections based on ICRP dose information (^{99m}Tc-MAG3) for all males and females with unilateral abnormal renal function [18]. The ELR (chances in 100,000) is depicted as a function of the age (years).

Figure 4.19 shows the estimated risk values calculated based on ICRP data [18] for renal abnormal renal function (bilateral). The ELR (per 100,000 persons) differences between genders were more considerable for 1-year-olds with females showing a higher risk (10%). In contrast, the adult ages presented small differences when comparing males to females (30-years-old adult: 2%; 60-years-old adult: –3.6%). In comparison to BARF, the UARF case showed higher risk values for males and females at all ages (Fig. 4.18 and 4.19), which can be associated with the slower biokinetics of the UARF[18]. As expected, for the cases of UARF and BARF, the ELR values decreased with the increase of the age at exposure.

Tables A8 and A9 (Annex) express the ELR per cancer site for renal blockage (unilateral) and abnormal renal function (bilateral) calculated based on ICRP values [18]. The organs with higher risk (ELR ≥ 1 per 100,000 persons) for the UARF case were: kidneys, bladder, lungs, and red marrow for the males; kidneys, bladder, lungs, stomach, and breast for the female. Moreover, for the BARF case, the organs which presented a higher risk (ELR ≥ 1 per 100,000 persons) were: kidneys, bladder, and colon for the males; kidneys, bladder, colon, lungs, thyroid, and breast for the females.

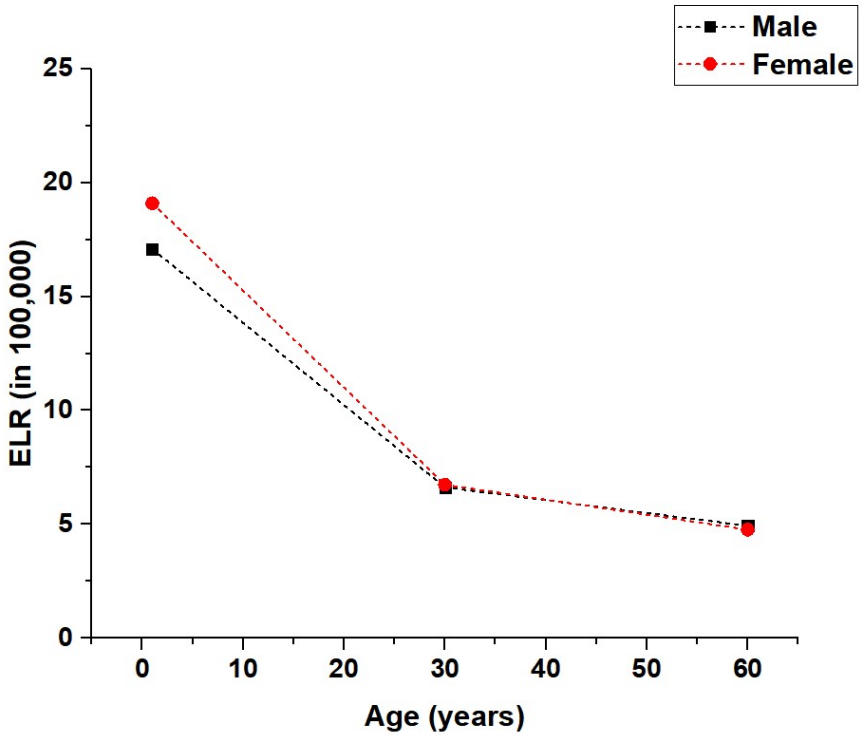

FIGURE 4.19. Risk projections based on ICRP dose information (^{99m}Tc-MAG3) [18] for males and females with abnormal renal function. The ELR (chances in 100,000) is depicted as a function of the age (years).

5. CONCLUSION

In this work, we retrospectively derived new data on biokinetics and dosimetry for infants with normal kidney function after undergoing renal ^{99m}Tc-MAG3 scans. In addition, we analyzed the associated age- and gender-specific excess lifetime risk associated with ionizing radiation. The absorbed and effective doses were low when using the EANM pediatric dosage card for calculating the injected activities. The radiation-associated stochastic risk increased with the organ doses considering age- and gender-specific influences. In comparison with adults, the pediatric patient data showed a slightly higher radiation-related risk (excess lifetime risk) for the same absorbed doses. Overall, however, the lifetime radiation risk associated with ^{99m}Tc-MAG3 scans is very low when compared to the general population's risk for developing cancer.

It is important to highlight that our method features a risk-adapted, TIAC-based approach applied for organ-specific absorbed dose calculations, instead of only reporting effective dose values obtained by multiplying the administered activities with constant values taken from ICRP tables such as ICRP 128. This approach might lead to improvements in future recommendations for pediatric dosages in nuclear medicine diagnostics.

6. REFERENCES

1. Lassmann, M. and G. Pedroli, *Dose optimization in nuclear medicine.* Clinical and Translational Imaging, 2016. **4**(1): p. 3-4.
2. Fahey, F.H., et al., *Standardization of administered activities in pediatric nuclear medicine: a report of the first nuclear medicine global initiative project, part 1-statement of the issue and a review of available resources.* J Nucl Med, 2015. **56**(4): p. 646-51.
3. Schauer, D.A. and O.W. Linton, *National Council on Radiation Protection and Measurements report shows substantial medical exposure increase.* Radiology, 2009. **253**(2): p. 293-6.
4. Fahey, F.H., et al., *Dose Estimation in Pediatric Nuclear Medicine.* Semin Nucl Med, 2017. **47**(2): p. 118-125.
5. ICRP, ICRP publication 103.The 2007 Recommendations of the International Commission on Radiological Protection. Ann ICRP, 2007. 37(2-4): p. 1-332.
6. International Atomic Energy Agency, and D. L. Bailey. Nuclear Medicine Physics: A Handbook for Teachers and Students. 2015.
7. ICRP, ICRP publication 60. 1990 recommendations of the International Commission on Radiological Protection. Ann ICRP, 1991. 21(1-3).
8. Fahey, F.H., et al., *Standardization of Administered Activities in Pediatric Nuclear Medicine: A Report of the First Nuclear Medicine Global Initiative Project, Part 2-Current Standards and the Path Toward Global Standardization.* J Nucl Med, 2016. **57**(7): p. 1148-57.
9. Gordon, I., et al., *Guidelines for standard and diuretic renogram in children.* Eur J Nucl Med Mol Imaging, 2011. **38**(6): p. 1175-88.
10. ICRP, ICRP publication 73. Radiological Protection and Safety in Medicine. Ann. ICRP, 1996. 26 (2).
11. Lassmann, M., et al., *The new EANM paediatric dosage card.* Eur J Nucl Med Mol Imaging, 2008. **35**(9): p. 1748.
12. Lassmann, M. and S.T. Treves, *Pediatric Radiopharmaceutical Administration: harmonization of the 2007 EANM Paediatric Dosage Card (Version 1.5.2008) and the 2010 North American Consensus guideline.* Eur J Nucl Med Mol Imaging, 2014. **41**(8): p. 1636.
13. Stabin, M., Taylor, A., Conway, J., Eshima, D., Wooten, W., Halama J. Radiation Dosimetry for Tc-99m-MAG3 in Adults and Children. In: Stelson A, Watson E, editors. Fifth International Radiopharmaceutical Dosimetry Symposium. Oak Ridge, TN: Oak Ridge Associated Universities; 1992. p. 434-43.
14. Eberlein, U., et al., *Biokinetics and dosimetry of commonly used radiopharmaceuticals in diagnostic nuclear medicine - a review.* Eur J Nucl Med Mol Imaging, 2011. **38**(12): p. 2269-81.
15. Soares Machado, J., et al., *Biokinetics, dosimetry, and radiation risk in infants after ^{99m}Tc-MAG3 scans.* EJNMMI Res, 2018. **8**(1): p. 10.
16. Tauhata, L., P.A. Salati, and A.R. Di Prinzio, *Radioprotecão e dosimetria: fundamentos*. 2003: CBPF. Retrieved [2018] from https://inis.iaea.org/collection/NCLCollectionStore/_Public/45/073/45073465.pdf.
17. International Atomic Energy Agency. Radiation Biology: A Handbook for Teachers and Students. Vienna: International Atomic Energy Agency, 2010.
18. ICRP, ICRP publication 128. Radiation Dose to Patients from Radiopharmaceuticals: A Compendium of Current Information Related to Frequently Used Substances. Ann. ICRP, 2015. 44(2S).
19. ICRU, International Commission on Radiation Units and Measurements. Fundamental Quantities and Units for Ionizing Radiation. Oxford: Oxford University Press, 2011.
20. Stabin, M.G., *Radiation Protection and Dosimetry: An Introduction to Health Physics*. 2007: Springer New York.

21. Mattsson, S., et al., *Radiation Dose to Patients from Radiopharmaceuticals: a Compendium of Current Information Related to Frequently Used Substances.* Ann ICRP, 2015. **44**(2 Suppl): p. 7-321
22. International Commission on Radiological Protection. Radiation Dose to Patients from Radiopharmaceuticals: Addendum 2 to ICRP Publication 53. Oxford: Published for the International Commission on Radiological Protection by Pergamon, 1999.
23. International Atomic Energy Agency. IAEA Human Health Series. Vienna: International Atomic Energy Agency, 2009. Retrieved [2017] from <http://www-pub.iaea.org/MTCD/publications/ProcessSeries.asp?id=140>.
24. Even-Sapir, E., et al., *^{18}F-Fluoride positron emission tomography and positron emission tomography/computed tomography.* Semin Nucl Med, 2007. **37**(6): p. 462-9.
25. Boeno, N.; Machado Nabinger, P.; Minghelli Schmitt, V.; (03 de setiembre de 2014). Revisão comparativa dos ^{68}Ga-DOTA-peptídeos. Alasbimn Journal, ISSN: 0717 - 4055. URL: http://www.alasbimnjournal.net/a/133.
26. Virgolini, I., et al., *Procedure guidelines for PET/CT tumour imaging with ^{68}Ga-DOTA-conjugated peptides: ^{68}Ga-DOTA-TOC, ^{68}Ga-DOTA-NOC, ^{68}Ga-DOTA-TATE.* Eur J Nucl Med Mol Imaging, 2010. **37**(10): p. 2004-10.
27. Machado, J.S., et al., *Recommended administered activities for ^{68}Ga-labelled peptides in paediatric nuclear medicine.* Eur J Nucl Med Mol Imaging, 2016. **43**(11): p. 2036-9.
28. Wester, H.J., et al., *Disclosing the CXCR4 expression in lymphoproliferative diseases by targeted molecular imaging.* Theranostics, 2015. **5**(6): p. 618-30.
29. Herrmann, K., et al., *Biodistribution and radiation dosimetry for the chemokine receptor CXCR4-targeting probe ^{68}Ga-pentixafor.* J Nucl Med, 2015. **56**(3): p. 410-6.
30. Piepsz, A., et al., *Technetium-99m-DMSA imaging and the obstructed kidney.* Clin Nucl Med, 1986. **11**(6): p. 389-91.
31. The International Commission on Rad.Protection, 2003. "The evolution of the system of radiological protection: the justification for new ICRP recommendations." Journal of Radiological Protection. 23, no. 2: 129-142.
32. *Advice on the implications of the conversion coefficients for external radiations published in ICRP Publication 74 and in ICRU report 57. Memorandum from the British Committee on Radiation Units and Measurements.* Br J Radiol, 1997. **70**(840): p. 1270-3.
33. National Institute of Diabetes and Digestive and Kidney Disease. Urine Blockage in Newborns. 2013. Retrieved [2017] from https://www.niddk.nih.gov/health-information/urologic-diseases/urine-blockage-newborns.
34. Hubbell, J.H.a.S., S.M., *X-Ray Mass Attenuation Coefficients - Tables of X-Ray Mass Attenuation Coefficients and Mass Energy-Absorption Coefficients (version 1.4)*. 1995, Originally published as NISTIR 5632, National Institute of Standards and Technology, Gaithersburg, MD (1995): United States of America. p. 111.
35. National Research Council. Health Risks from Exposure to Low Levels of Ionizing Radiation BEIR VII Phase 2. Washington, DC: National Acad. Press, 2006.
36. Jacobs, F., et al., *Optimised tracer-dependent dosage cards to obtain weight-independent effective doses.* Eur J Nucl Med Mol Imaging, 2005. **32**(5): p. 581-8.
37. Snyder, W. S. "S, Absorbed Dose Per Unit Cumulated Activity for Selected Radionuclides and Organs." New York: Society of Nuclear Medicine, 1975.
38. Stabin, MG, RB Sparks, and E Crowe. "Olinda/exm: the Second-Generation Personal Computer Software for Internal Dose Assessment in Nuclear Medicine." Journal of Nuclear Medicine: Official Publication, Society of Nuclear Medicine. 46.6 (2005): 1023-7.
39. Loevinger, R., et al., *MIRD Primer for Absorbed Dose Calculations*. 1988: Society of Nuclear Medicine.
40. Fahey, F. and M. Stabin, *Dose optimization in nuclear medicine.* Semin Nucl Med, 2014. **44**(3): p. 193-201.
41. Ozasa, K., et al., *Studies of the mortality of atomic bomb survivors, Report 14, 1950-2003: an overview of cancer and noncancer diseases.* Radiat Res, 2012. **177**(3): p. 229-43.

42. Preston, D.L., et al., *Effect of recent changes in atomic bomb survivor dosimetry on cancer mortality risk estimates.* Radiat Res, 2004. **162**(4): p. 377-89.
43. Little, M.P., *Heterogeneity of variation of relative risk by age at exposure in the Japanese atomic bomb survivors.* Radiat Environ Biophys, 2009. **48**(3): p. 253-62.
44. Council, N.R., *Health Effects of Exposure to Low Levels of Ionizing Radiations: Time for Reassessment?* 1998, Washington, DC: The National Academies Press. 86.
45. Simon, A. K., Hollander, G. A., McMichael, A. 2015. "Evolution of the Immune System in Humans from Infancy to Old Age." Proceedings of the Royal Society B: Biological Sciences. 282, no. 1821: 20143085.
46. Berrington de Gonzalez, A., et al., *RadRAT: a radiation risk assessment tool for lifetime cancer risk projection.* J Radiol Prot, 2012. **32**(3): p. 205-22.
47. Tran-Gia, J., Schlogl, S. and Lassmann, M. *Design and Fabrication of Kidney Phantoms for Internal Radiation Dosimetry using 3D Printing Technology.* J Nucl Med, 2016.
48. Bouchet, L.G., et al., *MIRD Pamphlet No 19: absorbed fractions and radionuclide S values for six age-dependent multiregion models of the kidney.* J Nucl Med, 2003. **44**(7): p. 1113-47.
49. BfS, B.f.S.- *Bekanntmachung der aktualisiert diagnostischen referenzwerte für nuklearmedizinische Untersuchungen.* 2012. p. 6. Retrieved [2016] from https://www.bfs.de/SharedDocs/Downloads/BfS/DE/fachinfo/ion/drw-nuklearmedizin.pdf?__blob=publicationFile&v=4.
50. Gelfand M.J., Parisi M.T., and Treves S.T. 2011. "Pediatric Radiopharmaceutical Administered Doses: 2010 North American Consensus Guidelines". Journal of Nuclear Medicine. 52, no. 2: 318-322.
51. Cristy, M., Eckerman K.F. Specific absorbed fractions of energy at various ages from internal photon sources. Oak Ridge, TN: Oak Ridge National Laboratory. ORNL/TM-8381/V1. 1987.
52. ICRP, ICRP Publication 53. Radiation Dose to Patients from Radiopharmaceuticals. Ann. ICRP, 1988. 18(1-4).
53. ICRP, ICRP Publication 80. Radiation Dose to Patients from Radiopharmaceuticals. Sage Publications Ltd, 2015.
54. United Nations. Effects of Ionizing Radiation: UNSCEAR 2006 Report to the General Assembly, with Scientific Annexes. Vol. II, Vol. II. New York: United Nations, 2009.
55. UN Scientific Committee on the Effects of Atomic Radiation (54th sess. : 2006 : Vienna). United Nations Scientific Committee on the Effects of Atomic Radiation: Report on the 54th Session (29 May-2 June 2006). New York: UN, 2006.
56. Cancer in German 2011/2012. 10th edition. Robert Koch Institute (ed.) and Association of Population-based Cancer Registries in Germany (ed.). Berlin, 2016 Retrieved [2017] from http://www.krebsdaten.de/Krebs/EN/Content/Publications/Cancer_in_Germany/cancer_chapters_2011_2012/cancer_germany_2011_2012.pdf?__blob=publicationFile.
57. American Cancer Society. Lifetime Risk of Developing or Dying from Cancer. 2016. Retrieved [2017] from https://www.cancer.org/cancer/cancer-basics/lifetime-probability-of-developing-or-dying-from-cancer.html#written_by.
58. Sgouros, G., et al., *An approach for balancing diagnostic image quality with cancer risk: application to pediatric diagnostic imaging of ^{99m}Tc-dimercaptosuccinic acid.* J Nucl Med, 2011. **52**(12): p. 1923-9.
59. Scott, J.E., et al., *Ultrasound measurement of renal size in newborn infants.* Arch Dis Child, 1990. **65**(4 Spec No): p. 361-4.
60. Yang, S.S. and S.J. Chang, *The effects of bladder over distention on voiding function in kindergarteners.* J Urol, 2008. **180**(5): p. 2177-82; discussion 2182.
61. Sandstrom, M., et al., *Comparative biodistribution and radiation dosimetry of ^{68}Ga-DOTATOC and ^{68}Ga-DOTATATE in patients with neuroendocrine tumors.* J Nucl Med, 2013. **54**(10): p. 1755-9.
62. Hartmann, H. et al., Radiation Exposure of Patients During ^{68}Ga-DOTATOC PET/CT Examinations. Nuklearmedizin. Nuclear Medicine, 2009. 48, no. 5: 201.

63. Almen, A. and S. Mattsson, *The radiation dose to children from X-ray examinations of the pelvis and the urinary tract.* Br J Radiol, 1995. **68**(810): p. 604-13.

III. ANNEX

In this section are provided additional results for organ sizes, absorbed dose coefficients, absorbed doses, time-integrated activity coefficients (^{68}Ga peptides), and risk assessment (excess lifetime risk per cancer site).

TABLE A1. Patient-specific organ sizes clustered by renal function.

Patient	Age (Months)	Anatomical Data						
		Right Kidney			Left Kidney			Bladder
		RF	Depth (cm)	Volume (ml)	RF	Depth (cm)	Volume (ml)	Volume (ml)
P1	1.6	N	1.6	17.0	N	2.7	20.0	34.0
P2	2.0	N	2.5	28.1	N	2.5	24.3	35.0
P3	3.0	N	2.3	19.1	N	2.2	14.1	37.5
P4	3.0	N	2.6	18.0	N	2.0	15.6	11.6
P5	4.0	N	2.1	19.0	N	2.6	11.4	40.0
P6	4.0	N	2.3	24.0	N	2.3	19.0	11.0
P7	5.0	N	2.6	18.0	N	2.5	18.0	42.5
P8	5.0	N	2.3	29.1	N	2.3	19.8	42.5
P9	5.0	N	2.7	18.0	N	2.4	17.0	42.5
P10	5.0	N	2.5	16.7	N	2.4	15.0	5.0
P11	6.0	N	2.7	28.1	N	2.5	24.3	45.0
P12	7.0	N	2.7	19.0	N	2.1	20.0	6.0
P13	7.0	N	2.4	14.0	N	2.7	20.0	51.0
P14	7.0	N	2.4	31.0	N	2.3	29.0	19.0
P15	8.0	N	1.6	17.0	N	1.7	20.0	30.0
P16	9.0	N	3.2	19.3	N	2.7	25.6	52.5
P17	11.0	N	3.0	25.0	N	2.2	23.0	19.0
P18	13.0	N	1.7	60.0	N	1.8	46.0	92.5
P19	14.0	N	1.8	20.0	N	2.6	21.0	60.0
P20	20.0	N	2.2	30.0	N	2.8	35.0	65.0
P21	1.3	AB	1.6	12.0	AB	2.1	12.0	14.0
P22	1.3	N	2.5	34.0	AB	2.1	12.0	12.0
P23	1.5	AB	2.8	41.0	N	2.0	21.0	6.0
P24	1.5	AB	2.5	36.0	AB	2.8	26.0	20.0
P25	2.0	N	2.9	37.0	AB	2.6	27.0	8.9
P26	3.0	N	2.0	20.0	AB	2.1	15.0	4.0
P27	5.0	AB	2.2	15.0	N	2.5	14.0	13.0
P28	5.0	AB	2.5	19.0	N	2.9	27.0	9.0
P29	5.0	AB	2.9	27.0	AB	2.2	25.0	6.0
P30	5.0	AB	2.6	26.0	AB	2.6	9.0	6.3
P31	6.0	AB	2.4	23.0	N	3.0	22.0	15.0
P32	5.0	AB	2.4	28.0	AB	2.4	28.0	3.0
P33	8.0	AB	2.8	26.0	N	2.7	31.0	8.0
P34	12.0	AB	2.5	34.0	AB	2.2	24.0	53.2
MEAN±SD	6.0±4.1		2.4±0.4	25.0±9.4		2.4±0.3	21.5±7.3	27.1±21.7

RF = Renal Function; N = Normal; AB = Abnormal
As the individual patients' depth information for bladder could not be extracted from the ultrasound exams, it was applied 5.0 cm for all patients

TABLE A2. Organ-specific absorbed dose coefficients (mGy/MBq) and effective dose coefficients (mSv/MBq) for patients with normal renal function (clustered into age groups).

Age group	Patient	Absorbed Dose (mGy/MBq)			Effective Dose (mSv/MBq)
		Kidneys	Bladder	Remainder	
Newborns (1.6-11.0 months; M: 13; F: 4)	P01	7.4E–02	1.8E–01	9.0E–03	1.9E–02
	P02	4.9E–02	1.2E–01	5.2E–03	1.2E–02
	P03	6.2E–02	4.6E–01	7.8E–03	3.3E–02
	P04	2.5E–02	8.8E–02	4.0E–03	8.9E–03
	P05	3.6E–02	1.3E–01	1.9E–02	2.7E–02
	P06	3.3E–02	1.4E–01	1.6E–02	2.4E–02
	P07	2.7E–02	9.3E–01	1.1E–02	6.3E–02
	P08	2.8E–02	8.0E–01	1.0E–02	5.5E–02
	P09	1.2E–02	5.4E–01	6.1E–03	3.6E–02
	P10	1.7E–02	1.9E–01	3.5E–03	1.4E–02
	P11	1.8E–02	4.8E–02	4.8E–03	7.6E–03
	P12	6.4E–02	4.4E–01	6.9E–03	3.1E–02
	P13	1.5E–02	2.0E–02	2.7E–03	3.9E–03
	P14	3.4E–02	2.6E–01	1.2E–02	2.6E–02
	P15	2.2E–02	1.2E–02	1.4E–03	2.5E–03
	P16	1.3E–01	2.7E–01	1.5E–02	3.0E–02
	P17	2.5E–02	5.0E–02	1.2E–02	1.5E–02
	MEAN±SD	3.9E–02±2.9E–02	2.7E–01±2.6E–01	8.6E–03±4.8E–03	2.4E–02±1.6E–02
1-year-olds (13.0-20.0 months; M: 1; F: 2)	P18	7.7E–03	1.5E–01	2.1E–03	1.1E–02
	P19	2.5E–02	3.0E–01	4.4E–03	2.1E–02
	P20	4.1E–03	2.8E–01	4.1E–03	2.1E–02
	MEAN±SD	1.2E–02±9.0E–03	2.5E–01±6.5E–02	3.5E–03±1.0E–03	1.8E–02±4.8E–03
ALL	MEAN±SD	3.5E–02±2.9E–02	2.7E–01±2.4E–01	7.8E–03±4.8E–03	2.3E–02±1.5E–02
ICRP 128 [18] (1-year-old)		1.5E–02	3.1E–01	3.6E–03	2.2E–02

M = Males;
F = Females

TABLE A3. Organ-specific absorbed dose coefficients (mGy/MBq) and effective dose coefficients (mSv/MBq) for patients with abnormal renal function (clustered into age groups).

Age group	Patient	Renal Abnormality Type	Absorbed Dose (mGy/MBq)			Effective Dose (mSv/MBq)
			Kidneys	Bladder	Remainder	
Newborns (1.3-8.0 months; M: 10; F: 3)	P21	Bilateral	9.3E–01	9.1E–01	2.4E–02	9.0E–02
	P22	Unilateral	6.7E–01	9.9E–01	2.1E–02	7.4E–02
	P23	Unilateral	8.1E–02	2.8E–01	1.5E–02	3.1E–02
	P24	Bilateral	1.0E+00	2.9E–01	2.0E–02	5.5E–02
	P25	Bilateral	1.3E–01	1.2E–01	5.6E–03	1.5E–02
	P26	Unilateral	1.3E–01	4.5E–01	1.2E–02	3.7E–02
	P27	Unilateral	6.2E–02	1.9E–01	9.8E–03	2.1E–02
	P28	Unilateral	1.1E–01	6.1E–01	2.0E–02	5.4E–02
	P29	Bilateral	2.6E–01	7.6E–01	1.2E–02	5.5E–02
	P30	Bilateral	8.6E–01	2.2E–01	1.6E–02	7.4E–02
	P31	Unilateral	2.7E–01	1.3E+00	1.6E–02	8.6E–02
	P32	Bilateral	5.5E–01	1.4E–01	1.1E–02	4.4E–02
	P33	Unilateral	2.7E–02	1.4E–02	1.4E–03	2.7E–03
	MEAN±SD		3.9E–01±3.5E–01	4.8E–01±3.7E–01	1.4E–02±6.2E–03	4.6E–02±2.6E–02
1-year-olds (12 months; M)	P34	Bilateral	4.5E–01	2.4E–01	2.0E–02	4.2E–02
ALL	MEAN±SD		4.0E–01±3.4E–01	4.6E–01±3.7E–01	1.5E–02±6.2E–03	4.5E–02±2.5E–02
ICRP 128 [18] (1-year-olds)		Unilateral	8.1E–01	1.7E–01	8.0E–03	3.8E–02
		Bilateral	5.9E–02	2.3E–01	6.0E–03	1.9E–02

M = Males; F = Females

TABLE A4. Time-integrated activity coefficients for ^{68}Ga peptides.

Organ	TIAC (h)			
	^{68}Ga-DOTATATE Sandström et al. [61]	^{68}Ga-DOTATOC Sandström et al. [61]	^{68}Ga-DOTATOC Hartmann et al. *[62]	^{68}Ga-Pentixafor Herrmann et al. *[29]
Liver	1.6E–01	1.3E–01	2.4E–01	5.4E–02
Spleen	3.8E–02	3.8E–02	9.8E–02	2.0E–02
Kidneys	5.6E–02	4.8E–02	1.3E–01	2.0E–02
Adrenals	3.0E–03	3.0E–03	2.5E–03	–
Bone Marrow	3.2E–02	3.8E–02	2.7E–02	2.8E–02
Bladder	7.0E–02	8.6E–02	4.5E–02	6.1E–02
Heart	1.2E–02	1.4E–02	–	2.9E–02
Small intestine	2.1E–02	1.8E–02	–	–
Upper Large colon	8.0E–03	7.0E–03	–	–
Lower Large colon	1.0E–03	1.0E–03	–	–
Lung	5.0E–03	6.0E–03	–	–
Remainder	1.2E+00	1.1E+00	8.8E-01	1.2E+00
* Males				

TABLE A5. Organ-specific absorbed doses and respective estimated excess lifetime risk per cancer site (chances in 100,000 persons) for NRF patients clustered by gender (mean±SD).

Organs	Male (14 Patients)		Female (6 Patients)	
	Dose (mGy)	**Risk (in 100,000)**	**Dose (mGy)**	**Risk (in 100,000)**
Stomach Wall	0.1±0.1	0.3±0.2	0.1±0.1	0.2±2.0
Colon	0.3±0.2	1.0±0.6	0.3±0.2	0.8±0.4
Liver	0.1±0.1	0.2±0.1	0.1±0.1	0.1±0.1
Gallbladder Wall	0.1±0.1	0.0±0.0	0.1±0.1	0.0±0.0
Pancreas	0.2±0.1	0.1±0.1	0.1±0.1	0.1±0.1
Lungs	0.1±0.1	0.4±0.3	0.1±0.1	0.6±0.7
Urinary Bladder	4.3±4.8	11.7±12.4	6.0±3.5	15.6±9.2
Kidneys	0.6±0.3	0.5±0.2	0.7±0.9	0.4±0.6
Brain	0.1±0.1	0.1±0.1	0.1±0.1	0.0±0.0
Thyroid	0.1±0.1	0.3±0.2	0.1±0.1	0.9±1.0
Red Marrow	0.1±0.1	0.4±0.4	0.1±0.1	0.3±0.3
Ovaries	–	–	0.3±0.2	0.3±0.2
Breasts	–	–	0.1±0.1	0.8±0.7
Uterus	–	–	0.6±0.3	0.4±0.2
RadRAT Tool - Lifetime Risk of developing Cancer of the Exposed organs with 90% uncertainty range [46]				

TABLE A6. Organ-specific absorbed doses and estimated excess lifetime risk per cancer site (chances in 100,000 persons) for adults and 1-year-olds with normal renal function (NRF) clustered by gender.

Organs	Adult			1-year-old		
	[+]Dose (mGy)	Male Risk (in 100,000)	Female Risk (in 100,000)	[+]Dose (mGy)	Male Risk (in 100,000)	Female Risk (in 100,000)
Stomach Wall	2.7E–02	1.5E–02	1.8E–02	5.8E–02	1.0E–01	1.2E–01
Colon	2.3E–01	3.3E–01	2.2E–01	2.3E–01	8.3E–01	5.5E–01
Liver	2.1E–02	8.3E–03	4.5E–03	4.8E–02	5.7E–02	3.2E–02
Gallbladder Wall	3.9E–02	0.0E+00	0.0E+00	6.5E–02	0.0E+00	0.0E+00
Pancreas	2.7E–02	6.5E–03	6.6E–03	5.8E–02	3.5E–02	3.6E–02
Lungs	1.0E–02	1.2E–02	3.1E–02	2.3E–02	8.0E–02	1.9E–01
Urinary Bladder	7.6E+00	7.6E+00	7.4E+00	7.4E+00	1.9E+01	1.9E+01
Kidneys	2.3E–01	7.6E–02	4.7E–02	3.5E–01	2.9E–01	1.9E–01
Brain	6.9E–03	1.6E–03	4.2E–04	1.4E–02	1.4E–02	3.9E–03
Thyroid	8.9E–03	1.4E–03	7.0E–03	1.9E–02	3.6E–02	2.0E–01
Red Marrow	6.4E–02	5.5E–02	4.3E–02	4.8E–02	1.3E–01	1.2E–01
[*]**Ovaries**	3.7E–01	–	1.9E–02	3.2E–01	–	2.3E–01
[*]**Breasts**	6.9E–03	–	1.4E–01	1.9E–02	–	3.6E–01
[*]**Uterus**	8.2E–01	–	1.7E–01	7.2E–01	–	4.6E–01

[+]The dose (mGy) values were calculated stem from the effective dose coefficients (mGy/MBq) published in ICRP publication 128 [18]

[*]Gender-specific organs

TABLE A7. Organ-specific absorbed doses and respective estimated excess lifetime risk per cancer site (chances in 100,000 persons) for ARF patients clustered by gender (mean±SD).

Organs	Male (14 Patients)		Female (6 Patients)	
	Dose (mGy)	Risk (in 100,000)	Dose (mGy)	Risk (in 100,000)
Stomach Wall	0.2±0.1	0.3±0.2	0.2±0.1	0.5±0.1
Colon	0.4±0.2	1.3±0.8	0.5±0.2	1.3±0.5
Liver	0.2±0.1	0.2±0.2	0.2±0.1	0.2±0.1
Gallbladder Wall	0.3±0.1	0.0±0.0	0.3±0.1	0.0±0.0
Pancreas	0.3±0.1	0.2±0.1	0.3±0.1	0.2±0.1
Lungs	0.1±0.1	0.4±0.2	0.2±0.03	1.3±0.2
Urinary Bladder	6.7±5.9	17.6±16.2	10.8±5.5	28.5±14.7
Kidneys	6.0±5.3	5.1±4.7	7.7±5.7	4.9±3.3
Brain	0.1±0.1	0.1±0.1	0.1±0.02	0.03±0.01
Thyroid	0.1±0.1	0.2±0.1	0.1±0.02	1.3±0.2
Red Marrow	0.2±0.1	0.5±0.3	0.1±0.02	0.6±0.1
Ovaries	–	–	0.1±0.01	1.3±0.1
Breasts	–	–	0.5±0.2	0.6±0.2
Uterus	–	–	1.0±0.4	0.6±0.3

RadRAT Tool - Lifetime Risk of developing Cancer of the Exposed organs with 90% uncertainty range [46]

TABLE A8. Organ-specific absorbed doses and estimated excess lifetime risk per cancer site (chances in 100,000 persons) for adults and 1-year-olds with unilateral abnormal renal function (UARF) clustered by gender.

Organs	Adult			1-year-old		
	[+]Dose (mGy)	Male	Female	[+]Dose (mGy)	Male	Female
		Risk (in 100,000)	Risk (in 100,000)		Risk (in 100,000)	Risk (in 100,000)
Stomach Wall	2.7E–01	1.5E–01	1.8E–01	2.8E–01	5.0E–01	6.0E–01
Colon	2.7E–01	3.7E–01	2.5E–01	3.5E–02	1.3E–01	8.4E–02
Liver	3.0E–01	1.2E–01	6.4E–02	3.9E–01	4.6E–01	2.6E–01
Gallbladder Wall	4.3E–01	0.0E+00	0.0E+00	5.3E–01	0.0E+00	0.0E+00
Pancreas	5.1E–01	1.2E–01	1.2E–01	6.7E–01	4.1E–01	4.2E–01
Lungs	7.6E–02	9.1E–02	2.3E–01	1.7E–01	5.8E–01	1.4E+00
Urinary Bladder	3.8E+00	3.9E+00	3.8E+00	3.9E+00	1.0E+01	9.9E+00
Kidneys	1.4E+01	4.5E+00	2.8E+00	1.9E+01	1.6E+01	1.1E+01
Brain	7.6E–03	1.7E–03	4.7E–04	1.7E–02	1.7E–02	4.8E–03
Thyroid	1.2E–02	1.9E–03	9.2E–03	3.7E–02	7.1E–02	4.0E–01
Red Marrow	2.1E–01	1.8E–01	1.4E–01	1.9E–01	5.3E–01	4.7E–01
Ovaries	2.6E–01	–	7.2E–02	3.5E–01	–	8.5E–01
Breasts	2.6E–02	–	1.0E–01	6.9E–02	–	3.9E–01
Uterus	4.9E–01	–	1.0E–01	5.1E–01	–	3.3E–01

[+]The dose (mGy) values were calculated stem from the effective dose coefficients (mGy/MBq) published in ICRP publication 128 [18]

TABLE A9. Organ-specific absorbed doses and estimated excess lifetime risk per cancer site (chances in 100,000 persons) for adults and 1-year-olds with bilateral abnormal renal function (BARF) clustered by gender.

Organs	Adult			1-year-old		
	[+]Dose (mGy)	Male Risk (in 100,000)	Female Risk (in 100,000)	[+]Dose (mGy)	Male Risk (in 100,000)	Female Risk (in 100,000)
Stomach Wall	8.2E–02	4.6E–02	5.5E–02	1.4E–01	2.5E–01	3.0E–01
Colon	2.4E–01	3.3E–01	2.2E–01	2.5E–01	9.3E–01	6.1E–01
Liver	9.6E–02	3.7E–02	2.0E–02	1.5E–01	1.8E–01	1.0E–01
Gallbladder Wall	1.1E–01	0.0E+00	0.0E+00	1.5E–01	0.0E+00	0.0E+00
Pancreas	1.0E–01	2.4E–02	2.5E–02	1.7E–01	1.1E–01	1.1E–01
Lungs	5.4E–02	6.5E–02	1.6E–01	1.0E–01	3.6E–01	8.7E–01
Urinary Bladder	5.7E+00	5.7E+00	5.6E+00	5.3E+00	1.4E+01	1.3E+01
Kidneys	9.6E–01	3.1E–01	1.9E–01	1.4E+00	1.1E+00	7.4E–01
Brain	4.2E–02	9.6E–03	2.6E–03	8.3E–02	8.1E–02	2.3E–02
Thyroid	5.0E–02	7.9E–03	4.0E–02	1.0E–01	1.9E–01	1.1E+00
Red Marrow	1.0E–01	8.9E–02	7.0E–02	1.2E–01	3.2E–01	2.9E–01
Ovaries	3.4E–01	–	1.0E–01	3.2E–01	–	9.1E–01
Breasts	3.7E–02	–	1.3E–01	7.4E–02	–	3.6E–01
Uterus	6.9E–01	–	1.4E–01	6.2E–01	–	4.0E–01

[+]The dose (mGy) values were calculated stem from the effective dose coefficients (mGy/MBq) published in ICRP publication 128 [18]

Radiation Risk Assessment Tool - Lifetime Cancer Risk from Ionizing Radiation

Radiation Risk Assessment Tool Summary Report

RadRAT 4.1.1 using Analytica/ADE 4.5 64-bit

Report Date: 10/27/2017 08:57:46 AM

Information Used In Lifetime Risk Calculation

Gender	Female
Birth Year	2013
Population	U.S. 2000-2005

Assumptions and Settings

Number of Iterations	300
Random Number Seed	99
User Defined Uncertainty Distribution	Fixed Value (1)
Current Year Setting	2017

General Exposure Information

Event #	Exposure Year	Organ	Organ Dose (mGy)	Exposure Rate
1	2015	Brain/CNS	Fixed Value (0.0097)	acute
1	2015	Breast	Fixed Value (0.014)	acute
1	2015	Gallbladder	Fixed Value (0.0442)	acute
1	2015	Colon	Fixed Value (0.391)	acute
1	2015	Stomach	Fixed Value (0.0558)	acute
1	2015	Kidney	Fixed Value (0.099)	acute
1	2015	Liver	Fixed Value (0.0374)	acute
1	2015	Lung	Fixed Value (0.016)	acute
1	2015	Ovary	Fixed Value (0.418)	acute
1	2015	Pancreas	Fixed Value (0.0531)	acute
1	2015	Leukemia	Fixed Value (0.052)	acute
1	2015	Thyroid	Fixed Value (0.0122)	acute
1	2015	Bladder	Fixed Value (6.72)	acute
1	2015	Uterus	Fixed Value (0.986)	acute

Risk Estimates

Lifetime Risk of Developing Cancer of the Exposed Organs (chances in 100,000) with a 90% Uncertainty Range

	Lower Bound	Mean	Upper Bound
Excess Lifetime Risk*	7.17	19.1	37.2

* Risk from the time of exposure to the end of the expected lifetime

Excess Lifetime Risk per Cancer Site* with a 90% Uncertainty Range

Cancer Site	Lower Bound	Mean	Upper Bound
Stomach	0.0145	0.116	0.444
Colon	0.368	0.917	1.8
Liver	0.00223	0.0236	0.0881
Gallbladder	< 0	< 0	0.00492
Pancreas	0.0057	0.0323	0.0731
Lung	0.0555	0.129	0.277
Breast	0.0876	0.164	0.274
Ovary	0.111	0.45	1.05
Uterus	< 0	0.612	2.08
Bladder	5.36	16.4	34.7
Kidney	0.00659	0.0515	0.132
Nervous System	0.000637	0.00247	0.00549
Thyroid	0.0288	0.121	0.301
Leukemia	0.0139	0.104	0.317

* Risk from the time of exposure to the end of the expected lifetime

FIGURE A1. Example of an input (organ absorbed doses) and an output (ELR values) of the RadRAT Tool for patient P20 (normal renal function).

IV. ABBREVIATION LIST

ALARA	As low as reasonably achievable
ANOVA	Analysis of Variance
ARF	Abnormal Renal Function
BARF	Bilateral Abnormal Renal Function
BfS	Bundesamt für Strahlenschutz
BL	bladder
Bq	Becquerel (SI unit for activity: 1 Bq = s^{-1})
CI	Confidence Intervals
CT	Computed Tomography
DNA	Deoxyribonucleic acid
DRL	Diagnostic Reference Levels
EANM	European Association of Nuclear Medicine
EFR	Excess Future Risk
ELR	Excess Lifetime Risk
ER	Excess Risk
^{18}F-FDG	^{18}F- fluoro-2-deoxy-D-glucose
Gy	Gray (SI unit for absorbed dose: 1 Gy = 1 J/kg)
IAEA	International Atomic Energy Agency
i.v.	intravenous
SPECT/CT	Single Photon Emission Computed Tomography
PET/CT	Positron Emission Tomography/Computed Tomography
MRI	Magnetic Resonance Imaging
ICRP	International Commission on Radiological Protection
IVU	Intravenous Urography
KD	kidneys
LB	Lower Bound
LEHR	Low-energy high-resolution
LET	Linear Energy Transfer
^{99m}Tc-MAG3	^{99m}Tc-mercaptoacetyltriglycine
^{99m}Tc-DMSA	^{99m}Tc-dimercaptosuccinic acid
MIRD	Committee on Medical Internal Radiation Dose
NACG	North America Consensus Guideline
NM	Nuclear Medicine
NRF	Normal Renal Function
OLINDA/EXM	Organ Level Internal Dose Assessment/Exponential Modeling
PEDNM	Pediatric Nuclear Medicine
PLR	Population Lifetime Risk
RadRAT	Radiation Risk Assessment Tool
RKI	Robert Koch Institute's
RLR	Relative Lifetime Risk
ROI	Region of Interest
RRA	Radiation Risk Analysis
SD	Standard deviation
SEER	Surveillance Epidemiology and End Results
SNMMI	Society of Nuclear Medicine and Molecular Imaging
Sv	Sievert (defined unit for effective dose by the ICRP: 1 Sv = 1 J/kg)
TAC	Time-Activity Curves
TIAC	Time-Integrated Activity Coefficients
T_{max}	Maximum Uptake Time-Point
UARF	Unilateral Abnormal
UB	Upper Bound
UKW	Universität Klinikum Würzburg
WB	Whole Body

V. TABLES LIST

VI. EQUATIONS LIST

VII. COMPLIANCE WITH ETHICAL STANDARDS

Funding: Part of the work was financed by a scholarship of CAPES - Coordenação de Aperfeiçoamento de Pessoal de Nível Superior, the development agency of the Brazilian Federal Government.

Ethical approval: As the data for this retrospective analysis were acquired within a clinical routine, our local ethics committee waived the need for further approval.

VIII. AFFIDAVIT / EIDESSTATTLICHE ERKLÄRUNG

Affidavit

I hereby confirm that my thesis entitled *Morphological and Functional Ultrashort Echo Time (UTE) Magnetic Resonance Imaging of the Human Lung* is the result of my own work. I did not receive any help or support from commercial consultants. All sources and / or materials applied are listed and specified in the thesis.

Furthermore, I confirm that this thesis has not yet been submitted as part of another examination process neither in identical nor in similar form.

_____ _____

Place, Date Signature

Eidesstattliche Erklärung

Hiermit erkläre ich an Eides statt, die Dissertation *Morphologische und funktionelle Magnetresonanztomographie der menschlichen Lunge mit ultrakurzen Echozeiten (UTE)* eigenständig, d.h. insbesondere selbständig und ohne Hilfe eines kommerziellen Promotionsberaters, angefertigt und keine anderen als die von mir angegebenen Quellen und Hilfsmittel verwendet zu haben.

Ich erkläre außerdem, dass die Dissertation weder in gleicher noch in ähnlicher Form bereits in einem anderen Prüfungsverfahren vorgelegen hat.

_____ _____

Ort, Datum Unterschrift

IX. ACKNOWLEDGMENTS

I would like to thank and express my eternal gratitude to my supervisor Prof. Dr. Michael Lassmann for welcoming me into his team, for all support, and for giving me the opportunity for developing my doctoral research in a perfect work environment. The knowledge I acquired from him I will care with me for life.

I would like to thank the CAPES - Coordenação de Aperfeiçoamento de Pessoal de Nível Superior, the development agency of the Brazilian Federal Government, the Universitätsklinikum Würzburg (associated with the University of Würzburg), the Graduate School of Life Science (GSLS), and the DAAD - Deutscher Akademischer Austauschdienst for supporting my research financially.

I would like to thank my thesis committee, Prof. Dr. Gerhard Glatting and Prof. Andreas K. Buck for advising me and provide guidance.

I would like to express my deep gratitude to my “teammate” Dr. Johannes Tran-Gia, for the precious mentoring, great support, and patience during my study time.

I would like to thank Susanne Schlögl for passing me valuable knowledge, and for the patience while instructing me, especially during my research experiments.

I would like to thank the GSLS Team for guidance and support during all stages of my Ph.D.

I am glad for being part of such harmonious group as the Physics Department of the Clinic and Policlinic for Nuclear Medicine of the Universitatsklinikum Würzburg, and I would like to thank my colleagues Dr. Uta Eberlein, Sara Schumann, Julius Neba, Andreas Hinsch, Dr. Heribert Hänscheid, Harald Schlotter for all support during my doctorate.

I am grateful for having Seval Beykan as my work colleague, my best friend, my sister. I would like to thank her for passing through so many important moments with me during the last years, for the constant emotional support and motivation.

I consider myself “blessed” since I have an amazing Family who always gave me so much love, support, and guidance even from “an ocean distance.” Therefore, I thank my mother Maria Lucia M. Soares Machado, my father Antonio Soares Machado, my sister Joyce Soares Machado, my brother Júlio C. Soares Machado, and my grandmother Ilda Júlio for the emotional support, for encouraging me to pursue and live my dreams, without you I would not come so far.

I would like to express my deep gratitude to my lovely husband Oliver G. Soares Machado who is “walking through all the way by my side” during the last years, giving me much support, unconditional love, and motivating me always.

I would like to thank my friends “another family” for unconditional support, encouragement, and love. In special I would like to thank Lenon Mendes Pereira, Alan Tonello, Gülayse Gürsoy, Maikol Salas, Felipe Arias, Juan Salcedo, and Adam Whisnant.

“Viver e não ter a vergonha de ser feliz cantar e cantar e cantar a beleza de ser um eterno aprendiz”
“Ah meu Deus!”
“Eu sei, eu sei que a vida devia ser bem melhor e será mas isso não impede que eu repita é bonita, é bonita e é bonita”

“O que é? O que é?”
Luiz Gonzaga (Gonzaguinha)

PUBLICATIONS

Original Research:

- Soares Machado, J., Tran-Gia, J., Schlögl, S., Buck, A.K., Lassmann, M. Biokinetics, Dosimetry and Radiation Risk in Infants after 99mTc-MAG3 Scans. Eur J Nucl Med Mol Imaging – Research (2018) 8:10 DOI 10.1186/s13550-017-0356-2 https://ejnmmires.springeropen.com/articles/10.1186/s13550-017-0356-2

- Soares Machado, J., Beykan, S., Herrmann, K., Lassmann, M. Recommended Administered Activity for Ga-68-labelled peptides in Pediatric Nuclear Medicine. Eur J Nucl Med Mol Imaging (2016) 43: 2036. doi:10.1007/s00259-015-3289-x https://link.springer.com/article/10.1007%2Fs00259-015-3289-x

- MACHADO, J. S. Análise das Doses Ocupacionais em Operações de Manutenção e Intervenção em Áreas Restritas do Centro de Radiofarmácia do IPEN. 2013. Dissertation (Master). Instituto de Pesquisas Energéticas e Nucleares -IPEN / CNEN. São Paulo. 96 p www.teses.usp.br/teses/disponiveis/85/85131/tde...085528/.../2013MachadoAnalise.pdf

- MACHADO, Jessica S.; RAMOS, Felipe C. Radiobiologia: Efeitos Biológicos das Radiações. 2009. Dissertation (Bachelor). Centro Universitário São Camilo. São Paulo -SP.76 p

Conference Contributions:

- **EANM - European Association of Nuclear Medicine, 30th Annual Congress**, 21st – 25th October 2017, Vienna Austria. Presentation title: “Dosimetry and Radiation Risk in Infants after 99mTc-MAG3 Scans.”

- **EANM - European Association of Nuclear Medicine, 28th Annual Congress**, 15th – 19th October 2016, Barcelona Spain. Presentation title: “Biokinetics and Dosimetry of 99mTc-MAG3 scans in Infants”.

- **EANM - European Association of Nuclear Medicine, 27th Annual Congress**, 10th – 14th October 2015, Hamburg Germany. Presentation title 1: “Dosage in Pediatric Nuclear Medicine Diagnostics in Daily Practice.” Presentation title 2: “Recommended Administered Activity for 68Ga-labelled peptides in Pediatric Nuclear Medicine”.

- **RADIO 2011 - II Congress of Radiation Protection of the Community of Portuguese Language Countries**. II Brazilian Congress on Radiological Protection. V International Congress on Industrial Radiation Protection. Machado, J. S., Gerulis, E., Rodrigues Jr, O., Todo, A. S. Otimização da radioproteção em manutenções de celas de produção de radiofármacos. Instituto de Pesquisas Energéticas e Nucleares IPEN -CNEN / SP.